UNSTEADY WAVES ON AN OPEN TWO LAYER FLUID

A thesis

presented for the degree

of

Doctor of Philosophy

at the

University of Canterbury

Christchurch

New Zealand

by

P. W. Sharp

1983

Acknowledgements

My biggest thanks is to my supervisor, Dr. P.J. Bryant, whose knowledge and encouragement has been greatly appreciated throughout the three years of my Ph.D. study. I also wish to thank Dr. I.D. Coope and Mr. R.L. Broughton whose suggestions led to improvements in the numerical schemes employed in my thesis. For the efficient typing of this manuscript my thanks go to Mrs. A. Tindall. The use of the Harwell subroutine NS02AD is also gratefully acknowledged.

Finally I would like to pay a special tribute to the PRIME 750 which showed that neither man nor machine is perfect.

Mathematical Symbols, Notation, Abbreviations

In all summations, for example

$$\sum_{k=\ell}^{m} a_k$$

if $m < \ell$ no sum is performed.

Partial differentiation is denoted by a post subscript.

Widely used symbols and notation are:

$*$ - the complex conjugate

$\sim$ - as an underline denotes a vector

$\|\cdot\|_2$ - the L_2 norm of a vector

a - a measure of the surface wave height

A - coefficient matrix (3.2.11), initial value of non-zero surface harmonic amplitudes for unsteady solutions

$A_k(t)$ - amplitude of harmonic, with wavenumber k, in general Fourier series expansion of the surface displacement

$a_k(t)$ - amplitude of surface harmonic, with wavenumber k, in a particular solution

b - a measure of the interface wave height

$B_k(t)$ - amplitude of harmonic, with wavenumber k, in general Fourier series expansion of the interface displacement

$b_k(t)$ - amplitude of interface harmonic, with wavenumber k, in a particular solution

c - for constant amplitude, the surface group speed and interface phase speed

$C(\alpha)$ - complete integral of the first kind for the parameter α

CNM - the classical Newton's method

DNM - the damped Newton's method

$E(x,t)$ - envelope function in unsteady solutions for surface wave

$\underset{\sim}{f}(\underset{\sim}{x})$ - system of nonlinear algebraic equations for harmonic amplitudes in steady solutions

g - gravity

$\underset{\sim}{g}(\underset{\sim}{x},\theta)$ - auxiliary function in general continuation method

h - depth of upper layer, step size in integration schemes

i - when not used as a subscript or superscript denotes $(-1)^{\frac{1}{2}}$

IVP1 - initial value problem in Davidenko's continuation approach

IVP2 - initial value problem in the method of incremental loading

IVP3 - initial value problem for harmonic amplitudes in unsteady solutions

J - Jacobian of $\underset{\sim}{f}(\underset{\sim}{x})$

K $\equiv$ $R_{3m+1,-1}$, used in the unsteady three wave analytical results

k - general wavenumber, order of predictor in integration schemes

k_1 - smallest surface wavenumber

k_2 - largest surface wavenumber

L - $2\pi L$ is the fundamental wavelength

ℓ - general wavenumber

m - on the linear theory the central wavenumber of the surface spectrum

M $\equiv$ $R_{3m,1}$, used in the unsteady three wave analytical results

n_1 - number of interface harmonics

n_2 - number of surface harmonics

P $\equiv$ $R_{2l,m}$, used in the unsteady three wave analytical results

PHM - Powell's hybrid method

r - geometric ratio in ordering of interface harmonics (3.2.8)

$R_{1k,\ell}$ - interaction coefficient for two interface harmonics interacting with a third interface harmonic

$R_{2k,\ell}$ - interaction coefficient for two surface harmonics interacting with an interface harmonic

$R_{3k,\ell}$ - interaction coefficient for a surface and an interface harmonic interacting with a second surface harmonic

S_{max} - the maximum allowable slope of harmonics in steady solutions

t - coordinate time, time scale for phase changes

T - period of energy oscillations in unsteady three wave analytical solution

$T_k \equiv \tanh k\mu$

x - horizontal space coordinate

$X \equiv a_{m+1}$, used in unsteady three wave analytical results

$\underset{\sim}{x}_0$ - initial estimate of a steady solution

y - vertical space coordinate

$Y \equiv a_m$, used in unsteady three wave analytical results

$\underset{\sim}{y}$ - eigenvector of (3.2.11)

$Z \equiv b_1$, used in unsteady three wave analytical results

α - for steady solutions, the frequency of the surface wave relative to the group

$\bar{\Delta}C$ - in the unsteady solutions the speed of the wave system relative to the frame of reference moving with speed $\omega_{B1}\mu^{-1}$

ΔC - the time average of ΔC

$\varepsilon \equiv b/h$, perturbation parameter, measure of the wave slopes

ε^i - initial value of ε in our form of the method of incremental loading

ε^f - final value of ε in our form of the method of incremental loading

εV - horizontal velocity at free surface due to lowest interface harmonic

$\eta(x,t)$ - the interface displacement

θ - general continuation parameter

λ - constraint on surface amplitudes in steady solutions

μ $\equiv$ h/L

$\xi(x,t)$ - surface displacement

ρ - ratio of lower to upper layer densities

ρ_1 - lower layer density

ρ_2 - upper layer density

τ $\equiv$ εt, time scale of amplitude changes

ϕ_1 - velocity potential for lower layer

ϕ_2 - velocity potential for upper layer

ω_k - linear frequency of harmonic with wavenumber k

ω_{Ak} - linear frequency of surface harmonic with wavenumber k

ω_{Bk} - linear frequency of interface harmonic with wavenumber k

TABLE OF CONTENTS

Abstract

The interaction and evolution of small amplitude gravity waves on an open two layer fluid is investigated. The surface and interface displacements are represented as spatially periodic Fourier series with time dependent coefficients, for which evolution equations with all significant quadratic interactions included, are derived. Both steady and unsteady solutions to these equations are found, analytically for a small number of wave modes, and numerically for a larger number of modes. The steady numerical solutions are obtained using a robust variation of Davidenko's continuation method while an efficient integration scheme is used to find the unsteady solutions. Numerical examples are given to illustrate general properties of the interactions and evolution.

CHAPTER 1

Introduction

This thesis deals with the evolution of small amplitude gravity waves on a stable two layer fluid. The system consists of two homogeneous layers of comparable density with no stream velocities and an open upper surface.

For this system it has long been known theoretically (see for example Lamb [24]) that two types of gravity wave modes are possible. One is a fast surface mode with a small interface amplitude. The second is a slow interface mode with a small surface amplitude. Briscoe [7] in a historical note cites two early observations of this internal wave mode, with the more interesting being that of the explorer Nansen. He found in 1893 when sailing in Norwegian fiords which had a thin layer of freshwater upon saltwater that the speed of his ship was noticeably less than the surface conditions would suggest. The reduction in speed was attributed to part of the ship's energy being used to generate internal waves on the interface between the freshwater and saltwater.

In this thesis instead of having a travelling pressure field at the surface we have considered the situation of a surface wave field with the mutual interaction between the surface and internal waves being studied. The type of interaction considered is based on that due to Phillips [32].

In the classical theory of water waves the linear theory predicts that gravity waves will propagate independently of one another and hence without the transfer of energy between them. With the inclusion of the nonlinear terms the theoretical work of Stokes [40], Boussinesq [5], Korteweg and De Vries [23] (see, for example, Whitham [44] for a

discussion of these results) has demonstrated that permanent wave forms on a homogeneous fluid are possible.

Phillips showed for surface gravity waves on deep water that with the nonlinear terms included it was possible for significant amounts of energy to be transferred to a wave mode if a resonance condition (to be stated later) was satisfied. In particular he showed that three wave modes could interact to generate a mode not initially present. The rate of interaction was of $O(\varepsilon^2)$ where $\varepsilon << 1$ is a measure of the wave slopes. Thus for a complete description of the wave field evolution over a time interval of $O(\varepsilon^{-2})$ the linear theory had to be extended to include the nonlinear terms. Because Phillips assumed that the interaction did not affect the original wave modes, the perturbation scheme he used was not valid when the new mode was of size comparable to the original modes. Hence Phillips was only able to obtain the initial growth of the new mode.

Benney [2] removed the above singularity by allowing the amplitudes of the wave modes to vary slowly with time. Using this approach he derived evolution equations for the amplitudes of the wave modes and showed that the solution consisted of energy oscillations between the modes. Bretherton [6] formalised Benney's approach by using a two time expansion with the phase changes of the wave modes occurring on the fast time scale and the amplitude changes on the slow time scale. Bretherton also introduced the idea of near resonance for which the resonance condition is satisfied to $O(\varepsilon)$. This enabled wave modes which were not at resonance but made a significant contribution to the evolution to be included.

Following the above theoretical work the existence of the resonant interactions was established experimentally by Longuet-Higgins and Smith [27], and McGoldrick, Phillips, Huang, Hodgson [29], with good agreement

being obtained between the observed and estimated initial growth rates.

Meanwhile the idea of resonant wave interactions was applied to other types of wave systems. McGoldrick [28] considered the interaction between gravity-capillary waves, Ball [1] the interaction between internal and surface gravity waves on a two layer fluid and Thorpe [41] the interaction for a continuously stratified fluid. Ball showed that it was possible for two surface waves with frequencies $\omega_{\underset{\sim}{k}}$, $\omega_{\underset{\sim}{k}+\underset{\sim}{\ell}}$ and wavenumbers $\underset{\sim}{k}$, $\underset{\sim}{k} + \underset{\sim}{\ell}$ and one interface wave with frequency $\omega_{\underset{\sim}{\ell}}$ and wavenumber $\underset{\sim}{\ell}$ to satisfy the resonance condition which for this situation was

$$\omega_{\underset{\sim}{k}+\underset{\sim}{\ell}} - \omega_{\underset{\sim}{k}} - \omega_{\underset{\sim}{\ell}} = 0 \qquad 1.1.1$$

with $\|\underset{\sim}{k}\|_2 >> \|\underset{\sim}{\ell}\|_2$. Using the perturbation scheme of Phillips this type of interaction occurs at an $O(\varepsilon)$ rate. Thus for gravity waves on deep water with both surface-surface and surface-interface resonant wave interactions present the latter dominates the wave field evolution up to a time of $O(\varepsilon^{-1})$. The existence of these surface-interface wave interactions was verified experimentally by Lewis, Lake and Ko [25] and by Joyce [22].

Having shown that resonant interactions between surface and internal waves were possible it then became necessary to establish the importance of their dynamic role in the evolution of wave fields. Thorpe [42] in a concise review of internal waves discussed physical processes that have been used to explain their generation, interaction and dissipation. His list of possible sources of generation included travelling pressure fields, travelling stress fields, travelling buoyancy fluxes, coupling between the surface mixing layer and the underlying water, bottom topography generation as well as resonant wave interactions. This variation together with the possibility that

several processes may occur at the same time makes the problem of deciding the importance of resonant wave interactions difficult.

Recent theoretical studies of the evolution of waves on a two layer fluid include the work of Watson, West and Cohen [43], Rizk and Ko [38] and Ma [30] as well as that in the text by Phillips [33]. Watson et al using a statistical approach, with both the surface and interface wave fields being linear, were able to obtain an estimate of the energy transferred from the surface to the internal waves. Rizk and Ko considered, using the technique of multiple scales, the interaction between Stokes waves on the surface and long internal waves. By rigorously ordering the terms in the expansion they were able to estimate the relative effects of the resonant and other terms. Ma derived evolution equations for the interaction between long internal and short surface waves. The exact form of these equations depended on the wave slopes in the two wave fields and the ratio of wavelengths.

The approach we have used has been to take both the surface and interface displacements as unknown functions resolved into as many wave modes as required. The surface and interface wave fields are not restricted to being linear and the interface wavelengths are taken to be far greater than the surface wavelengths. By having as many wave modes as required we have ensured that all the wave modes that make a significant contribution to the evolution are present. The use of nonlinear wave fields means as will be seen that the interaction between interface wave modes together with that between surface and interface modes must be included.

To simplify the algebra we have taken the wave propagation to be unidirectional and the lower layer to be of depth far greater than any wavelengths present. A limit is placed on the slopes of the wave modes to exclude large amplitude waves. The waves are represented as

spatially periodic Fourier series with coefficients which vary slowly with time.

In chapter 2 evolution equations with all the significant quadratic interactions included are derived for the rates of change of the Fourier coefficients. The cubic and higher interactions are omitted because as stated above they occur on a longer time scale than the quadratic interactions. Steady solutions to these evolution equations are given in chapter 3. Analytical results are obtained for a small number of harmonics while the general solutions are found numerically. The steady solutions are used to illustrate properties of the nonlinear interactions and to form a basis with which to compare the unsteady solutions of chapter 4. For these unsteady solutions, as in chapter 3, analytical results are possible when a small number of harmonics are present but the general solution must be found numerically. The numerical solutions given are used to illustrate general properties of the evolution as well as properties that are unique to different sets of solutions.

To obtain the steady numerical solutions it was necessary to solve a system of nonlinear algebraic equations. Schemes based on Newton-like formulae were found to perform unsatisfactorily. Our experience with these methods led us to develop a successful scheme based on Davidenko's continuation method [14]. In this approach the emphasis was on having a robust scheme. This emphasis contrasted with that for the numerical scheme used to find the unsteady solutions. Here it was necessary to solve an initial value problem as efficiently as possible. We selected a standard integration scheme which was designed to be efficient on our type of problem. However by modifying the implementation and underlying algorithm of the integrator we were able to increase its speed by up to a factor of 2.

CHAPTER 2

Evolution Equations

2.1 Introduction

In this chapter the evolution equations for the Fourier amplitudes, with all significant interactions included, are derived. For the derivation we have assumed that the flow is inviscid, incompressible and irrotational. Discussions on the validity of the assumptions for water wave models are given in texts such as by Lighthill [26] and Phillips [33].

In our two layer situation the largest viscous effect is in the internal dissipation of energy. Using the linear theory Lighthill gives an estimate of the time required for this dissipation to decrease the energy of a surface wave by a factor of e. For waves with wavelengths 1m and 10m the time is 8000 and 250,000 wave periods respectively. Thus for our case in which the wavelengths were generally greater than 10m viscous effects can be neglected.

The absence of viscous effects means that the vorticity is confined to the interface. The fluid velocity can then be represented as the gradient of a scalar function which because of the incompressibility condition satisfies Laplace's equation.

Although the flow has been taken to be incompressible we have not made the further simplifying assumption of the Boussinesq approximation. Thus variations in the density which affect the inertia terms are not neglected.

In choosing the horizontal scale of our model we have kept all wavelengths less than 1000m. This length is small compared with the Earth's radius and thus in the derivation now given it is sufficient to use a Cartesian coordinate system.

2.2 Derivation

Our two layer model consists of an upper layer of density ρ_2 and mean depth h and a lower layer of infinite depth and density ρ_1, where the density difference $\rho_1 - \rho_2$ is small compared with ρ_1 and ρ_2. The parameters a, b, to be defined more precisely later, are measures of the surface and interface wave heights. The interface displacement $\eta(x,t)$ and surface displacement $\xi(x,t)$ are in units of b and the corresponding velocity potentials $\phi_1(x,t)$ and $\phi_2(x,t)$ in units of $(gh)^{\frac{1}{2}}b$ where g is gravity. The horizontal and vertical coordinates are x, y respectively in units of h with the origin on the mean interface level. The time t is in units of $(hg^{-1})^{\frac{1}{2}}$ and the principal parameter is $\varepsilon = b/h \ll 1$. The equations of motion in dimensionless form for this inviscid, irrotational, incompressible flow are then

$$
\begin{aligned}
&\xi_t + \varepsilon \phi_{2x}\xi_x = \phi_{2y} && y = 1 + \varepsilon\xi \\
&\phi_{2t} + \frac{1}{2}\varepsilon(\phi_{2x}^2 + \phi_{2y}^2) + \xi = 0 && y = 1 + \varepsilon\xi \\
&\eta_t + \varepsilon \phi_{1x}\eta_x = \phi_{1y} && y = \varepsilon\eta \\
&\eta_t + \varepsilon \phi_{2x}\eta_x = \phi_{2y} && y = \varepsilon\eta \\
&\rho\phi_{1t} + \rho\eta + \frac{\varepsilon}{2}\rho(\phi_{1x}^2 + \phi_{1y}^2) \\
&\qquad = \phi_{2t} + \eta + \frac{\varepsilon}{2}(\phi_{2x}^2 + \phi_{2y}^2) && y = \varepsilon\eta \\
&\phi_{1xx} + \phi_{1yy} = 0 \qquad -\infty < y < \varepsilon\eta \\
&\phi_{2xx} + \phi_{2yy} = 0 \qquad \varepsilon\eta < y < 1 + \varepsilon\xi \\
&\phi_{1y} \to 0 \quad \text{as} \quad y \to -\infty && 2.2.1
\end{aligned}
$$

where $\rho = \rho_1/\rho_2$. The first two equations are the free surface kinematic and dynamic boundary conditions while the next three are the kinematic and dynamic interface boundary conditions. The last three equations are from the incompressibility of the flow and the bottom boundary condition. When the surface boundary conditions are expanded in ε about y = 1 and the interface boundary conditions about y = 0

equations 2.2.1 become

$$\begin{aligned}
&\xi_t + \varepsilon\,(\xi\phi_{2x})_x = \phi_{2y} + O(\varepsilon^2) && y = 1\\
&\phi_{2t} + \varepsilon\,\{\xi\phi_{2yt} + \tfrac{1}{2}(\phi_{2x}^{\,2} + \phi_{2y}^{\,2})\} + \xi = O(\varepsilon^2) && y = 1\\
&\eta_t + \varepsilon\,(\eta\phi_{1x})_x = \phi_{1y} + O(\varepsilon^2) && y = 0\\
&\eta_t + \varepsilon\,(\eta\phi_{2x})_x = \phi_{2y} + O(\varepsilon^2) && y = 0\\
&\rho\phi_{1t} + \rho\eta + \varepsilon\rho\eta\phi_{1yt} + \frac{\rho\varepsilon}{2}\,(\phi_{1x}^{\,2} + \phi_{1y}^{\,2})\\
&\qquad = \phi_{2t} + \eta + \varepsilon\eta\phi_{2yt}\\
&\qquad\quad + \frac{\varepsilon}{2}(\phi_{2x}^{\,2} + \phi_{2y}^{\,2}) + O(\varepsilon^2) && y = 0\\
&\phi_{1xx} + \phi_{1yy} = 0 \qquad -\infty < y < 0\\
&\phi_{2xx} + \phi_{2yy} = 0 \qquad 0 < y < 1\\
&\phi_{1y} \to 0 \quad \text{as} \quad y \to -\infty
\end{aligned} \tag{2.2.2}$$

where in the first, third and fourth equations the quadratic terms have been simplified using Laplace's equation for ϕ_1, ϕ_2. With $\mu = h/L$ where $2\pi L$ is the fundamental wavelength we have sought spatially periodic solutions of the form

$$\begin{aligned}
\xi(x,t) &= \frac{1}{2}\sum_{k=1}^{\infty} A_k(t)\,\mathrm{expi}(k\mu x - \omega_k t) + *\\
\eta(x,t) &= \frac{1}{2}\sum_{k=1}^{\infty} B_k(t)\,\mathrm{expi}(k\mu x - \omega_k t) + *\\
\phi_1(x,t) &= \frac{1}{2}\sum_{k=1}^{\infty} C_{1k}(t)\,e^{k\mu y}\,\mathrm{expi}(k\mu x - \omega_k t) + *\\
\phi_2(x,t) &= \frac{1}{2}\sum_{k=1}^{\infty} (C_{2k}(t)\cosh\{k\mu y\} + D_{2k}(t)\sinh\{k\mu y\})\\
&\qquad\qquad \mathrm{expi}(k\mu x - \omega_k t) + *\,.
\end{aligned} \tag{2.2.3}$$

Here * denotes the complex conjugate, k is the wavenumber in units of L^{-1} and the frequency ω_k is in units of $(g/h)^{\frac{1}{2}}$.

When the above Fourier series are substituted into equations 2.2.2 with the $O(\varepsilon)$ and higher terms neglected the linear solution

$$B_k = (1 - T_k k\mu/\omega_k^2)\cosh\{k\mu\}A_k$$
$$= (i\, k\mu/\omega_k)C_{1k} = (i\, k\mu/\omega_k)D_{2k}$$
$$= i\, k\mu/\omega_k\,(\omega_k^2/k\mu - T_k)/(1 - T_k\omega_k^2/k\mu)\,C_{2k} \qquad 2.2.4$$

and the linear dispersion relation

$$(\rho + T_k)(\omega_k^2/k\mu)^2 - \rho(1 + T_k)\omega_k^2/k\mu + (\rho - 1)T_k = 0$$

where $T_k = \tanh\{k\mu\}$ are obtained.

The two roots of the dispersion relation are

$$\omega_{Ak}^2/k\mu = 1$$

and

$$\omega_{Bk}^2/k\mu = (\rho - 1)(T_k/(\rho + T_k)).$$

The larger root ω_{Ak} which is the frequency of the free surface wave mode is the same as for gravity waves in deep water, indicating that these modes propagate independently of the properties of the interface. Using equations 2.2.4 the interface amplitude B_k for this mode is

$$B_k = A_k e^{-k\mu}$$

showing the exponential attenuation with depth as in the linear theory for gravity waves on deep water.

The smaller root ω_{Bk} is the frequency of a free interface wave mode. Using equations 2.2.4 the surface amplitude A_k for this mode is

$$A_k = -(\rho - 1)B_k e^{-k\mu}$$

again showing the exponential attentuation with depth. When $k\mu \gg 1$, corresponding to waves of length small compared with the interface depth

$$\omega_{Bk}^2 \simeq \left(\frac{\rho - 1}{\rho + 1}\right) k\mu$$

which is the same as ω_{Ak} except that gravity is replaced by the reduced

gravity $(\rho - 1)g/(\rho + 1)$. If $k\mu << 1$, corresponding to waves of length large compared with the interface depth

$$\omega_{Bk} \simeq \left(\frac{\rho - 1}{\rho}\right)^{1/2} k\mu$$

which is the same as for shallow water gravity waves except that gravity is replaced by the reduced gravity $(\rho - 1)g/\rho$. This approximate linear dependence of ω_{Bk} on $k\mu$ is of importance in deciding the final form of the evolution equations.

Using the linear solutions the quadratic terms in equations 2.2.2 can be evaluated and C_{1k}, C_{2k}, D_{2k} eliminated to give two second order ordinary differential equations involving A_k, B_k. One of these equations can be integrated twice and the other once to give the equations which form the basis of this thesis. The details of this method of elimination and subsequent integrations are given by Bryant [11] and only the important points will be presented here.

The way in which C_{1k}, C_{2k}, D_{2k} are eliminated depends on whether they occur in the linear or nonlinear terms. If the former, the elimination is by simultaneous solution. If the latter, C_{1k}, C_{2k}, D_{2k} are eliminated by substituting for them in terms of B_k from equations 2.2.4. With ε non-zero the value of C_{1k}, C_{2k}, D_{2k} differ from those in equations 2.2.4 by $O(\varepsilon)$. This difference, when included in the nonlinear terms, becomes of $O(\varepsilon^2)$ and can be neglected.

The resulting differential equations, after the integrations are

$$\begin{aligned}
&\frac{dA_k}{dt} + (\rho - 1)(1 - T_k k\mu/\omega_k{}^2)\cosh\{k\mu\}\,\frac{dB_k}{dt} \\
&\quad = \frac{1}{2} i\varepsilon \sum_{\ell=1}^{k-1} \frac{P_{k,-\ell} B_\ell B_{k-\ell}}{(\omega_\ell + \omega_{k-\ell} + \omega_k)} \exp -i(\omega_\ell + \omega_{k-\ell} - \omega_k)t \\
&\quad + i\varepsilon \sum_{\ell=1}^{\infty} \frac{P_{k,\ell} B_\ell{}^* B_{k-\ell}}{(\omega_{k+\ell} - \omega_\ell + \omega_k)} \exp -i(\omega_{k+\ell} - \omega_\ell - \omega_k)t \\
&\quad + O(\varepsilon^2) \qquad k = 1,2,\ldots
\end{aligned} \tag{2.2.5}$$

and $B_k - (1 - T_k k\mu/\omega_k^2)\cosh\{k\mu\}A_k$

$$= -\frac{1}{2}\varepsilon \sum_{\ell=1}^{k-1} \frac{Q_{k,-\ell}B_\ell B_{k-\ell}\exp -i(\omega_\ell + \omega_{k-\ell} - \omega_k)t}{(\omega_\ell + \omega_{k-\ell})^2 - (\omega_{Ak}\omega_{Bk}/\omega_k)^2}$$

$$- \varepsilon \sum_{\ell=1}^{\infty} \frac{Q_{k,\ell}B_\ell^* B_{k+\ell}\exp -i(\omega_{k+\ell} - \omega_\ell - \omega_k)t}{(\omega_{k+\ell} - \omega_\ell)^2 - (\omega_{Ak}\omega_{Bk}/\omega_k)^2}$$

$$+ O(\varepsilon^2) \qquad k = 1,2,... \qquad 2.2.6$$

where $P_{k,\ell}$, $Q_{k,\ell}$ with $\omega_k = -\omega_{-k}$ $k < 0$ are given in appendix 1.

The first term in equations 2.2.5, 2.2.6 represents the sum interactions in which two harmonics with wavenumbers ℓ, $k - \ell$ respectively interact with a third harmonic whose wavenumber k is greater than ℓ and $k - \ell$. The second term in each equation gives the difference interactions consisting of two harmonics with wavenumbers $k + \ell$, ℓ interacting with a third harmonic whose wavenumber k is less than the maximum of $k + \ell$, ℓ.

A comparison between the left hand sides of equations 2.2.6 and the first equality in equations 2.2.4 shows that the right hand sides of equations 2.2.6 give the quadratic corrections to the linear solution. Equation 2.2.5 cannot be integrated further because the factors $(\omega_\ell + \omega_{k-\ell} - \omega_k)$ and $(\omega_{k+\ell} - \omega_\ell - \omega_k)$ that would be introduced into the denominator can be zero or of $O(\varepsilon)$. However the integrations used to obtain equations 2.2.6 are valid because as will be shown the factors $(\omega_\ell + \omega_{k-\ell} - \omega_{Ak}\omega_{Bk}/\omega_k)$, $(\omega_{k+\ell} - \omega_\ell - \omega_{Ak}\omega_{Bk}/\omega_k)$ are of $O(1)$. Finally while it is possible at this stage to uncouple the linear terms in equations 2.2.5, 2.2.6 this is not done until the final form of the non-linear terms has been obtained.

In deciding this form there are six types of quadratic interactions to consider. The three that have been included are

(i) Two interface wave modes interacting with a third interface wave. The resonance condition requires

$$\left(\frac{(k+\ell)\mu T_{k+\ell}}{\rho + T_{k+\ell}}\right)^{\frac{1}{2}} - \left(\frac{\ell\mu T_{\ell}}{\rho + T_{\ell}}\right)^{\frac{1}{2}} - \left(\frac{k\mu T_{k}}{\rho + T_{k}}\right)^{\frac{1}{2}} = 0 .$$

In general this cannot be satisfied. However for long interface waves the left hand side of the above condition is of $0(\mu^2)$ enabling the near resonance condition to be satisfied when $\varepsilon = 0(\mu^2)$. Because $(\omega_{Bk+\ell} - \omega_{B\ell} - \omega_{Ak})$ is of 0(1) equation 2.2.6 is valid and this type of interaction has therefore been included in order to consider long interface waves. Both sum and difference interactions are possible.

(ii) Two surface wave modes interacting with an interface wave mode. The resonance condition is then

$$\{(k+\ell)\mu\}^{\frac{1}{2}} - (\ell\mu)^{\frac{1}{2}} - \left\{\frac{(\rho-1)T_k k\mu}{\rho + T_k}\right\}^{\frac{1}{2}} = 0 .$$

This can be satisfied by taking

$$\mu = \frac{1}{2k}\, ln\{(\rho-1)(1+\beta)/[(\rho-1) - (\rho+1)\beta]\}$$

where $\beta = 2\alpha + 1 - 2(\alpha^2+\alpha)^{\frac{1}{2}}$, $\alpha = \ell/k$. The factor $(\omega_{Ak+\ell} - \omega_{A\ell} - \omega_{Ak})$ is of 0(1) making equation 2.2.6 valid and this interaction is included. Because $\omega_{Ak} >> \omega_{Bk}$ only the difference interactions are significant.

(iii) An interface wave mode and a surface wave mode interacting with a surface wave mode. This is similar to (ii), except both sum and difference interactions are possible, and is included.

The three types of interaction that have been excluded are -

(iv) Two surface waves interacting with a third surface wave mode. The resonance condition would require $\omega_{Ak+\ell} - \omega_{A\ell} - \omega_{Ak}$ to be zero. As stated above this expression is of 0(1) and hence this type of interaction is excluded.

(v) An interface wave mode and a surface wave mode interacting with an interface wave mode. The smallness of the interface wavenumber compared with the surface wavenumber means it is not possible to satisfy the resonance or near resonance condition and this interaction is excluded.

(vi) Two interface wave modes interacting with a surface wave mode. This is excluded for the same reasons as (v) above.

With the first three types of interaction (i) - (iii) included equations 2.2.5, 2.2.6 give the evolution equations

$$\frac{dB_k}{dt} = \frac{1}{2} i\varepsilon \sum_{\ell=1}^{k-1} R_{1k,-\ell}{}^{B}{}_{\ell}{}^{B}{}_{k-\ell} + i\varepsilon \sum_{\ell=1}^{\infty} R_{1k,\ell}{}^{B}{}_{\ell}{}^{*B}{}_{k+\ell}$$

$$+ i\varepsilon \sum_{\ell=1}^{\infty} R_{2k,\ell}{}^{A}{}_{\ell}{}^{*A}{}_{k+\ell} + O(\varepsilon^2) \qquad k = 1,2,...$$

$$\frac{dA_k}{dt} = i\varepsilon \sum_{\ell=1}^{k-1} R_{3k,-\ell}{}^{B}{}_{\ell}{}^{A}{}_{k-\ell} + i\varepsilon \sum_{\ell=1}^{\infty} R_{3k,\ell}{}^{B}{}_{\ell}{}^{*A}{}_{k+\ell}$$

$$+ O(\varepsilon^2) \qquad k = 1,2,... \quad .$$

CHAPTER 3

Steady Solutions

3.1 Introduction

In this chapter steady solutions to the evolution equations are given. These solutions are used to illustrate general properties of the nonlinear interactions studied in this thesis and to form a basis with which to compare the unsteady solutions of the next chapter.

The form of the steady solution sought depends upon Benney's [3] interpretation of the resonance condition 1.1.1. He showed that if two small scale waves and one large scale wave formed a resonant triad then it could be restated as requiring the phase speed of the large scale wave to equal the group speed of the small scale waves. When the nonlinear terms are included this interpretation is no longer strictly true. However the discrepancy is $O(\varepsilon)$ where we have $\varepsilon << 1$. We have therefore found steady solutions consisting of a free surface wave group with a permanent envelope and a permanent interface wave with the surface group speed equal to the interface phase speed. The parameter μ was selected so that

$$\frac{d\omega_{Am}}{dk\mu} = \frac{\omega_{B1}}{\mu} \qquad 3.1.1$$

was satisfied for some integer $m >> 1$, in order to investigate the resonant interaction involving the lowest interface harmonic and two surface harmonics.

The unknowns in the above form of solution are the harmonic amplitudes, the group speed and the frequency of the surface wave relative to the group. In section 2 the system of algebraic equations for these unknowns is given. In general, because the system is nonlinear, it must be solved numerically by methods such as those given in

section 3. However, for the simple case when the surface amplitudes are small, analytical results are possible and these are also given in section 2. They are used in two ways: To provide starting points for the numerical schemes and to illustrate properties of the general solution. In particular it is shown that multiple solutions are possible.

In section 3 two numerical schemes are discussed. The first scheme based on Newton-like methods was the one initially used to find the general solutions of the nonlinear equations in section 2. It showed the existence of multiple solutions but was unsatisfactory because it could not always find the required solution. A discussion of it is included since our experience with it led to the development of the second and successful method discussed in this section. This method was based on the continuation approach (see for example Rabinowitz [36]) and was found to be very robust.

In the last section numerical examples are given. The parameters ρ, ε and μ were selected to have the same value as in the next chapter to enable comparisons to be made between the steady and unsteady solutions. The solutions given in this section have been divided into two sets distinguished by different values of ρ. Within each set solutions are given for contrasting values of μ to demonstrate different properties of the nonlinear interactions.

3.2 Theoretical

Steady solutions of the form

$$\eta(x,t) = \sum_{k=1}^{n_1} b_k \cos\{k\mu(x - ct)\} \qquad 3.2.1$$

$$\xi(x,t) = \sum_{k=k_1}^{k_2} a_k \cos\{k\mu(x - ct) - \alpha t\} \qquad 3.2.2$$

are sought where $b_k (1 \leqslant k \leqslant n_1)$, $a_k (k_1 \leqslant k \leqslant k_2)$ are real and constant and n_1, k_1, k_2 are found numerically by trial and error so that the introduction of further harmonics alters the solution by less than a prescribed amount.

Equations 3.2.1 and 3.2.2 describe an interface wave and a surface wave group propagating in the positive x direction with the phase speed c of the interface wave equal to the surface group speed. The unknown α is the frequency of the surface wave relative to the group.

When the amplitudes A_k, B_k from 2.2.3 are expressed in terms of a_k and b_k the evolution equations become

$$(\omega_{Bk} - k\mu c) b_k = \frac{1}{2}\varepsilon \sum_{\ell=1}^{k-1} R_{1k,-\ell}\, b_\ell b_{k-\ell} + \varepsilon \sum_{\ell=1}^{n_1-k} R_{1k,\ell}\, b_\ell b_{k+\ell} + \varepsilon \sum_{\ell=k_1}^{k_2-k} R_{2k,\ell}\, a_\ell a_{k+\ell} + O(\varepsilon^2)$$

$$1 \leqslant k \leqslant n_1 \qquad 3.2.3$$

$$(\omega_{Ak} - k\mu c - \alpha) a_k = \varepsilon \sum_{\ell=1}^{\min(n_1, k-k_1)} R_{3k,-\ell}\, b_\ell a_{k-\ell} + \varepsilon \sum_{\ell=1}^{\min(n_1, k_2-k)} R_{3k,\ell}\, b_\ell a_{k+\ell} + O(\varepsilon^2)$$

$$k_1 \leqslant k \leqslant k_2 \ . \qquad 3.2.4$$

Two further equations are required. These define a and b the parameters which measure the size of the surface and interface displacements respectively. For the interface, 2b is defined to be the height of the interface wave from trough to crest. With the origin of $(x - ct)\mu$ in the trough we have

$$\sum_{k \text{ odd}} b_k = -1 \ . \qquad 3.2.5$$

For the surface group the maximum height of the envelope above the free surface is defined to be a. Since the height of the surface

wave is independent of the interface wave height we have

$$\sum_{k\ \mathrm{odd}} a_k = \lambda \qquad 3.2.6$$

where λ is a constant.

Equations 3.2.3 - 3.2.6, denoted by $\underset{\sim}{f}(\underset{\sim}{x})$, form a system of non-linear algebraic equations for the unknowns $b_k (1 \leqslant k \leqslant n_1)$, $a_k (k_1 \leqslant k \leqslant k_2)$, c and α. As stated before in section 1, that although in general this system of algebraic equations must be solved by numerical methods, analytical results are possible when the surface amplitudes are small. The interface spectrum is then dominated by the near resonant interactions between interface harmonics and equations 3.2.3, 3.2.5 become

$$(\omega_{Bk} - k\mu c) b_k = \frac{1}{2}\varepsilon \sum_{\ell=1}^{k-1} R_{1k,-\ell,\ell} b_\ell b_{k-\ell} + \varepsilon \sum_{\ell=1}^{n_1-k} R_{1k,\ell,\ell} b_\ell b_{k+\ell} + O(\varepsilon^2)$$

$$1 \leqslant k \leqslant n_1$$

$$\sum_{k\ \mathrm{odd}} b_k = -1 . \qquad 3.2.7$$

Equations of this form have been solved by Bryant, both analytically [10] and numerically [10,11]. In [10] Bryant ordered the nonlinear terms in equations 3.2.7 by assuming that the interface harmonics approximated the geometric series

$$b_k \alpha r^{k-1} . \qquad 3.2.8$$

with $r^{n_1-1} \sim \varepsilon$. The equations were then solved by successive approximations with each solution being made consistent with the ordering 3.2.8 by relating μ to ε.

Using this approach the first approximation is with $r \sim \varepsilon$. The non-trivial equations from 3.2.7 are

$$(\omega_{B1} - \mu c)b_1 = O(\varepsilon^2)$$

$$(\omega_{B2} - 2\mu c)b_2 = \frac{1}{2}\varepsilon R_{12,-1}b_1^2 + O(\varepsilon^2)$$

$$b_1 = -1 + O(\varepsilon^2)$$

with the solution

$$b_1 = -1 + O(\varepsilon^2)$$

$$b_2 = -\frac{1}{2}\varepsilon R_{12,-1}/(2\omega_{B1} - \omega_{B2}) + O(\varepsilon^2)$$

$$c = \omega_{B1}\mu^{-1} + O(\varepsilon^2)\ . \qquad 3.2.9$$

A Taylor's series expansion shows that $2\omega_{B1} - \omega_{B2}$ is $O(\mu^2)$ and μ is therefore taken to be $O(1)$ to make 3.2.9 consistent with 3.2.8.

The above solution shows that there is very little interaction between interface harmonics for this value of μ. The phase speed c is equal to its linear value $\omega_{B1}\mu^{-1}$ and the interface displacement is almost sinusoidal.

With $r \sim \varepsilon$ equations 3.2.4 for the surface harmonics become

$$(\omega_{Ak} - k\mu c - \alpha)a_k = -\varepsilon R_{3k,-1}a_{k-1} - \varepsilon R_{3k,1}a_{k+1} + O(\varepsilon^2) \qquad k_1 \leqslant k \leqslant k_2\ . \qquad 3.2.10$$

These can be expressed as the eigenvalue problem

$$A\underset{\sim}{y} = \alpha\underset{\sim}{y} + O(\varepsilon^2) \qquad 3.2.11$$

where $a_{i,i} = \omega_{Ak_1+i-1} - (k_1 + i - 1)\omega_{B1} \qquad i = 1,\ldots,n_2$

$$a_{i,i+1} = \varepsilon R_{3k_1+i-1,1}\ , \quad a_{i+1,i} = \varepsilon R_{3k_1+i-1,-1} \qquad i = 1,\ldots,n_2 - 1$$

$$y_i = a_{k_1+i-1} \qquad i = 1,\ldots,n_2,\ \ n_2 = k_2 - k_1 + 1$$

In general 3.2.11 will have a complete set of eigenvectors giving n_2 different forms of the surface spectrum and n_2 solutions to the system $\underset{\sim}{f}(\underset{\sim}{x})$ for this value of μ. It will be seen in section 4 that this property of multiple solutions occurs for general values of μ.

The eigenvalues of A are

$$\omega_{Ak} - k\omega_{Bl} + O(\varepsilon) \qquad k_1 \leqslant k \leqslant k_2$$

which becomes using the definition of μ

$$\frac{1}{2}\omega_{Am} + O(d^2\omega_{Ak}/dk^2, \varepsilon) \qquad 3.2.12$$

where $d^2\omega_{Ak}/dk^2 < 0$. The maximum value of α is therefore approximately $\frac{1}{2}\omega_{Am}$ with the remaining values close to this.

Equations 3.2.10 can also be expressed in the form

$$a_{k+1} - 2a_k + a_{k-1} + f(k)a_k = O(\varepsilon) \qquad k_1 \leqslant k \leqslant k_2 \qquad 3.2.13$$

where $f(k) = (\omega_{Ak} - k\omega_{Bl} - \alpha + 2\varepsilon R_{3k,1}) / (\varepsilon R_{3k,1})$ and $R_{3k,1} \simeq R_{3k,-1}$.

If 3.2.13 is compared with the differential equation

$$d^2y/dx^2 + f(x)y = 0$$

the surface spectrum is seen to be oscillatory in k for $f(k) > 0$ and monotonic in k for $f(k) < 0$. The maximum value of f(k) is

$$\alpha^2/(\varepsilon R_{3k,1})\{\alpha^{-1} - 2\omega_{Am}^{-1}\} + 2 \qquad 3.2.14$$

at $k = 4\alpha^2\mu^{-1} \simeq m$ (using equation 3.2.12). In deriving 3.2.14 we have used the result from appendix 1 that $R_{3k,1} \simeq \gamma k$ where γ is independent of k.

Because $\alpha^{-1} \geqslant 2/\omega_{Am} + O(\varepsilon)$ the solution for $a_k (k_1 \leqslant k \leqslant k_2)$ is seen to be oscillatory for a range of k in a neighbourhood of m and monotonically decreasing to zero outside this range.

The second approximation to equations 3.2.7 is for $r^2 \sim \varepsilon$ with equations 3.2.7 becoming

$$(\omega_{B1} - \mu c)b_1 = \varepsilon R_{11,1} b_1 b_2 + O(\varepsilon^2)$$
$$(\omega_{B2} - 2\mu c)b_2 = \frac{1}{2}\varepsilon R_{12,-1} b_1^2 + O(\varepsilon^2)$$
$$(\omega_{B3} - 3\mu c)b_3 = \varepsilon R_{13,-1} b_1 b_2 + O(\varepsilon^2)$$
$$b_1 + b_3 = -1 + O(\varepsilon^2) .$$

The solution is

$$b_1 = -1 + \frac{1}{2}\varepsilon^2 R_{12,-1} R_{13,-1} / \{(2\omega_{B1} - \omega_{B2})(3\omega_{B1} - \omega_{B3})\} + O(\varepsilon^2)$$
$$b_2 = -\frac{1}{2}\varepsilon R_{12,-1} / (2\omega_{B1} - \omega_{B2}) + O(\varepsilon^{3/2})$$
$$b_3 = -\frac{1}{2}\varepsilon^2 R_{12,-1} R_{13,-1} / \{(2\omega_{B1} - \omega_{B2})(3\omega_{B1} - \omega_{B3})\} + O(\varepsilon^2)$$
$$c = \{\omega_{B1} + \frac{1}{2}\varepsilon^2 R_{11,1} R_{12,-1} / (2\omega_{B1} - \omega_{B2})\}\mu^{-1} + O(\varepsilon^2) \qquad 3.2.15$$

with $\mu^4 = O(\varepsilon)$ to make the solution consistent with 3.2.8.

There are two interesting differences between 3.2.15 and 3.2.9. The phase speed is no longer equal to its linear value $\omega_{B1}\mu^{-1}$, but depends on the nonlinear terms. For the values of ρ and μ used in this thesis $R_{11,1}$, $R_{12,-1} > 0$. The phase speed has therefore been increased above its linear value. Secondly the distinction between the nominal and true order in the perturbation scheme is illustrated. If only the explicit powers of ε were considered b_2 would be $O(\varepsilon)$, the nominal order. However because $\mu^4 = O(\varepsilon)$ b_2 is $O(\varepsilon^{\frac{1}{2}})$ showing the effect of the near resonance term $(2\omega_{B1} - \omega_{B2})^{-1}$.

For smaller values of μ Bryant used numerical methods to solve equations 3.2.7. These results showed that as μ was decreased holding ε constant the number of harmonics increased as the higher harmonics moved closer to resonance. For the surface an increase in n_1 means that more near resonant triads containing one surface harmonic and one interface harmonic interacting with a second surface harmonic are possible, broadening the surface spectrum.

If the surface amplitudes are no longer restricted to small values the original equations $\underset{\sim}{f}(\underset{\sim}{x})$ are regained. The methods used to solve

these equations numerically are now given.

3.3 Numerical Scheme

The first numerical scheme used which we have called the standard approach was based on Newton-like methods. These methods were selected because they could be implemented quickly and were efficient when convergence occurred.

In the standard approach an initial estimate of the required solution was found by setting

$$b_1 = -1, \quad c = \omega_{B1}\mu^{-1}, \quad \alpha = \beta, \quad a_{k_1+i-1} = y_i \qquad i = 1,\ldots,n_2$$

where β, $\underset{\sim}{y}$ are the appropriate eigenvalue and eigenvector respectively from 3.2.11. The wavenumbers k_1, k_2 were chosen so that the addition of an extra surface harmonic to the system changed the solution by less than a prescribed accuracy (10^{-3}). Using one of three nonlinear equation solvers $\underset{\sim}{f}(\underset{\sim}{x}) = \underset{\sim}{0}$ was then solved, the number of harmonics increased and $\underset{\sim}{f}(\underset{\sim}{x}) = \underset{\sim}{0}$ resolved. The previous solution with added variables set to zero was used as the initial estimate of the new solution. This process was continued until either the addition of more harmonics altered the solution by less than 10^{-3} or an error return was given. If the former occurred the previous solution was taken as the required one.

The three nonlinear equation solvers used were the Classical Newton's method (CNM), the Damped Newton's method (DNM) and Powell's Hybrid method (PHM). There are several versions of the first two methods. The versions we used are given in appendix 2.

The results obtained using the CNM showed that multiple solutions existed with the surface spectrum being of the form given following 3.2.14. However the CNM was not sufficiently robust for the required

range of ρ,μ,ε and λ. In general satisfactory convergence was obtained for the lowest solution (that with the least amount of oscillation) while divergence occurred for the higher solutions (those with progressively more oscillations) and in particular for the even solutions. The divergence which included convergence to the wrong solution was at first attributed to the initial estimates of the solutions being poor.

Several techniques were used to improve the estimates with the biggest gain being from the use of extrapolation to estimate the value of new variables rather than setting them to zero. This was very noticeable for the interface harmonics. With n_1 being started at 1 it meant that it was possible to have n_1 small compared with its correct value. The true value of the interface harmonics that had to be added could then be significantly greater than zero, giving poor initial estimates if they were set to zero.

Three types of extrapolation were used with the most satisfactory being based on equations 3.2.3, 3.2.4. For an increase in n_1 we have from equations 3.2.3 with $k = n_1 + 1$ that

$$b_{n_1+1} = (\omega_{Bn_1+1} - (n_1+1)\mu c)^{-1}\left\{\frac{1}{2}\varepsilon \sum_{\ell=1}^{n_1} R_{1n_1+1,-\ell}\, b_\ell\, b_{n_1+1-\ell} + \varepsilon \sum_{\ell=k_1}^{k_2-n_1-1} R_{2n_1+1,\ell^a \ell+n_1+1}\right\}. \qquad 3.3.1$$

Every variable on the right has a value from the previous solution and the value of b_{n_1+1} can be estimated. Similar expressions are possible from equations 3.2.4 for a decrease in k_1 or an increase in k_2. This form of extrapolation was used in subsequent calculations.

Despite the improvements in the initial estimates divergence still occurred. The conditioning of the Jacobian of $\underset{\sim}{f}(\underset{\sim}{x})$ was then considered. An ill-conditioned Jacobian can cause the CNM to diverge by making the Newton step too large or in the wrong direction. The

normalised determinant of the Jacobian (see appendix 2 for our definition of this) was found to vary from approximately 10^{-10} to 10^{-42} indicating that the Jacobian was ill-conditioned and that a more robust solver would be needed to find the solutions.

To test if the divergence of the CNM was caused by the Newton step being too large the DNM was tried. In this approach the aim is to retain the convergence properties of the CNM when the iterates are near the solution and to prevent divergence when the iterates are far from it. The Newton step is scaled so that for each new estimate of the solution there is a reduction in the function residues. Although the DNM converged satisfactorily for a greater range of ρ,ε,μ and λ than did the CNM it still was not sufficiently robust. Failure was due to divergence or because the Newton direction was not a descent direction.

The last nonlinear equation solver used in the standard approach was PHM. In this method which is fully discussed in [37] the search direction is a linear combination of the steepest descent and Newton direction. This method never failed to solve $\underset{\sim}{f}(\underset{\sim}{x}) = \underset{\sim}{0}$ but like the CNM and the DNM it did not always find the required solution.

The results from the standard approach showed that if a nonlinear equation solver was to find the required solution of $\underset{\sim}{f}(\underset{\sim}{x}) = \underset{\sim}{0}$ in the presence of other solutions it had to ensure that all the iterates from it were close to the required solution. Or more generally the iterates had to be close to a transformation of $\underset{\sim}{f}(\underset{\sim}{x}) = \underset{\sim}{0}$, the solution of which could be related to the required solution. Consideration of this last idea led to a successful scheme based on the method of continuation.

In the continuation approach the problem of solving $\underset{\sim}{f}(\underset{\sim}{x}) = \underset{\sim}{0}$ is replaced by that of solving a sequence of subproblems. The sequence is selected so that:

(i) each subproblem can be easily solved;

(ii) the solution of the first is known, and

(iii) the solution of the last is the required solution.

A simple way to create this sequence is to introduce a parameter θ and define the auxiliary function

$$\underset{\sim}{g}(\underset{\sim}{x},\theta) = \underset{\sim}{f}(\underset{\sim}{x}) - \theta\underset{\sim}{f}(\underset{\sim}{x}_0) \qquad 3.3.2$$

where $\underset{\sim}{x}_0$ solves $\underset{\sim}{g}(\underset{\sim}{x},\theta) = \underset{\sim}{0}$ for $\theta = 1$. If θ is reduced from 1 to 0 in small steps to give the sequence $\{\theta_i\}_{i=1}^{N}$, as yet unspecified, the sequence of subproblems given by

$$\underset{\sim}{g}(\underset{\sim}{x},\theta_i) = \underset{\sim}{f}(\underset{\sim}{x}) - \theta_i\underset{\sim}{f}(\underset{\sim}{x}_0) \qquad i = 1,\ldots,N \qquad 3.3.3$$

satisfies (ii) and (iii) above. Property (i) is satisfied by choosing the decrements $d\theta_i (\equiv \theta_{i+1} - \theta_i)$ to be small and by using the solution from the ith subproblem as an initial estimate of the solution of the next.

In the above continuation method the choice of $\{\theta_i\}_{i=1}^{N}$ depends on establishing a balance between robustness and efficiency. If $d\theta_i$ is very small each subproblem can be solved efficiently but there will be many to solve, reducing the overall efficiency. If $d\theta_i$ is large few subproblems have to be solved but the solution of each may be difficult to obtain, again reducing the overall efficiency. With large values of $d\theta_i$ it is also possible to have the iterates far enough away from the solution of 3.3.3 that divergence occurs. Davidenko's [14] form of the method of continuation which is now discussed provides a way of selecting a near optimal value of $d\theta_i$.

If the function $\underset{\sim}{g}(\underset{\sim}{x},\theta) = \underset{\sim}{0}$ has a solution for all $0 \leqslant \theta \leqslant 1$ then $\underset{\sim}{x}$ can be regarded as a function of θ. The locus of points $\underset{\sim}{x}(\theta)$ is called the Davidenko path. Differentiating 3.3.2 with respect to θ gives

$$\frac{d\underset{\sim}{x}}{d\theta} = \frac{1}{\theta} J^{-1} \underset{\sim}{f}(\underset{\sim}{x}) \qquad 3.3.4$$

provided J (the Jacobian of $\underset{\sim}{f}(\underset{\sim}{x})$) is non-singular. Along with the condition $\underset{\sim}{x}(1) = \underset{\sim}{x}_0$ equation 3.3.4 forms an initial value problem (IVP1). If this is solved by an efficient integrator which keeps the error in $\underset{\sim}{x}$ below a prescribed tolerance the problems associated with the selection of $d\theta_i$ are overcome. By using a severe error tolerance our basic requirement that each iterate be close to a solution of the transformed $\underset{\sim}{f}(\underset{\sim}{x})$ is satisfied. It may seem that the problem of selecting $d\theta_i$ still exists because we have to provide an integrator with the appropriate properties. However this presents no difficulties because there are many such integrators. Examples are STRIDE [13], EPISODE [21], GEAR [20], STEP [39] and DC02AD [18].

The scheme we used was based on the method of incremental loading (see for example Oden [31]) which is a variation of Davidenko's method. In the incremental loading approach the parameter θ is taken to be one already in the system. Equation 3.3.4 becomes

$$\frac{d\underset{\sim}{x}}{d\theta} = - J^{-1} \underset{\sim}{f}_{\theta}(\underset{\sim}{x}(\theta)) \qquad 3.3.5$$

where $\underset{\sim}{f}_{\theta} \equiv \frac{\partial \underset{\sim}{f}}{\partial \theta}$, with θ being stepped from θ^i to θ^f. Along with the condition $\underset{\sim}{x}(\theta^i) = \underset{\sim}{x}_0$ equation 3.3.5 forms an initial value problem (IVP2).

One important difference between IVP1 and IVP2 is that in IVP2 $\underset{\sim}{x}_0$ is no longer arbitrary. It must be a solution of $\underset{\sim}{g}(\underset{\sim}{x},\theta)$ for $\theta = \theta^i$. Some generality compared with IVP1 has therefore been lost. The gain is that subproblems are created which are physically as well as mathematically related. Advantage can be taken of continuities in θ of the original problem leading to greater efficiency and robustness if $\underset{\sim}{x}_0$ can be found easily.

Before solutions can be found to $\underset{\sim}{f}(\underset{\sim}{x}) = \underset{\sim}{0}$ using the above approach three parts of the scheme have to be specified. The form of the integeration scheme, the choice of θ and θ^i and what to use as the initial solution $\underset{\sim}{x}_0$.

In solving IVP1 and IVP2 two basic approaches are possible. The first is to solve the initial value problem without using $\underset{\sim}{f}(\underset{\sim}{x}) = \underset{\sim}{0}$ while the second is to make use of. Authors such as Boggs [4] and Broughton [8] have used the first while the second has been used by Deist and Sefor [15]. We have used the second approach. We think that because it uses more information than the first it can be made more efficient and more robust. In particular the integrated solution can be refined using $\underset{\sim}{f}(\underset{\sim}{x}) = \underset{\sim}{0}$ reducing the error compared with the first approach.

In our integration scheme we used a prediction-correction approach. For the prediction a variable-order, variable-step Adams-Bashforth formula was used. This was a modification of the integrator STEP already mentioned and discussed in the next chapter. The step size was varied to enable control of the error in $\underset{\sim}{x}$ and to improve the efficiency while the order was varied primarily to improve the efficiency. For the correction which was done on $\underset{\sim}{f}(\underset{\sim}{x}) = \underset{\sim}{0}$ PHM was used. This was selected in place of say the CNM because our experience from the standard approach showed that a method as robust as PHM was required.

The parameters ρ, μ, ε and λ were available to be used as θ. The first two were not selected because they occurred in a complicated way in $\underset{\sim}{f}(\underset{\sim}{x})$. Of ε and λ, the former was chosen because it is a more fundamental parameter than λ. For the initial solution $\underset{\sim}{x}_0$ we used the same one as in the standard approach, that is

$$b_1 = -1\ ,\ c = \omega_{B1}\mu^{-1},\ \alpha = \beta,\quad a_{k_1+i-1} = y_i \qquad i = 1,\ldots,n_2$$

where β, $\underset{\sim}{y}$ are the appropriate eigenvalue and eigenvector respectively from 3.2.11.

We chose ε^i ($< \varepsilon^f$ and based on numerical experience) so that if b_2 was added it would cause a change in the solution of less than our prescribed accuracy tolerance (10^{-3}). In general it was found, and as the results of the previous section show, that increasing ε broadens both spectra, requiring variables to be added. The above choice of ε^i meant that provided it was done at the correct value of ε, the true value of any new variable was the smallest possible, that is, when it caused a change of 10^{-3} in the solution. This contrasts with the standard approach in which it was possible for a new variable to make a difference to the solution significantly greater than 10^{-3}. In the present method the possibility of slow convergence or divergence due to poor initial estimates is considerably less.

A brief outline of our algorithm is:

1. Find $\underset{\sim}{x}_0$.
2. If $\varepsilon = \varepsilon^f$ terminate otherwise take a step of the initial value problem

$$\underset{\sim}{x}(\varepsilon^i) = \underset{\sim}{x}_0 \quad , \quad \frac{d\underset{\sim}{x}}{d\varepsilon} = - J^{-1} \underset{\sim}{f}_\varepsilon$$

   using a variable-order, variable-step Adams-Bashforth predictor and correcting in $\underset{\sim}{f}(\underset{\sim}{x}) = \underset{\sim}{0}$ using PHM.
3. Test if n_1, k_1, k_2 need to be changed. If not proceed to step 2. Otherwise alter them by one as necessary, use extrapolation to estimate the value of variables added, solve $\underset{\sim}{f}(\underset{\sim}{x}) = \underset{\sim}{0}$ using PHM and proceed to step 2.

3.4 Numerical Examples

The solutions given here have been divided into two sets, distinguished by different values of ρ, with the emphasis on the lowest solution. Because we are investigating small amplitude waves we have kept the slope of all harmonics less than 0·1.

The first set of solutions has $\rho = 1{\cdot}05$. The first example considered within this set is for a small value of μ. We have taken $\rho = 1{\cdot}05$, $\varepsilon = 0{\cdot}015$, $\mu = {\cdot}3192$ and the maximum slope $S_{max} = 0{\cdot}04$. The surface and interface spectra for the lowest 3 solutions are given in figure 3.1(a) while the free surface wave groups are plotted in figure 3.1(b). The interface displacement is considered later in this set of solutions.

Equation 3.1.1 predicts with $\mu = {\cdot}3192$ that the central wavenumber of the surface group will be 22. From figure 3.1(a) it is significantly less for the lowest solution. An estimate (see for example Bryant [11]) of the central wavenumber can be obtained if the resonance condition (using Benney's interpretation) is modified to the form

$$c = d\omega_{Ak}/dk\mu + \varepsilon V \qquad 3.4.1$$

where εV is the horizontal velocity at the free surface due to the lowest interface harmonic b_1. This velocity, calculated using equations 2.2.3, 2.2.4, is sinusoidal with a positive maximum at the centre of the wave group and a negative minimum at the ends. For the lowest solution $c = {\cdot}197$ and $-{\cdot}002 \leqslant \varepsilon V \leqslant {\cdot}002$. Equation 3.4.1 therefore gives the central wavenumber to be 20·5 in agreement with measurements from figure 3.1(a).

The interface spectra show two general properties of solutions for small values of μ. The first is that the spectra for the higher

solutions are not monotonically decreasing sequences as the ordering scheme 3.2.8 might suggest, but display small oscillations. Their influence on the interface displacement is discussed later. Secondly the effect of the near resonant interactions involving b_2 is shown. This harmonic is a significant fraction (in this case 18% for the lowest solution) of b_1. The effect is not as large in the higher solutions because of the oscillations in the spectra.

If S_{max} is now increased the surface amplitudes become larger and the second type of interaction has a greater effect on the shape of the interface spectrum. The surface and interface spectra for the lowest solution with $S_{max} = \cdot 04, \cdot 05, \cdot 06$ are given in figure 3.1(c), the free surface wave groups in figure 3.1(d) and the interface displacements in figure 3.1(e).

Figure 3.1(c) shows that as S_{max} has increased there have been significant decreases in the central wavenumber of the surface group as well as the increases in the surface amplitudes. The phase speeds for $S_{max} = \cdot 05, \cdot 06$ are $\cdot 205$ and $\cdot 215$ respectively. Equation 3.4.1 with $-\cdot 002 \leqslant \varepsilon V \leqslant \cdot 002$ then gives estimated central wavenumbers of 19 and 17 in agreement with figure 3.1(c).

For the interface both the spectrum has become broader and the ratio b_2/b_1 larger as S_{max} has increased. The increase in the number of harmonics has meant that the interface displacement has deviated more from a sinusoidal shape. As shown in figure 3.1(e) the crest has become lower and wider while the trough has become deeper and narrower.

To illustrate the effects of the oscillations in the interface spectra for the higher solutions the spectra and displacements for the 3 lowest solutions with $S_{max} = 0 \cdot 06$ are given in figures 3.1(f), 3.1(g). The oscillations in the spectra are more pronounced than in figure 3.1(b) with the shape of the surface envelope being imposed on the

interface displacement.

If μ is increased the nonlinear interactions between the interface harmonics move away from resonance and the interface spectrum is dominated by the second type of interaction. The example we have selected to illustrate this is with $\rho = 1{\cdot}05$, $\varepsilon = 0{\cdot}005$, $\mu = 1{\cdot}354$ and $S_{max} = {\cdot}04$. The surface spectra and surface wave groups for the 2 lowest solutions are given in figure 3.2(a). The interface displacement is not given because it is almost sinusoidal with $|b_2| < {\cdot}009$.

The predicted value from equation 3.1.1 of the central wavenumber for the surface wave group is eleven which agrees with the results in figure 3.2(a). Equation 3.4.1 is also consistent with this. The small value of ε and the large value of μ have made the horizontal velocity at the free surface due to b_1 very small ($\leqslant 10^{-4}$). This along with c equalling $\omega_{B1}\mu^{-1}$ to an accuracy of 10^{-3} has meant that equation 3.4.1 is the resonance condition 3.1.1 to the same accuracy.

The results obtained for the lowest solution when S_{max} is increased are given in figure 3.2(b). The interface displacement retains its almost sinusoidal shape with $|b_2| \leqslant {\cdot}013$. The surface amplitudes have been increased but unlike the first example there has been little change in the central wavenumber. The main effect of increasing S_{max} has been to vertically scale the spectrum.

The second set of solutions has $\rho = 1{\cdot}02$. The decrease in ρ means that in equation 3.1.1 m will be greater while the near resonance condition can be satisfied by a larger number of triads. It can therefore be anticipated and is found to be true that the solutions for $\rho = 1{\cdot}02$ will have broader spectra with the central wavenumbers of the surface wave groups being larger.

The first example is with $\rho = 1{\cdot}02$, $\varepsilon = {\cdot}01$, $\mu = {\cdot}3096$ and $S_{max} = {\cdot}04$. The results corresponding to those in figures 3.1(a) - (g)

are given in 3.3(a) - (g). As in figures 3.1(a) and 3.1(c) the central wavenumber of the surface group is less than that given by equation 3.1.1 (m = 55) with the wavenumber becoming smaller as S_{max} increases. Equation 3.4.1 again provides good estimates of those wavenumbers. An example is for $S_{max} = \cdot 06$ in figure 3.3(c). The phase speed c is $\cdot 147$ and $-\cdot 001 \leqslant \varepsilon V \leqslant \cdot 001$ which gives an estimate of 38 compared with 39 from figure 3.3(c).

Figure 3.3(f) shows that for the higher solutions oscillations have occurred in the interface spectra as in figure 3.1(f). However these oscillations are smaller with the result, shown in figure 3.3(g), that the shape of the envelope has been impressed less on the interface displacement than in figure 3.1(g).

For the lowest solution as S_{max} has been increased the interface wave (figure 3.3(e)) has deviated more from a sinusoidal shape with the crests becoming broader and the troughs deeper as in figure 3.1(e). However the effects are greater for $\rho = 1 \cdot 02$ because the interface spectrum contains more harmonics.

The example in this set for a large value of μ is with $\rho = 1 \cdot 02$, $\varepsilon = 0 \cdot 004$, $\mu = 1 \cdot 373$ and $S_{max} = 0 \cdot 04$. The results are given in figures 3.4(a) - (b). The interface displacement as for the second example of the first set is almost sinusoidal with $|b_2| \leqslant \cdot 015$. The predicted value of the central wavenumber is 27 which agrees with the result in figure 3.4(a). However unlike figure 3.2(b) as S_{max} is increased there is a noticeable decrease in this wavenumber as seen in figure 3.4(b). But as before because of the small horizontal velocity at the free surface due to b_1 and the closeness of c to $\omega_{B1}\mu^{-1}$ equation 3.4.1 is essentially equation 3.1.1.

CHAPTER 4

Unsteady Solutions

4.1 Introduction

In this chapter unsteady solutions to the evolution equations are given. These solutions, like the steady solutions, are used to illustrate general properties of the nonlinear interactions.

Following the work in the previous chapter we have sought solutions consisting of an interface wave and a surface wave group with the harmonic amplitudes now being time dependent. In choosing a frame of reference to view the evolution Benney's interpretation of the resonance condition was used. As stated in section 3.1, for our two layer model the resonance condition 1.1.1 is equivalent to requiring the phase speed of the interface waves to equal the group speed of the surface waves, with the centre of the surface waveband at k. When the nonlinear terms are included this interpretation is no longer strictly true. However the discrepancy is of $O(\varepsilon)$ where we have $\varepsilon << 1$ and the centre of the waveband will be in a small neighbourhood of k. In this sense a frame of reference moving with speed $d\omega_{Ak}/(dk\mu)$ in the positive x direction represents the 'best' frame in which to study the evolution. With this choice we selected μ so that

$$\frac{d\omega_{Am}}{dk\mu} = \frac{\omega_{B1}}{\mu}$$

for some integer $m >> 1$, in order to investigate the resonant interaction between the lowest interface harmonic and two surface harmonics.

In section 2 the system of nonlinear differential equations for the harmonic amplitudes is given. Because of the nonlinearity the general solution to this system must be found numerically by a scheme such as that discussed in section 3. However when only the harmonics

B_1, A_m, A_{m+1} are present analytical results are possible and these are also given in section 2. The results are used in two ways: To form a basis with which to compare the general unsteady solutions and to test the accuracy of the numerical scheme used to find them.

The discussion in section 3 of this scheme first considers the features of the above problem which influenced our choice of an integrator based on the requirements that the solution be found efficiently and with control over the integration error. We then consider the way in which the scheme we selected attempts to satisfy these requirements and how well it controls the error. Finally a modification to the integrator which improved its efficiency is discussed.

In the last section numerical examples are given with the parameters ρ, ε and μ selected to have the same values as in the last chapter. The solutions are divided into two sets distinguished by different values of ρ. Within each set contrasting values of μ are used to demonstrate different properties of the evolution. It is also shown that the frame of reference moving with speed $d\omega_{Am}/(dk\mu)$ is numerically efficient.

4.2 Theoretical

Unsteady solutions of the form

$$\eta(x,t) = \sum_{k=1}^{n_1} b_k(t)\,\mathrm{expi}(k\mu x - \omega_{Bk}t) + *\ ,$$

$$\xi(x,t) = E(x,t)\,\mathrm{expi}(m\mu x - \omega_{Am}t) + *$$

were sought where $E(x,t) = \sum_{k=k_1}^{k_2} a_k(t)\,\mathrm{expi}\{(k-m)\mu(x-ct)\}\ (c = \omega_{B1}\mu^{-1})$ is the envelope function, the amplitudes $b_k (1 \leqslant k \leqslant n_1)$, $a_k (k_1 \leqslant k \leqslant k_2)$ are complex and the wavenumber limits n_1, k_1, k_2 are found by trial and error in a similar way to those of the previous chapter. If the

amplitudes are real and constant the expression for ξ describes a wave group of central wavenumber m and central frequency ω_{Am} propagating in the positive x direction with a group speed c. The expression for η is then that of a wave moving in phase with the surface group and with a phase speed c.

When A_k, B_k from equations 2.2.3 are expressed in terms of a_k and b_k the evolution equations become

$$\frac{db_k}{d\tau} + \frac{i(\omega_{Bk} - k\mu c)b_k}{\varepsilon} = \frac{1}{2}i \sum_{\ell=1}^{k-1} R_{1k,-\ell}\, b_\ell b_{k-\ell} + i \sum_{\ell=1}^{n_1-k} R_{1k,\ell}\, b_\ell^* b_{k+\ell} + i \sum_{\ell=k_1}^{k_2-k} R_{2k,\ell}\, a_\ell^* a_{k+\ell} + O(\varepsilon) \qquad 1 \leqslant k \leqslant n_1 \qquad 4.2.1$$

$$\frac{da_k}{d\tau} + \frac{i(\omega_{Ak} - (k-m)\mu c - \omega_{Am})a_k}{\varepsilon} = i \sum_{\ell=1}^{\min(n_1,k-k_1)} R_{3k,-\ell}\, b_\ell a_{k-\ell} + i \sum_{\ell=1}^{\min(n_1,k_2-k)} R_{3k,\ell}\, b_\ell^* a_{k+\ell} + O(\varepsilon) \qquad k_1 \leqslant k \leqslant k_2 \qquad 4.2.2$$

where $\tau = \varepsilon t$. The need for this second time scale is demonstrated by forming the expression for the rate of change of the amplitudes. For example we have

$$\frac{d|b_k|^2}{d\tau} = \frac{1}{2}i \sum_{\ell=1}^{k-1} R_{1k,-\ell}\, b_\ell b_{k-\ell} b_k^* + i \sum_{\ell=1}^{n_1-k} R_{1k,\ell}\, b_\ell^* b_{k+\ell} b_k^* + i \sum_{\ell=k_1}^{k_2-k} R_{2k,\ell}\, a_\ell^* a_{k+\ell} b_k^* + * + O(\varepsilon) \qquad 1 \leqslant k \leqslant n_1 . \qquad 4.2.3$$

This shows that the amplitude changes occur on the slow time scale τ while from equation 4.2.1 the changes in phase occur on the fast time scale t.

Equations 4.2.1, 4.2.2 along with suitable initial conditions form an initial value problem (IVP3). As stated in the previous section, that although in general solutions to this problem must be found numerically, analytical results are possible when only b_1, a_m, a_{m+1} are present. In this case equations 4.2.1, 4.2.2 become

$$X' = iKYZ \qquad 4.2.4$$

$$Y' = iMXZ^* \qquad 4.2.5$$

$$Z' = iPXY^* \qquad 4.2.6$$

where ' denotes $\frac{d}{d\tau}$, $X = a_{m+1}$, $Y = a_m$, $Z = b_1$, $K = R_{3m+1,-1}$, $M = R_{3m,1}$, $P = R_{21,m}$, $K > M$ for the values of ρ, μ used in this thesis and we have taken $d\omega_{Am}/dk \simeq \omega_{Am+1} - \omega_{Am}$ as in Benney's interpretation of the resonance condition and have omitted the $O(\varepsilon)$ terms.

Two independent complete integrals for equations 4.2.4 - 4.2.6 are

$$P|X|^2 + K|Z|^2 = C_1 \qquad 4.2.7$$

$$P|Y|^2 - M|Z|^2 = C_2 \qquad 4.2.8$$

where C_1, C_2 are constants evaluated using the initial conditions. These two integrals can be combined to give

$$|X|^2 + |Y|^2 + (K-M)/P|Z|^2 = (C_1 + C_2)/P\,. \qquad 4.2.9$$

In general $(K-M)/P << 1$ and equation 4.2.9, for $Z \sim X,Y$, gives on the linear theory (see for example Phillips [34]) an estimate of the energy of the two surface harmonics.

From equations 4.2.4 - 8 we have

$$|Z|^{2''} = (2C_1C_2 + 4|Z|^2(C_1M - KC_2) - 6KM|Z|^4)\,.$$

Multiplying by $|Z|^{2'}$ and integrating gives

$$|Z|^{2\,'2} = 4|Z|^2(C_1C_2 + |Z|^2(C_1M - KC_2) - KM|Z|^4) + C_3 \qquad 4.2.10$$

where C_3 is evaluated using the initial conditions. The solution of 4.2.10 can be expressed in terms of the Jacobi elliptic functions for general initial conditions (see for example Hashizume and Ikeda [19]). However this is unnecessary for the present work and we have used two sets of initial conditions to illustrate properties of the solutions of 4.2.10.

The first set, $X(0) = A$, $Y(0) = A$, $Z(0) = 0$ $(A > 0)$ has all the energy initially in the surface spectrum. Equation 4.2.10 becomes

$$|Z|^{2\,'2} = -4|Z|^2KM(|Z|^2 - A^2P/K)(|Z|^2 + A^2P/M)$$

where P/K, $P/M > 0$. For a physically realistic solution $|Z|^{2\,'2}$ and $|Z|^2$ must both be non-negative which together with $|Z|^{2\,''} > 0$ at $|Z|^2 = 0$ and $|Z|^{2\,''} < 0$ at $|Z|^2 = A^2P/K$ means that $|Z|^2$ oscillates between 0 and A^2P/K. From equations 4.2.7, 4.2.8 $|X|^2$, $|Y|^2$ then oscillate between A^2 and 0 and, A^2 and $A^2(1 + M/K)$ respectively. The solution to equations 4.2.4 - 4.2.6 with the present initial conditions is that of a continual transfer of energy between harmonics with no steady state being possible.

The oscillation of energy is of two types. Between surface harmonics and between the interface and surface harmonics. Because the energy of Z is proportional to $\rho - 1 \ll 1$ (see for example Phillips [35]) and $|Z|$ is bounded by A (since $P < K$) the first type of energy oscillation involves the greater amount of energy. The interface harmonic acts as a catalyst enabling a large proportion of the total energy to be transferred between the two components of the surface spectrum.

The period T of the oscillation is

$$T = 2/\{A^2KP(1+\alpha)\}^{1/2} C(\alpha/(1+\alpha))$$

where $\alpha = MK^{-1}$ and C is the complete integral of the first kind for the parameter $\alpha/(1+\alpha)$. Because $K \simeq M$, $C = 1{\cdot}85$ and

$$T = 2{\cdot}62/(A^2PK)^{\frac{1}{2}} .$$

The effect of the interaction coefficients and initial amplitude on T is shown by holding the maximum amplitude of Z at a fixed value Z_{max}. The period then becomes

$$T = 2{\cdot}62/\{K(Z_{max}A)^{\frac{1}{2}}\} .$$

The time taken for the interface harmonic to grow to its largest value is thus inversely dependent on K and A, results in accord with physical reasoning. The coefficient K is a measure of the strength of interaction between the interface and surface harmonics. The larger K is for a given A the stronger the interaction and the quicker the transfer of energy to the interface. If K is held constant and A increased the surface amplitudes are larger, again increasing the rate of energy transfer to the interface. The perturbation scheme used by Phillips [32] suggests that $T \propto A^{-2}$. However this scheme neglects changes in the surface amplitudes and hence the decrease in the rate of energy transfer when the product of the surface amplitudes becomes small.

The second set of initial condition, $X(0) = A$, $Y(0) = A$, $Z(0) = B$ is the same as the first except energy has been added to the interface spectrum.

Equations 4.2.10 becomes

$$|Z|^{'2} = -4KM(|Z|^2 - B^2)(|Z|^2 - r_1)(|Z|^2 - r_2) \qquad 4.2.11$$

where $r_1 = \{\gamma - (\gamma^2 + 4P^2KMA^4)^{\frac{1}{2}}\}/(2KM) < 0$

$r_2 = \{\gamma + (\gamma^2 + 4P^2KMA^4)^{\frac{1}{2}}\}/(2KM) > 0$

$\gamma = KMB^2 + PA^2(M - K)$

If $A \neq \{(K - M)/P\}^{\frac{1}{2}}B$, the roots B^2, r_1, r_2 are distinct giving an oscillatory solution as before with $|Z|^2$ bounded by B^2 and r_2, $|X|^2$ by A^2 and $A^2 - K/P(r_2 - B^2)$ and $|Y|^2$ by A^2 and $A^2 + M/P(r_2 - B^2)$. The period of the oscillations is

$$T = 2/\{KM(r_2 - r_1)\}^{\frac{1}{2}}C((r_2 - B^2)/(r_2 - r_1)) \qquad r_2 > B^2$$

$$T = 2/\{KM(B^2 - r_1)\}^{\frac{1}{2}}C((B^2 - r_2)/(B^2 - r_1)) \qquad B^2 > r_2 \qquad 4.2.12$$

For a given B/A equations 4.2.12 show that $T \propto A^{-1}$ as for the previous set of initial conditions. However for a given A the dependence of T on B/A is not as simple. To illustrate this dependence the period together with the bounds on the oscillations $|X|$, $|Y|$, $|Z|$ as a function of B/A are given in figure 4.1(a) - (d) for $\rho = 1{\cdot}05$, $\mu = {\cdot}3096$ and $A = 1$.

When B/A is small the period and bounds in the oscillations are similar to those for the first set of initial conditions. As B is increased, for $B < A\{(K - M)/P\}^{-\frac{1}{2}}$ the roots r_2, B^2 move closer together and r_2, r_1 move apart. The period T (from equation 4.2.12) decreases and the oscillations in $|X|$, $|Y|$, $|Z|$ become smaller. For example with $B = 0$ the period is $5{\cdot}9$, $|Z|$ oscillates between 0 and ${\cdot}65$, $|X|$ between 0 and 1 and $|Y|$ between 1 and $1{\cdot}40$. With $B = 1$ the period is $4{\cdot}2$, $|Z|$ is bound by 1 and $1{\cdot}07$, $|X|$ by $1{\cdot}0$ and ${\cdot}80$ and $|Y|$ by $1{\cdot}0$ and $1{\cdot}16$.

When $B = A\{(K - M)/P\}^{-\frac{1}{2}}$ (equal to $4{\cdot}3$ for this example) the roots r_2, B^2 coalesce and no oscillation in the amplitudes are possible. The harmonic amplitudes are then of the form

$$X = Ae^{i\psi_1},\ Y = Ae^{i\psi_2},\ Z = Be^{i\psi_3}$$

where ψ_1, ψ_2, ψ_3 are real functions of τ. Using equations 4.2.4 - 6 and the initial conditions gives

$$\psi_1 = KA\tau,\ \psi_2 = MA\tau,\ \psi_3 = PA^2/B\tau\ .$$

For $B > A\{(K-M)/P\}^{-\frac{1}{2}}$, $B^2 > r_2$ with oscillations in the amplitudes again occurring.

When the number of surface harmonics was increased keeping $n_1 = 1$ it was not found possible to solve analytically the resulting initial value problem. However the following two independent complete integrals for an arbitrary number of surface harmonics were found.

$$|b_1|^2 + \sum_{\substack{i=k_1 \\ i\neq\ell}}^{k_2} \alpha_i |a_i|^2 = C_1 \qquad k_1 \leqslant \ell \leqslant k_2$$

and

$$\sum_{i=k_1}^{k_2} \beta_i |a_i|^2 = C_2$$

where α_i, β_i are functions of the interaction coefficients and C_1, C_2 are constants evaluated using the initial conditions. The explicit forms of α_i, β_i are not given because other complete integrals were used in subsequent calculations. A complete integral of a similar form to the above was also obtained for $n_1 = 2$, $n_2 = 3$.

For a larger number of harmonics the solutions to IVP3 were found numerically using the integration scheme now discussed.

4.3 Numerical Scheme

Our choice of an integrator to solve IVP3 was based on the need to find the solution efficiently and to a prescribed accuracy (10^{-3}). The features of IVP3 which influenced this choice were the stiffness, the cost of the derivative evaluation and the range of integration.

The traditional view of stiffness (see for example Gear [16]) for initial value problems is illustrated by the following example.

$$\frac{dy}{dt} = -y$$

$$\frac{dz}{dt} = -10^7 z \qquad 4.3.1$$

with initial conditions $y(0) = 1$, $z(0) = 1$. The analytical solution is $y(t) = e^{-t}$, $z(t) = e^{-10^7 t}$.

If the solution is found numerically using the forward Euler method then with exact arithmetic

$$y(t) = (1-h)^n$$

$$z(t) = (1-10^7 h)^n$$

where $t = nh$. For stability we require $h \leqslant 0(10^{-7})$. After say the first 100 steps z will be negligible compared to y and only the first equation in 4.3.1 will be significant. If the system 4.3.1 did contain only this equation h could be selected much greater than 10^{-7} for the remaining steps. However the presence of the second equation means that h must retain its small value. Problems of this type in which the step size is limited by an insignificant component of the solution are referred to as being stiff.

The above inefficiency in the selection of h can be overcome by using a different integration scheme. For example, the backward Euler method gives

$$y(t) = (1+h)^{-n}$$

$$z(t) = (1+10^7 h)^{-n}.$$

The instability due to z has been removed and after z becomes insignificant h can be much larger than 10^{-7}.

Problem 4.3.1 shows that if an efficient integrator is required the stiffness of the problem must be considered. For nonlinear problems such as IVP3 the stiffness will in general vary as the integration proceeds. It is then not known in advance whether an integrator using stiff formulae (e.g. Backward Differentiation) or one using non-stiff formulae (e.g. Adams) would be more efficient. A common way to decide this is to solve the problem for a typical set of initial conditions using both types of formulae and select the more efficient. Using this approach and the integrator DIFSUB [17], which has options for solving both stiff and non-stiff problems, we found that IVP3 could be regarded as non-stiff.

The efficiency of an integrator is also affected by the cost of evaluating the derivative. For equations 4.2.1, 4.2.2 this is approximately $7n_1$ multiplications per equation making the evaluation expensive. It was therefore important to select an integrator which made as few evaluations as possible.

For IVP3 the range of integration is long. This means that a large number of steps are needed in the integration and the accumulated error over these steps can be large compared with the errors made at each step. It was therefore necessary to have an integrator for which the error made at each step was small.

Based on the above points we chose, from those available, the integrator STEP written by Shampine and Gordon [39]. STEP was designed to find accurate solutions to non-stiff problems with expensive derivative evaluations. It uses a predictor-corrector approach with the predictor being an Adams-Bashforth formula while the corrector is an Adams-Moulton formula. At each step the integrator attempts to control a quantity called the local error. The relationship between this and other types of errors for a typical step of the initial value problem

$$\frac{dy}{dt} = f(y,t)$$
$$y(0) = y_0 \qquad 4.3.2$$

is shown in figure 4.2(a) where exact arithmetic is used. The curve y(t) is the true solution while u(t) is the solution to the initial value problem

$$\frac{du}{dt} = f(u,t)$$
$$u(t_n) = y_n$$

where y_n is the numerical solution of 4.3.2 at t_n. The local truncation error is the error made in taking a step along y(t) from $y(t_n)$ using the true values of the past points in the prediction and correction. It is the error in approximating the integral

$$\int_{t_n}^{t_{n+1}} f(y,t)dt \qquad (t_{n+1} = t_n + h)$$

by a finite sum. The local error is that made in taking a step along the curve u(t) from y_n using the numerical values of the past points in the prediction and correction. There are two possible contributions to this error: the local discretization error, analogous to the local truncation error, and the memorized error made by using the numerical rather than the true values of the past points.

In general, because of errors made at each step, $y_n \neq y(t_n)$. The local truncation error and hence the global error can not be easily controlled and STEP does not attempt to do so. Instead it approximates u(t) by controlling the local error. In [39] it is shown that the memorized error is O(h) smaller than the local discretization error. STEP therefore estimates and attempts to keep this latter error less than a prescribed tolerance. This is achieved by varying h so that the tolerance is satisfied and at the same time h is as large as possible

to make STEP efficient. The efficiency is further improved by varying the order of the predictor-corrector pair as the integration proceeds. The order and step size changing algorithms are given in appendix 3.

Because it is the local error and not the global error that is controlled by STEP no satisfactory conclusion can be made about the accuracy of a solution of IVP3 until further information has been obtained. Shampine and Gordon recommend the following method of estimating the global error.

The initial alue problem is solved twice, once with a tolerance of ε_1 and once with a tolerance ε_2, to give solutions y_1, y_2 respectively. The global errors e_1, e_2 for ε_1, ε_2 are then

$$e_1 = |y - y_1| \quad , \quad e_2 = |y - y_2| \qquad 4.3.3$$

where y is the true solution. The last step is to estimate e_1 as $|y_1 - y_2|$. For this to be realistic e_2 must be much less than e_1. Except when near limiting precision reducing the error tolerance generally decreases the global error. Using this and results from numerical experiments Shampine and Gordon suggest taking $\varepsilon_2 = 0{\cdot}1\varepsilon_1$. With this choice they found that the estimate of e_1 was rarely incorrect by more than a factor of 10.

To illustrate the relationship between the local error tolerance and the global error for IVP3, the solution for $\rho = 1{\cdot}05$, $\varepsilon = 0{\cdot}015$, $\mu = {\cdot}31$, $n_1 = 1$, $k_1 = 22$, $k_2 = 23$, $b_1(0) = 0$, $a_{22}(0) = a_{23}(0) = {\cdot}8$ was found. This solution was compared with the analytical solution, calculated using Bulirsch's [12] algorithm for the Jacobi elliptic functions, to give the global error as a function of τ. This is shown in figure 4.2(b) for the error tolerances 10^{-6}, 10^{-8}, 10^{-10}.

The two important features of the curves in figure 4.2(b) are that they are increasing functions and at a fixed value of τ the global error

dependence on the error tolerance is approximately linear. The first property means that to get the solution to an accuracy of 10^{-3} at the end of the integration the error tolerance must be less than 10^{-3}. For the range of ρ, ε, μ and initial conditions we used, a tolerance of 10^{-9} was found necessary. The second property shows that the method of estimating the global error given following 4.3.3 will be reliable. This method was used in all our numerical solutions of IVP3.

Our experience with STEP led us to make several changes to it. These modifications were primarily concerned with improving its efficiency with the most important being to the step size selecting algorithm. It was found that when STEP was solving IVP3 it used high orders ($\geqslant 8$) and took many consecutive steps of constant size. This meant, because STEP permitted only doubling when increasing the step size h, that it was possible for STEP to be inefficient by taking many steps with the local error far less than the error tolerance. For example, with the order k = 10, h = 0·1 and the largest acceptable value of h being 0·15 the local error is 86 times smaller than the tolerance. However if increases in h of 50% were permitted then in the above example, h would be increased to 0·15 and the problem solved more efficiently.

Based on this reasoning we modified the step size selecting algorithm so that increases in h as small as 10% were allowed after 2k + 1 consecutive steps of constant size and with $k \geqslant 6$ had been taken. The values of the above parameters were based on the need to make significant improvements in the efficiency but at the same time adversely affecting as little as possible STEP's performance on other problems. In particular all paths of the original order and step size selecting algorithm had to be considered before our modification could be acted upon. This modification along with those which improved the FORTRAN implementation of STEP meant that IVP3 was solved between 1·6 and 2·0

times faster than by the original form of STEP.

In solving IVP3 using STEP, the following procedure was applied. For a given ρ, μ, m and ε the solution was found with a small number of harmonics present. Harmonics were then added until the last one added altered the previous solution by less than a prescribed accuracy (10^{-2}). The previous solution was then taken as the required solution.

The initial conditions were of the same type as in the previous section. For the first set

$$b_k = 0 \qquad k = 1, \ldots, n_1$$

$$a_k = 0 \qquad k = k_1, \ldots\ m-1,\ m+2, \ldots, k_2$$

$$a_m = a_{m+1} = A$$

where A was chosen so that the time average of $\sum_{k\ \text{odd}} |b_k|$ was approximately 1 to enable comparisons to be made with the steady solutions of the last chapter. The parameter ε was selected so that the initial slope of a_m was approximately 0·1.

The second set of initial conditions was

$$b_1 = 1, \quad b_k = 0 \qquad k = 2, \ldots, n_1$$

$$a_k = 0 \qquad k = k_1, \ldots, m-1, m+2, \ldots, k_2$$

$$a_m = a_{m+1} = A$$

where A had the same value as in the previous set.

4.4 Numerical Examples

The solutions given here have been divided into two sets, characterized by different values of ρ. The first set has $\rho = 1{\cdot}05$ with the first example in the set being for a small value of μ. We have taken $\rho = 1{\cdot}05$, $\varepsilon = 0{\cdot}015$, $\mu = {\cdot}3192$ and the initial conditions

$$b_k = 0 \qquad k = 1,\ldots, n_1$$

$$a_k = 0 \qquad k = k_1,\ldots, 21,24,\ldots, k_2$$

$$a_{22} = a_{23} = 0{\cdot}8 .$$

Eight interface harmonics and twenty-five surface harmonics with wavenumbers eleven to thirty-five were required to describe the evolution to the prescribed accuracy of 10^{-2}. The interface displacement and surface envelope for two different time intervals are plotted in figures 4.3(a), (b) while figure 4.3(c) gives the time averaged spectra. Also included in figure 4.3(c) for comparison purposes are the spectra for the lowest steady solution with the same height in the surface spectrum and the right-hand side of equation 3.2.5 replaced by the average of

$$- \sum_{k \text{ odd}} |b_k| .$$

Figures 4.3(a), (b) show that unlike the analytical solutions of the previous section the evolution is not strictly periodic. For this example the integration was continued to $\tau = 400$ without the solution becoming strictly periodic or steady. This was found to occur for all the numerical solutions. However it was possible to refer to a period of the evolution, being that of $|b_1|$. This was 18 with the maximum amplitude of $|b_1|$ 1·1. The corresponding results for the three wave solution were 7·2 and ·52 respectively. Using the linear theory in which the energy of a harmonic is proportional to its amplitude squared, we have that compared with the three wave solution, the near resonant triads have enabled four times the amount of energy to be transferred to the interface in twice the time. This increase in the interface energy was found to occur for all the numerical solutions with the effect becoming greater as μ was decreased.

The influence of the three harmonics, b_1, a_m, a_{m+1} on the general solution can also be measured by finding the average of the complete integral 4.2.9 and expressing it as a fraction of the three wave value of $2A^2$. The influence of b_1, a_m, a_{m+1} on the evolution was then taken as a decreasing function of this fraction, which for this example was ·23.

Figures 4.3(a), (b) also show that the wave system, the centre of which is conveniently defined by the interface trough, propagates at a near constant speed ΔC relative to the frame of reference moving with speed $d\omega_{Am}/(dk\mu)$. An estimate of ΔC can be obtained by assuming that b_1 dominates the interface. Locally in t about t_0 we have

$$b_1(t) = b_1(t_0)\exp\{-i\psi(t)\}$$

where $\psi(t_0) = 0$. If $\psi(t)$ is expressed as

$$\psi(t) = \Delta C\mu(t - t_0) + 0((t - t_0)^2)$$

then from equations 4.2.1

$$\Delta C = \mathrm{Re}\left\{\left(\varepsilon \sum_{\ell=1}^{n_1-1} R_{11,\ell} b^*_\ell b_{\ell+1} + \varepsilon \sum_{\ell=k_1}^{k_2-1} R_{21,\ell} a^*_\ell a_{\ell+1}\right)/(-b_1\mu)\right\} \quad 4.4.1$$

where $\mathrm{Re}\{\ \}$ denotes the real part. The average $\bar{\Delta}C$ of this was ·009 while the value from figures 4.3(a), (b) was 0·01.

Equation 4.4.1 is also useful in testing whether the frame of reference moving with speed $d\omega_{Am}/(dk\mu)$ is numerically the most efficient. The above problem was resolved with $d\omega_{Am}/(dk\mu)$ replaced by

$$\frac{d\omega_{Am}}{dk\mu} - s\,\bar{\Delta}C$$

where s lies in a small range about zero. The results are summarized in table 4.1 below, in which the times have been expressed as a function of that for s = 0·0.

s	TIME
0	1•000
•2	•993
•4	•984
•6	•978
•75	•971
•80	•963
•85	•957
•90	•954
1•00	•982
1•20	1•000

Table 4.1 shows that for the optimal value of s the reduction in time is only 5%. Similar gains were found for other solutions. Based on this and the fact that $s\bar{\Delta}C$ is not known in advance we have used in subsequent calculations the frame of reference moving with speed $d\omega_{Am}/(dk\mu)$ in the positive x-direction.

The final results to be taken from figures 4.3(a), (b) is that the peaks in the surface envelope occurred above the region of convergence of the interface displacement and the troughs of the interface displacement were narrower than the crests.

The results in figure 4.3(c) show a good agreement between the steady and time averaged unsteady interface spectra. However for the surface the unsteady spectrum is broader with its central wavenumber closer to m. An estimate of this wavenumber can be found using the time average form of equation 3.4.1 with $C = \omega_{B1}\mu^{-1} + \Delta C$. This gave the wavenumber to be 20.6 in good agreement with that from figure 4.3(c).

The solution obtained for the second set of initial conditions

$$b_1 = 1 \qquad b_k = 0 \qquad k = 2,\ldots, n_1$$

$$a_k = 0 \qquad k = k_1,\ldots, 21,24,\ldots, k_2$$

$$a_{22} = a_{23} = \cdot 8$$

is given in figures 4.3(d) - (f).

The period of $|b_1|$ was 12 with it oscillating between ·3 and 1·3 while the fractional value of the complete integral 4.2.9 was ·19. For the three wave solution the period was 4·0 and the bounds on $|b_1|$ were 1·0, 1·025. As before greater amounts of energy have been transferred than for the three wave solution, with the influence of b_1, a_m, a_{m+1} on the evolution being approximately the same as the first set of initial conditions.

The average value of $|b_2|$ was 38% of $|b_1|$ compared with the result of 21% in figure 4.3(c). The increase in the size of $|b_2|$ has caused the solution in figures 4.3(d) - (f) to differ from that in figures 4.3(a) - (c) in two significant ways. The interface displacement now has extra peaks and triads such as b_2, a_{27}, a_{29}, which is very close to resonance, have a greater effect on the evolution widening the surface spectrum in the higher wavenumbers and causing the peak in the spectrum to be split.

If μ is increased the nonlinear interaction between interface harmonics moves away from resonance and the interface spectrum is dominated by the second type of interaction. It can be anticipated and is found to be true that this, along with the weaker interaction between harmonics on the two layers, will lead to a narrowing of the spectra.

To illustrate the evolution for a large value of μ we have taken $\rho = 1{\cdot}05$, $\varepsilon = {\cdot}005$, $\mu = 1{\cdot}354$ and the initial conditions

$$b_k = 0 \qquad k = 1,\ldots, n_1$$

$$a_k = 0 \qquad k = k_1,\ldots, 10,13,\ldots, k_2$$

$$a_{11} = a_{12} = 1{\cdot}0 .$$

Two interface harmonics and ten surface harmonics with wavenumbers seven to sixteen were required to describe the evolution to an accuracy of 10^{-2}. The interface displacement and surface envelope for two different time intervals are plotted in figures 4.4(a), (b) and the spectra in figure 4.4(c).

The period of $|b_1|$ was 4·6, the maximum amplitude 1·35 and the fractional value of the complete integral 4.2.9 was ·60. For the three wave solution the period was 3·5 and the maximum amplitude 0·86. As in the previous example there has been an increase, compared with the three wave solution, in the size of the energy oscillations. However the weaker interaction between harmonics has made the increase less than for $\mu = {\cdot}3192$.

The weaker interaction has meant that $|b_2|$ is small ($\leqslant 0{\cdot}04$) making the interface displacement almost sinusoidal as seen in figures 4.4(a), (b). The small value of $|b_2|$ has also led to the value, ·0019, of $\bar{\Delta}C$ estimated using equation 4.4.1 agreeing to the accuracy quoted with that in figure 4.4(a), (b). Finally the narrower spectra have meant that improved agreement between the steady and averaged unsteady spectra has been obtained.

The second set of solutions is with $\rho = 1{\cdot}02$. The decrease in the density difference, as for the steady solution, can be expected to have two significant effects on the solution. The central wavenumber of the surface group will be larger and, because more near resonant triads are possible, the spectra will be broader for a given initial energy.

The first example for $\rho = 1{\cdot}02$ is with $\mu = {\cdot}3096$, $\varepsilon = {\cdot}01$ and the two sets of initial conditions

$$b_k = 0 \qquad k = 1,\ldots, n_1$$

$$a_k = 0 \qquad k = k_1,\ldots, 54,57,\ldots, k_2$$

$$a_{55} = a_{56} = {\cdot}6$$

and

$$b_1 = 1, \quad b_k = 0 \qquad k = 2,\ldots, n_1$$

$$a_k = 0 \qquad k = k_1,\ldots, 54,57,\ldots, k_2$$

$$a_{55} = a_{56} = {\cdot}6 .$$

The figures corresponding to 4.3(a) - (f) are 4.5(a) - (f). For the first set of initial conditions the period was 20, the maximum amplitude of $|b_1|$ was $1{\cdot}1$ and the fractional value of 4.2.9 ${\cdot}14$. The larger number of near resonant triads has meant that the resonant interaction of b_1, a_m, a_{m+1}, has had less influence on the evolution than for the first example of the previous set.

The time average of equation 3.4.1 gave the central wavenumber of the surface wave group to be 52, a result confirmed by figure 4.5(c). The estimate of $\bar{\Delta}C$ from equation 4.4.1 was ${\cdot}005$ while that from figures 4.5(a), (b) was $0{\cdot}0045$.

For the second set of initial conditions the average value of $|b_2|$ was again increased this time from 17% to 31% of $|b_1|$. As before this has led to the interface displacement having more peaks and the surface spectrum being wider because of the greater effect of the near resonant triads containing b_2 such as b_2, a_{74}, a_{76}.

The example in this set for a large value of μ is with $\rho = 1{\cdot}02$, $\varepsilon = {\cdot}004$, $\mu = 1{\cdot}373$ and the initial conditions

$b_k = 0 \qquad k = 1,\ldots, n_1$

$a_k = 0 \qquad k = k_1,\ldots, 26,29,\ldots, k_2$

$a_{27} = a_{28} = \cdot 73$.

Two interface harmonics and fifteen surface harmonics with wave-numbers twenty to thirty-four were required. The results are given in figures 4.6(a) - (c). The period was 5·8, the maximum amplitude of $|b_1|$ 1·60 and the fractional value of the complete integral ·43. The period and maximum amplitude for the three wave solution were 3·2 and ·69. Thus as in the previous example the increase in the number of near resonant triads compared with the solution for $\rho = 1{\cdot}05$ has meant that the interaction of b_1, a_m, a_{m+1} has had less effect on the evolution.

The estimated value of $\bar{\Delta}C$ from equation 4.4.1 was ·0014 which because $|b_2|$ was small ($\leqslant \cdot 04$) agreed to this accuracy with that from figures 4.6(a), (b).

Discussion

The method used in this thesis of having both the interface and surface displacements as unknown functions, and allowing nonlinear wave fields and an arbitrary number of wave modes, has enabled us to solve the problem of the evolution of small amplitude gravity waves on an open two layer fluid in greater detail than in the past.

We found that although the analytical solution for a resonant triad is periodic, the solution when the neighbouring near-resonant triads were included are far from being periodic. There was no evidence that the solutions tended asymptotically towards a strictly periodic or steady solution for general initial conditions. These results on the periodicity contrast with the work of Bryant [9] for the one layer case. He found that the analytical solution with the three most significant wave modes present was periodic, and increasing the number of wave modes made the solution only slightly non-periodic.

The addition of wave modes to complete the description of the evolution allowed considerably more energy to be transferred to the interface and increased the period of evolution compared with the three wave mode solution. It was found as μ decreased, corresponding to longer interface waves or a shallower upper layer, that these effects increased. The decrease in μ also meant that more near-resonant triads were possible leading to an increase in the width of both the surface and interface spectra.

As the initial energy of the lowest interface harmonic was increased the average value of the second interface harmonic b_2 became greater. This enabled near resonant triads involving b_2 to have a greater effect on the evolution, causing the interface displacement to have more peaks and the surface spectrum to become broader.

A decrease in the density difference between the two layers meant that the central wavenumber of the surface spectrum was larger and that more near resonant triads were possible. This caused the spectra to be broader, the evolution period to be greater and more energy to be transferred to the interface.

If the lower layer was assumed to be of finite and not infinite depth and μ was large the analysis would be longer than that given here but we would expect similar results. However if μ was small, additional resonances would be possible and the evolution more complicated.

Finally to illustrate the time scale and the strength of the nonlinear interactions considered in this thesis, the results for the first numerical example in chapter 4 with $\rho = 1{\cdot}02$ and the first set of initial conditions are expressed as dimensioned quantities. With the depth of the upper layer taken to be 50m, two surface modes of wavelengths 17m, 19m respectively and initial amplitudes ·3m generate an interface wave of wavelength 970m and amplitude ·63. This takes 2480 seconds ($\simeq$ 41 minutes) corresponding to 720 surface wave periods or 6·5 interface wave periods.

References

[1] Ball, F.K. Energy transfer between external and internal gravity waves. J. Fluid Mech. 19 465-478 (1964).

[2] Benney, D.J. Non-linear gravity wave interactions. J. Fluid Mech. 14 577-587 (1962).

[3] Benney, D.J. Significant interactions between small and large scale surface waves. Stud. Appl. Math. 55 93-106 (1976).

[4] Boggs, P.T. The solution of nonlinear operator equations by A-stable integration techniques. Technical report No.72-72 (1970) Department of Computer Science, Cornell University, Ithaca, N.Y.

[5] Boussinesq, J. Théorie de l'intumescence liquide appeleé onde solitaire ou de translation se propagent dans un canal rectangulaire. Institut de France, Academie des Sciences, Comptes Rendus, p 755 (1871).

[6] Bretherton, F.P. Resonant interactions between waves. The case of discrete oscillations. J. Fluid Mech. 20 457-479 (1964).

[7] Briscoe, M.G. Introduction to collection of papers on oceanic internal waves. J. Geophys. Res. 80 289-290 (1975).

[8] Broughton, R.L. The solution of non-linear algebraic equations by continuation methods. M.Sc. dissertation (1974), Computing Centre, University of Essex, England.

[9] Bryant, P.J. Periodic waves in shallow water. J. Fluid Mech. 59, 625-644 (1973).

[10] Bryant, P.J. Stability of periodic waves in shallow water. J. Fluid Mech. 66, 81-96 (1974).

[11] Bryant, P.J. Permanent wave structures on an open two layer fluid. Stud. Appl. Math. 57 225-246 (1977).

[12] Bulirsch, R. Numerical calculation of elliptic integrals and elliptic functions. Num. Math. 7 78-90 (1965).

[13] Butcher, J.C., Burrage, K., Chipman, F.H. STRIDE: Stable Runge-Kutta integrator for differential equations. Computational Mathematics Report No.20, University of Auckland (1979).

[14] Davidenko, D.F. On a new method of numerical solution of systems of nonlinear equations. Math. Reviews 14 906 (1953).

[15] Deist, F.H., Sefor, L. Solutions of systems of nonlinear equations by parameter variation. Comp. J. 10 78-82 (1967).

[16] Gear, C.W. Numerical initial value problems in ordinary differential equations, (1 ed., 1971) p 209-210, Prentice-Hall.

[17] Reference 16 p 158-166.

[18] Harwell Subroutine Library (1980), DCO2AD, United Kingdom Atomic Energy Authority.

[19] Hashizume, Y., Ikeda, N. Resonant interactions of waves on a stratified fluid. Phys. Soc. Jap. 45 665-673 (1978).

[20] Hindmarsh, A.C. GEAR: Ordinary differential Equation System Solver, Lawrence Livermore Laboratory Report UCID-30001, Rev 3 (1974).

[21] Hindmarsh, A.C., Byrne, G.D. EPISODE: An experimental package for the integration of systems of ordinary differential equations, Lawrence Livermore Laboratory Report UCID-30112 (1975).

[22] Joyce, T.M. Nonlinear interactions among standing surface and internal gravity waves. J. Fluid Mech. 63 801-825 (1974).

[23] Korteweg, D.J., DeVries, G. On the change of form of long waves advancing in a rectangular canal and on a new type of long stationary waves. Phil. Mag. (5) 39 422 (1895).

[24] Lamb, H.H. Hydrodynamics (3 ed., 1906) p 355-356, Cambridge University Press.

[25] Lewis, J.E., Lake, B.M., Ko, D.R.S. On the interaction of internal waves and surface gravity waves. J. Fluid Mech. 63 773-800 (1974).

[26] Lighthill, M.J. Waves in fluids (1 ed., 1978) Cambridge University Press.

[27] Longuet-Higgins, M.S., Smith, N.D. An experiment on third-order resonant wave interactions. J. Fluid Mech. 25 417-435 (1966).

[28] McGoldrick, L.F. Resonant interactions among capillary-gravity waves. J. Fluid Mech. 21 305-331 (1965).

[29] McGoldrick, L.F., Phillips, O.M., Huang, N.E., Hodgson, T.H. Measurements of third order resonant wave interactions. J. Fluid Mech. 25 437-456 (1966).

[30] Ma, Yan-Chow. Effect of long internal waves on the evolution of deep-water surface gravity waves. Phys. Fluids 25 411-419 (1982).

[31] Oden, J.T. Finite elements of nonlinear continua, Advanced Engineering Series (1972) p 284-292, McGraw-Hill.

[32] Phillips, O.M. On the dynamics of unsteady gravity waves of finite amplitudes: Part 1: The elementary interactions. J. Fluid Mech. 9 193-217 (1960).

[33] Phillips, O.M. The dynamics of the upper ocean (2 ed., 1977) Cambridge University Press.

[34] Reference 33 p 38-39.

[35] Reference 33 p 215.

[36] Rabinowitz, P. editor Numerical Methods for nonlinear algebraic equations (1 ed., 1970) p 69-71, Gordon and Breach, Science Publishers.

[37] Reference 36 p 87-161.

[38] Rizk, M.H., Ko, D.R.S. Interaction between small-scale surface waves and large-scale internal waves. Phys. Fluids 21 1900-1907 (1978).

[39] Shampine, L.F., Gordon, M.K. Computer solution of ordinary differential equations. The initial value problem (1 ed., 1975). W.H. Freeman and Co.

[40] Stokes, G.G. On the theory of Oscillatory Waves. Camb Trans., t, 8.

[41] Thorpe, S.A. On wave interactions in a stratified fluid. J. Fluid Mech. 24 737-751 (1966).

[42] Thorpe, S.A. The excitation, dissipation, and interaction of internal waves in the deep ocean. J. Geophys. Res. 80 328-338 (1975).

[43] Watson, K.M., West, B.J., Cohen, B.I. Coupling of surface and internal gravity waves: a mode coupling model. J. Fluid Mech. 77 185-208 (1976).

[44] Whitham, G.B. Linear and nonlinear waves (1974) p 460-476. John Wiley and Sons.

APPENDIX 1

Interaction Coefficients

Defining $F_k = \omega_k^2 \cosh k\mu - k\mu \sinh k\mu$

$G_k = \omega_k^2 \sinh k\mu - k\mu \cosh k\mu$

gives

$$P_{k,\ell} = \frac{1}{2} F_k \left[(\rho - 1)(\omega_\ell^2 - \omega_\ell \omega_{k+\ell} + \omega_{k+\ell}^2) - \rho(\omega_{k+\ell}^2 - \omega_\ell^2) - \rho\omega_\ell\omega_{k+\ell} + \omega_\ell\omega_{k+\ell} \frac{G_\ell G_{k+\ell}}{F_\ell F_{k+\ell}} \right]$$

$$+ \frac{1}{2} G_k (\omega_{k+\ell} - \omega_\ell) \left(\omega_{k+\ell} \frac{G_{k+\ell}}{F_{k+\ell}} + \omega_\ell \frac{G_\ell}{F_\ell} \right)$$

$$+ \frac{1}{2} \frac{\omega_\ell^2 \omega_{k+\ell}^2}{F_\ell F_{k+\ell}} \left[\omega_k^2 \left(\omega_\ell^2 - \omega_\ell \omega_{k+\ell} + \omega_{k+\ell}^2 - \frac{\mu^2 \ell (k+\ell)}{\omega_\ell \omega_{k+\ell}} \right) - (\omega_{k+\ell} - \omega_\ell) \mu k \left(\frac{(k+\ell)\mu}{\omega_{k+\ell}} + \frac{\ell\mu}{\omega_\ell} \right) \right]$$

$$Q_{k,\ell} = \frac{\mu^2 k^2 T_k}{2\omega_k^2 (\rho + T_k)} \left[(\rho - 1)(\omega_\ell^2 - \omega_\ell \omega_{k+\ell} + \omega_{k+\ell}^2) - \rho(\omega_{k+\ell}^2 - \omega_\ell^2) - \rho\omega_\ell\omega_{k+\ell} + \omega_\ell\omega_{k+\ell} \frac{G_\ell G_{k+\ell}}{F_\ell F_{k+\ell}} \right.$$

$$+ (\omega_{k+\ell} - \omega_\ell) \left(\frac{\rho}{T_k} - \frac{(\rho-1)\mu k}{\omega_k^2} \right) \left(\omega_{k+\ell} \frac{G_{k+\ell}}{F_{k+\ell}} + \omega_\ell \frac{G_\ell}{F_\ell} \right)$$

$$\left. - \frac{(\rho-1)\omega_\ell^2 \omega_{k+\ell}^2 F_k}{\omega_k^2 F_\ell F_{k+\ell}} \left(\omega_\ell^2 - \omega_\ell \omega_{k+\ell} + \omega_{k+\ell}^2 - \mu\ell \frac{(k+\ell)\mu}{\omega_\ell \omega_{k+\ell}} \right) \right]$$

$$+ \frac{\mu k F_k}{2\omega_k^2} (\omega_{k+\ell} - \omega_\ell) \left(\frac{(k+\ell)\mu}{\omega_{k+\ell}} + \frac{\ell\mu}{\omega_\ell} \right) \frac{\omega_\ell^2 \omega_{k+\ell}^2}{F_\ell F_{k+\ell}}$$

$$R_{1k,\ell} = \left[\frac{\omega_k^{\,2} F_k P_{k,\ell}}{\omega_{k+\ell} - \omega_\ell + \omega_k} + \frac{\omega_k^{\,4}(\omega_{k+\ell} - \omega_\ell - \omega_k) Q_{k,\ell}}{(\omega_{k+\ell} - \omega_\ell)^2 - (\omega_{Ak}\omega_{Bk}/\omega_k)^2}\right] \Big/$$

$$((\rho - 1)F_k^{\,2} + \omega_k^{\,4}) \quad \text{with} \quad \omega_k = \omega_{Bk},\ \omega_\ell = \omega_{B\ell}$$

$$\omega_{k+\ell} = \omega_{Bk+\ell}\ .$$

$$R_{2k,\ell} = \frac{F_\ell F_{k+\ell}}{\omega_\ell^{\,2}\omega_{k+\ell}^{\,2}}\left[\frac{\omega_k^{\,2} F_k P_{k,\ell}}{(\omega_{k+\ell} - \omega_\ell + \omega_k)} + \frac{\omega_k^{\,4}(\omega_{k+\ell} - \omega_\ell - \omega_k) Q_{k,\ell}}{(\omega_{k+\ell} - \omega_\ell)^2 - (\omega_{Ak}\omega_{Bk}/\omega_k)^2}\right] \Big/$$

$$((\rho - 1)F_k^{\,2} + \omega_k^{\,2})$$

$$\text{with} \quad \omega_k = \omega_{Bk},\ \omega_\ell = \omega_{A\ell},\ \omega_{k+\ell} = \omega_{Ak+\ell}\ .$$

$$R_{3k,\ell} = \left[\frac{\omega_k^{\,4} P_{k,\ell}}{\omega_{k+\ell} - \omega_\ell + \omega_k} - \frac{(\rho-1)F_k\omega_k^{\,2}(\omega_{k+\ell} - \omega_\ell - \omega_k) Q_{k,\ell}}{(\omega_{k+\ell} - \omega_\ell)^2 - (\omega_{Ak}\omega_{Bk}/\omega_k)^2}\right] \frac{F_{k+\ell}}{\omega_{k+\ell}^{\,2}} \Big/$$

$$((\rho - 1)F_k^{\,2} + \omega_k^{\,4}) \quad \text{with} \quad \omega_k = \omega_{Ak},\ \omega_\ell = \omega_{B\ell}$$

$$\omega_{k+\ell} = \omega_{Ak+\ell}\ .$$

In numerical work the roundoff error in the expressions for $P_{k,\ell}$, $Q_{k,\ell}$, $R_{1k,\ell}$, $R_{2k,\ell}$, $R_{3k,\ell}$ can be reduced by using the explicit form of ω_k, F_k, G_k and collecting terms. This was not done in order to simplify the computer coding. However it was found necessary to reduce cancellation effects in the definitions of F_k, G_k by using the expressions for ω_k. With $\omega_k = \omega_{Bk}$

$$F_k = -\, k\mu e^{k\mu}\sinh k\mu/(\rho\cosh k\mu + \sinh k\mu)$$

$$G_k = -\, k\mu(\rho + e^{k\mu}\sinh k\mu)/(\rho\cosh k\mu + \sinh k\mu)$$

while for $\omega_k = \omega_{Ak}$

$$F_k = -\, G_k = k\mu e^{-k\mu}\ .$$

Approximate form of $R_{3k,1}$

When $\ell = 1$ and $e^{\mu} << e^{k\mu}$ the largest term in $P_{k,\ell}$, $Q_{k,\ell}$ for $R_{3k,1}$ is that containing F_k^{-1}. Neglecting the other terms, $R_{3k,1}$ becomes

$$\frac{\omega_1^2}{2F_1(\omega_{k+1} - \omega_1 + \omega_k)} \left\{\omega_k^2 \left[\omega_1^2 - 2\omega_{k+1} \frac{\mu}{\omega_1} + \mu\right]\right\} .$$

Using the approximation $\omega_{k+1} \simeq \omega_k + \frac{\mu}{2\omega_k}$ and taking ω_1^3 to be negligible compared with $2\omega_{k+1}\mu$ gives

$$R_{3k,1} \simeq - \frac{\omega_1 \mu^2 k}{2F_1} - \frac{\omega_1 \mu^2}{8F_1} .$$

Appendix 2

The Classical and Damped Newton's Method

The two algorithms given here are our form of the Classical Newton's Method (CNM) and the Damped Newton's Method (DNM) referred to in section 3 of Chapter 3. The following notation has been used in the description.

$f(\underset{\sim}{x}) = \underset{\sim}{0}$ - the system of nonlinear equations to be solved

n - the number of equations

$\underset{\sim}{x}_0$ - the initial estimate of the solution

$\underset{\sim}{x}^{(k)}$ - the k^{th} iterate generated by the method with $\underset{\sim}{x}^{(0)} = \underset{\sim}{x}_0$

$\delta\underset{\sim}{x}^{(k)}$ - the Newton step at the k^{th} iteration

J - the Jacobian of $\underset{\sim}{f}(\underset{\sim}{x})$

I_{max} - the maximum number of iterations allowed

u - the relative machine precision

TOL - the prescribed accuracy to which the solution is required

$\underset{\sim}{y}$ - a working vector

FLAG - a variable set when the method stops. Its values have the following meanings:

0 - convergence has been obtained with the last iterate being the solution to the required accuracy

1 - the method failed because too many iterations were taken

2 - the method failed because the Jacobian was singular

3 - applicable only to the DNM. The method failed because the Newton direction was not a descent direction.

CNM

Step 1 : Set $I_{max} = 3n$, $k = 0$, $\underset{\sim}{x}^{(0)} = \underset{\sim}{x}_0$

Step 2 : If $k > I_{max}$ set FLAG = 1 and stop.

Otherwise set $j = 0$

Step 3 : Calculate J, $\underset{\sim}{f}$ at $\underset{\sim}{x}^{(k)}$

Step 4 : Solve $J\delta\underset{\sim}{x}^{(k)} = -\underset{\sim}{f}$ for $\delta\underset{\sim}{x}^{(k)}$ if possible using Gaussian elimination with partial pivoting.

If J is singular and $j = 1$, set FLAG = 2 and stop.

If J is singular and $j = 0$, set $j = 1$

$x_i^{(k)} = x_i^{(k)} + 10^3 u$ $i = 1,\ldots,n$ and go to 3

Step 5 : If $\|\delta\underset{\sim}{x}^{(k)}\|_2 \leqslant$ TOL set FLAG = 0 and stop.

Otherwise set $\underset{\sim}{x}^{(k+1)} = \underset{\sim}{x}^{(k)} + \delta\underset{\sim}{x}^{(k)}$, $k = k + 1$ and go to 2

DNM

Step 1 : Set $I_{max} = 10n$, $k = 0$, $\underset{\sim}{x}^{(0)} = \underset{\sim}{x}_0$

Step 2 : If $k > I_{max}$ set FLAG = 1 and stop.

Otherwise set $j = 0$

Step 3 : Calculate J, $\underset{\sim}{f}$ at $\underset{\sim}{x}^{(k)}$

Step 4 : Solve $J\delta\underset{\sim}{x}^{(k)} = -\underset{\sim}{f}$ for $\delta\underset{\sim}{x}^{(k)}$ if possible using Gaussian elimination with partial pivoting.

If J is singular and $j = 1$, set FLAG 2 and stop.

If J is singular and $j = 0$, set $j = 1$

$x_i^{(k)} = x_i^{(k)} + 10^3 u$ $i = 1,\ldots,n$ and go to 3

Step 5 : If $\|\delta\underset{\sim}{x}^{(k)}\| \leqslant$ TOL set FLAG = 0 and stop.

Otherwise set $i = 0$

Step 6 : If $i > 9$ set FLAG = 3 and stop

Step 7 : Set $\underset{\sim}{y} = \underset{\sim}{x}^{(k)} + 2^{-i}\delta\underset{\sim}{x}^{(k)}$

If $\|\underset{\sim}{f}(\underset{\sim}{y})\|_2 > 0{\cdot}9\|\underset{\sim}{f}(\underset{\sim}{x}^{(k)})\|_2$ set $i = i + 1$ and go to 6

Otherwise set $\underset{\sim}{x}^{(k+1)} = \underset{\sim}{y}$, $k = k + 1$ and go to 2

Normalised Determinant

Given a nonsingular n × n matrix A the normalised determinant $\det_n$ of A is

$$\det_n(A) = \left(\prod_{i=1}^{n} s_i \right)^{-1} \det(A)$$

where $s_i = \left\{ \sum_{j=1}^{n} a_{ij}^2 \right\}^{\frac{1}{2}}$.

APPENDIX 3

Order and Step size selecting algorithm

The description given here is of the order and step size selecting algorithm used by the integrator STEP. The following notation and nomenclature has been used.

$$\underset{\sim}{y}(t_0) = \underset{\sim}{y}_0, \quad \frac{d\underset{\sim}{y}}{dt} = f(\underset{\sim}{y},t)$$

- the initial value problem being solved

k - the current order

h - the current step size

h_{user} - an upper bound on the step size provided by the user

h_{new} - the step size for the next step

n_c - the number of consecutive steps including the current one for which the step size has been constant

ε - the local error tolerance

E_i - an estimate of the discretization error that would be made in taking a step from the current point with step size h and order i

$r \equiv (0{\cdot}5\varepsilon/E_k)^{\frac{1}{k+1}}$

u - the relative machine precision

A failed step is one for which the local error is greater than the error tolerance. A general step is one which is neither a failed step nor one at the start of the integration.

Order Selection

General Step

After the prediction the order is lowered by 1 for the next step if

$$\max(E_{k-1},E_{k-2}) \leqslant E_k \qquad k > 2$$
$$E_{k-1} \leqslant \frac{1}{2}E_k \qquad k = 2$$

After the correction the order is lowered by 1 for the next step if

$$E_{k-1} \leqslant \min(E_k,E_{k+1}) \qquad k \geqslant 2$$

If there is no reduction in order it is raised by 1 if

$$n_c \geqslant k \quad \text{and}$$
$$E_{k+1} < E_k \qquad 1 < k < 12$$
$$E_{k+1} < 0{\cdot}5E_k \qquad k = 1$$

Start of Integration

At the start of the integration the order is rasied by 1 at each step until

(i) there is a step failure or

(ii) the order is to be lowered for the next step or

(iii) the order has reached the maximum of 12.

Failed Step

On the third and succeeding step failures at the current point the order is set at one until a successful step occurs.

Step size selecting algorithm

General step

If $r \leqslant 0{\cdot}5$	$h_{new} = h/2$
If $0{\cdot}5 < r < 0{\cdot}9$	$h_{new} = rh$
If $0{\cdot}9 \leqslant r < 1{\cdot}0$	$h_{new} = 0{\cdot}9h$
If $1{\cdot}0 \leqslant r < 2{\cdot}0$	$h_{new} = h$
If $r \geqslant 2{\cdot}0$	$h_{new} = 2h$

Start of integration

For the first step $h = \min\left\{h_{user}, \frac{1}{4}[\varepsilon/(2\|\underset{\sim}{f}(\underset{\sim}{y}_0, t_0)\|_2)]^{\frac{1}{2}}\right\}$

Thereafter h is doubled at each step until

(i) there is a step failure or

(ii) the order is to be reduced for the next step or

(iii) the order has reached the maximum of 12.

Failed Step

For the first 3 failed steps at the current point h is halved.

In the succeeding attempted steps from the current point

$$h = h * \min\left\{\frac{1}{2}, [\varepsilon/(2E_k)]\right\} .$$

Figures

For the surface wave groups depicted here the solid line represents the surface displacement at $t = 0$ while the dotted line is the surface envelope.

The points in the surface and interface spectra have been joined for clarity.

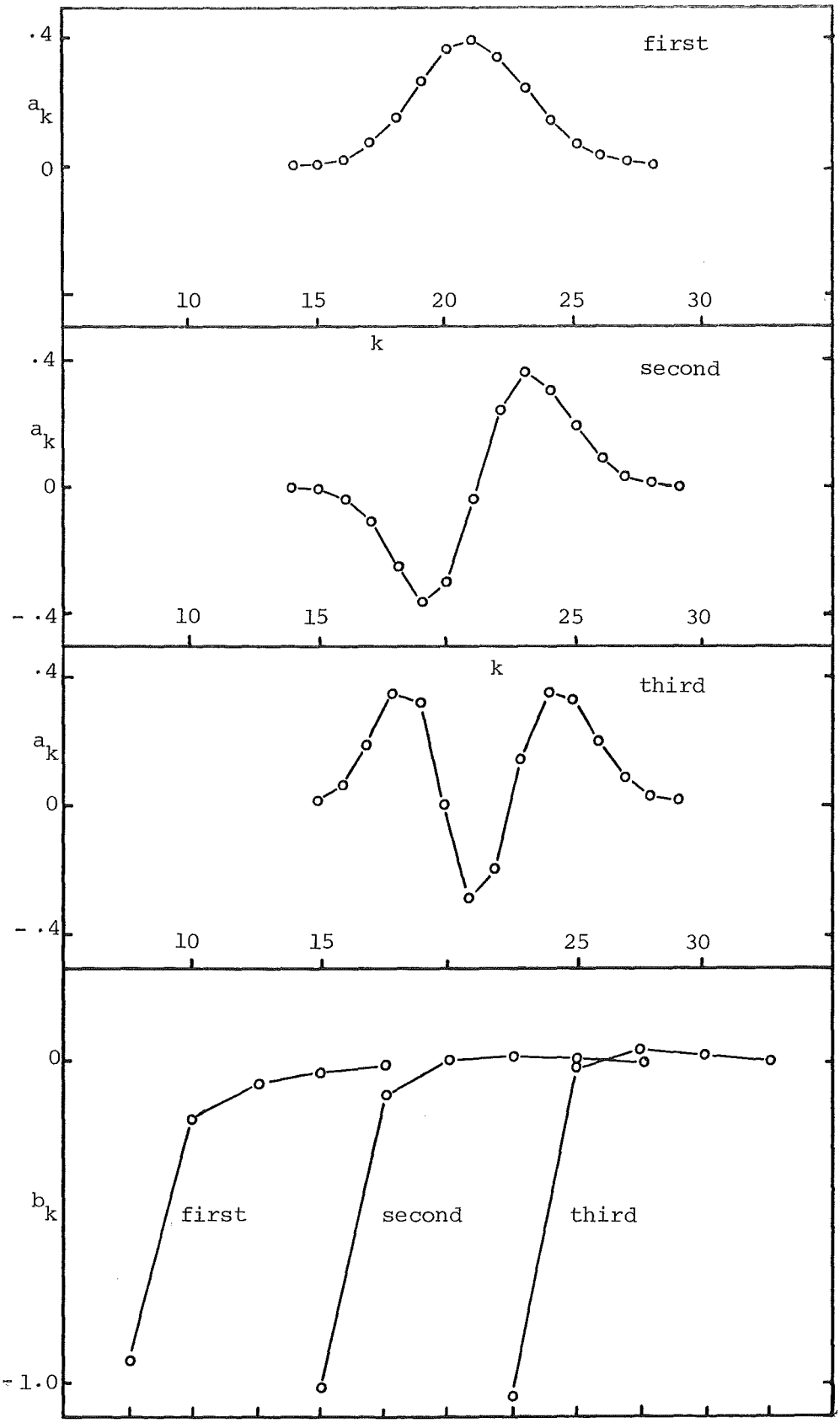

Figure 3.1(a): Surface (top) and interface spectra for the 3 lowest solutions with $\rho = 1{\cdot}05$, $\varepsilon = 0{\cdot}015$, $\mu = {\cdot}3192$, $S_{max} = 0{\cdot}04$.

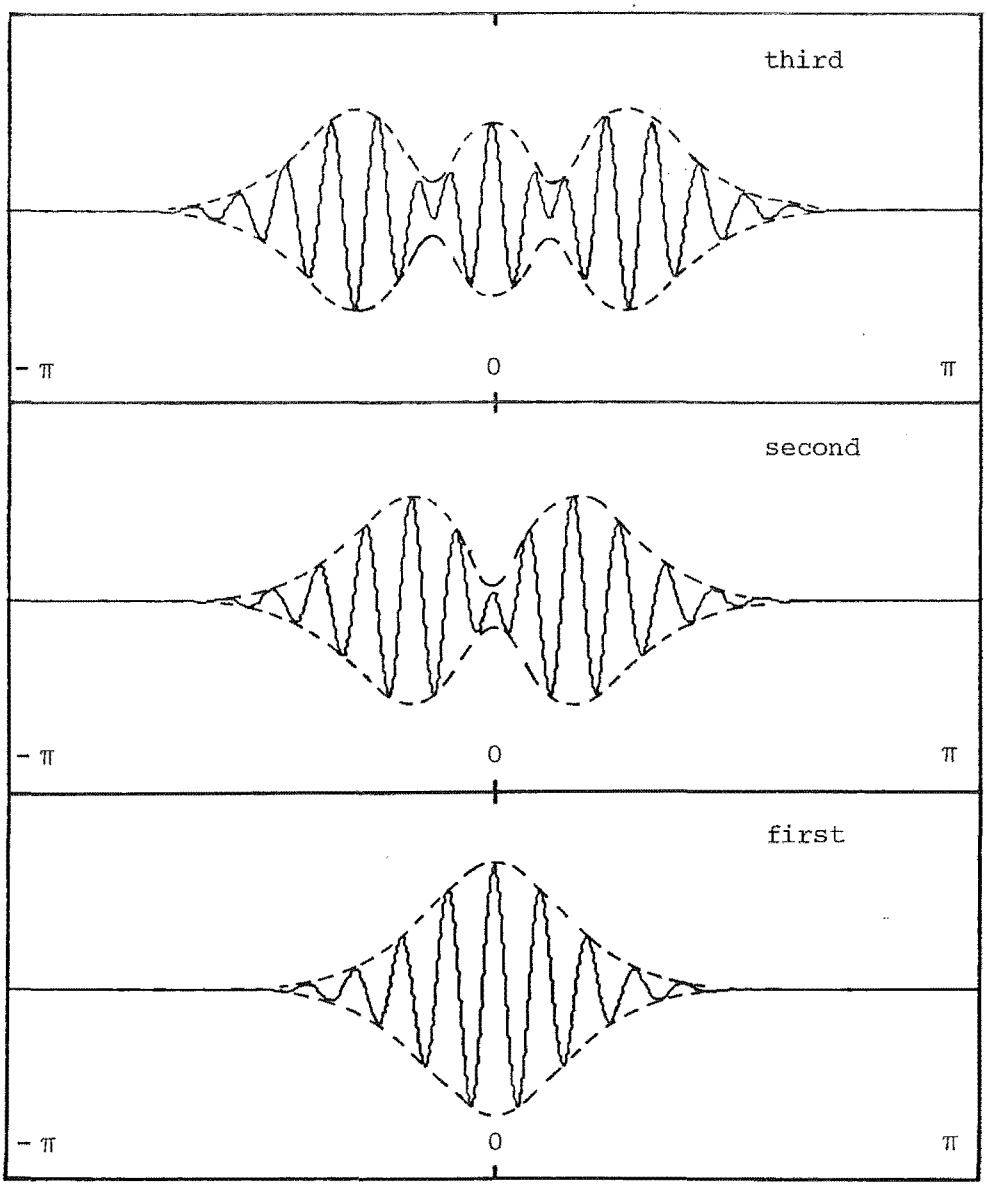

Figure 3.1(b): Free surface wave groups for the 3 lowest solutions with $\rho = 1{\cdot}05$, $\varepsilon = {\cdot}015$, $\mu = {\cdot}3192$, $S_{max} = {\cdot}04$. The vertical magnification is 30.

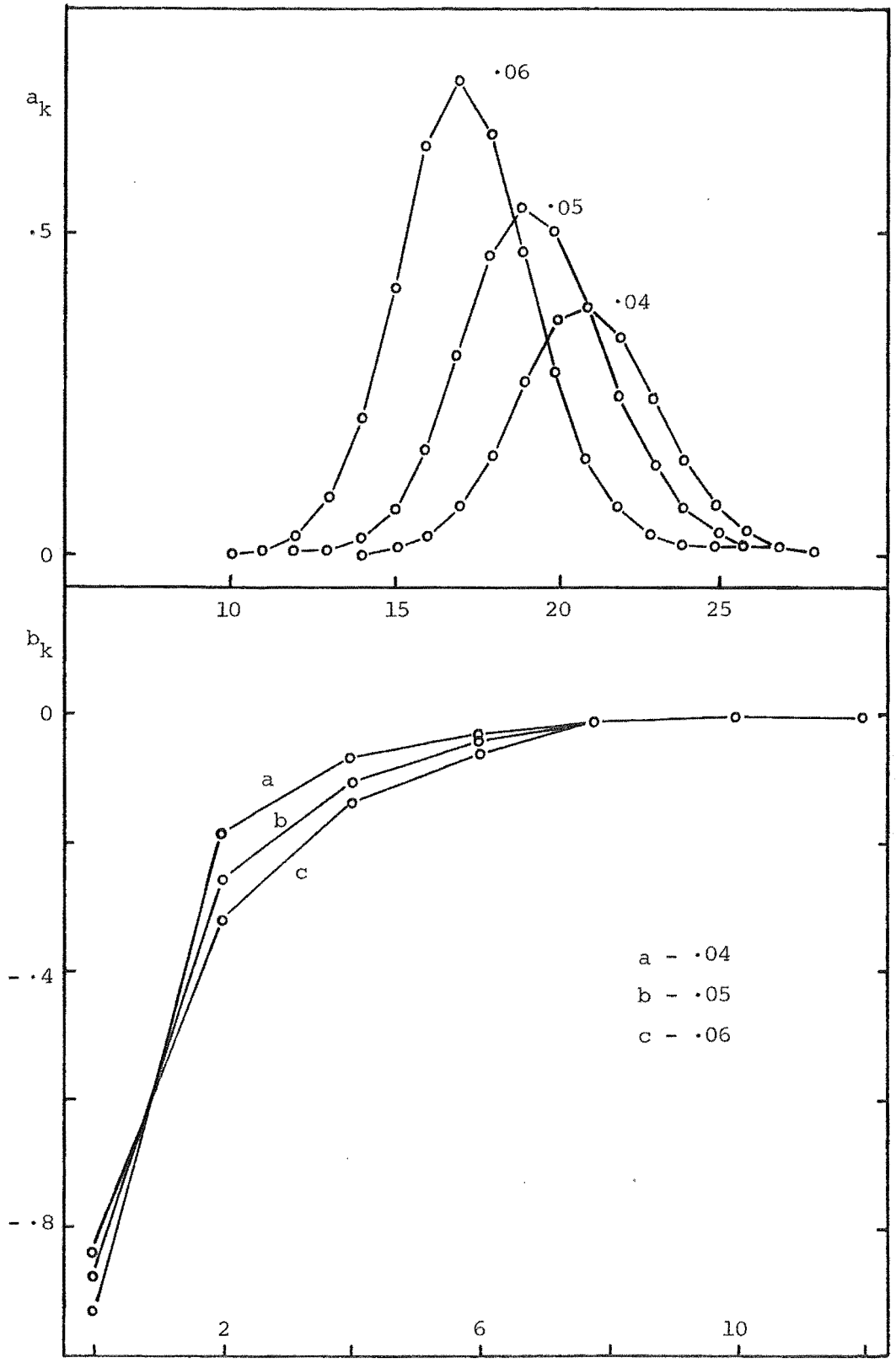

Figure 3.1(c): Surface (top) and interface spectra for the lowest solution with $\rho = 1{\cdot}05$, $\varepsilon = {\cdot}015$, $\mu = {\cdot}3192$, $S_{max} = {\cdot}04, {\cdot}05, {\cdot}06$.

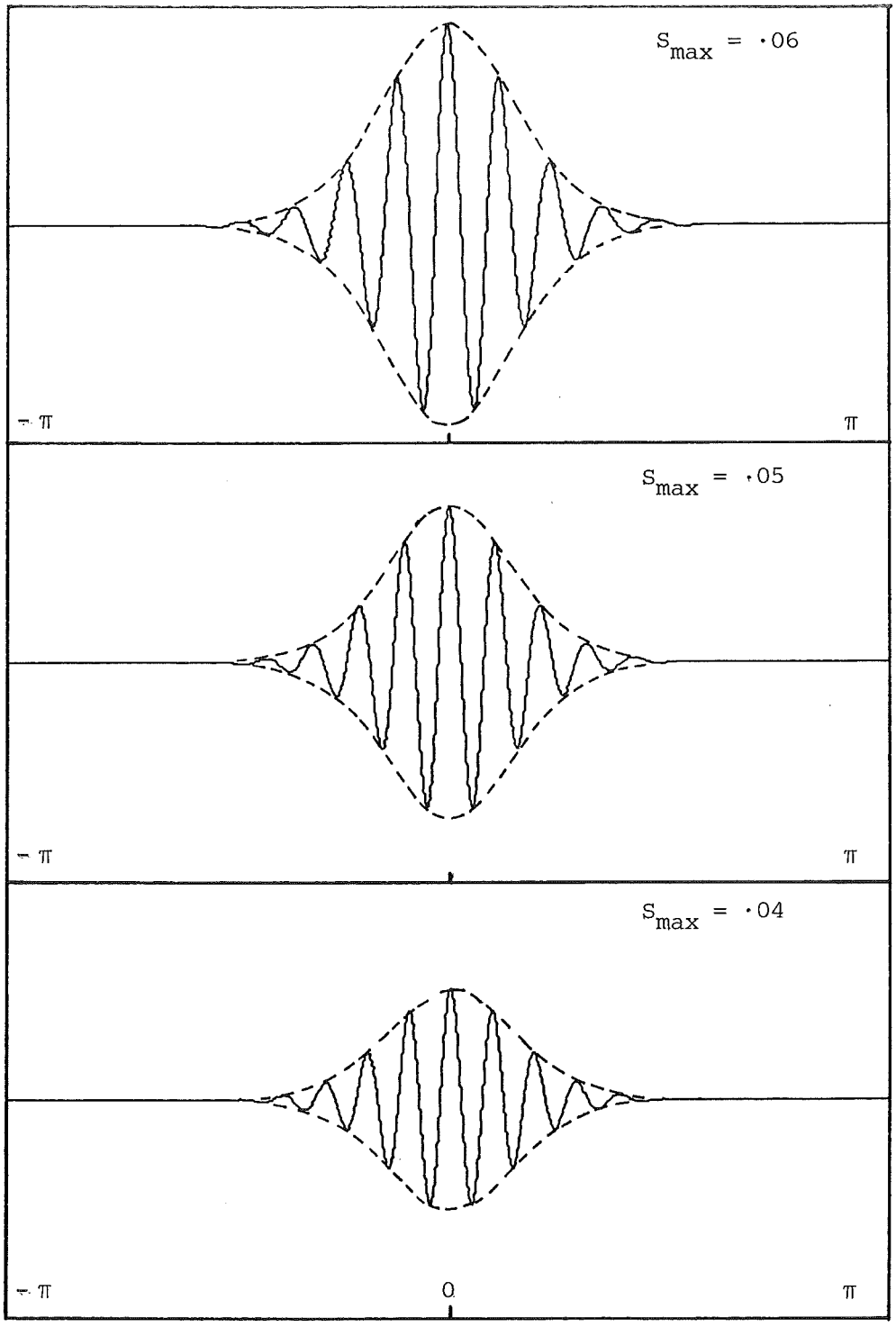

Figure 3.1(d): Free surface wave groups for the lowest solution with ρ = 1·05, ε = ·015, μ = ·3192, S_{max} = ·04, ·05, ·06. The vertical magnification is 30.

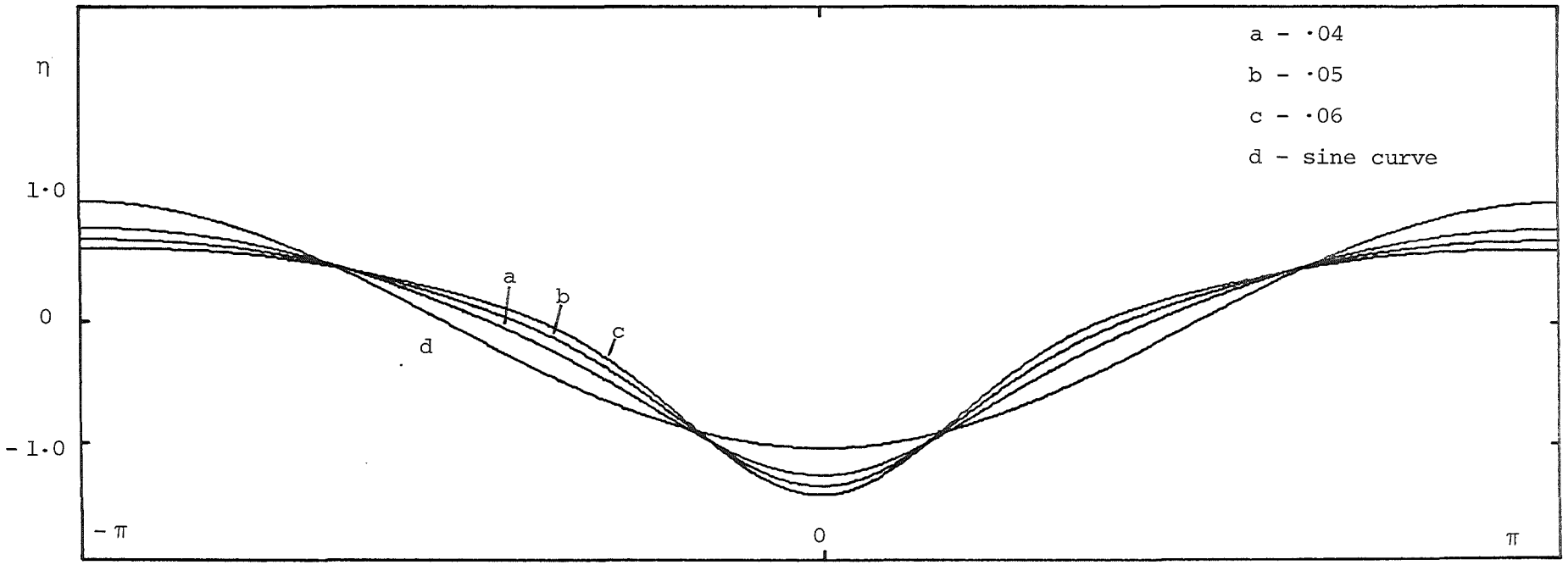

Figure 3.1(e): Interface displacements and sine curve for the lowest solution with $\rho = 1{\cdot}05$, $\varepsilon = {\cdot}015$, $\mu = {\cdot}3192$, $S_{max} = {\cdot}04, {\cdot}05, {\cdot}06$. The vertical magnification is 75.

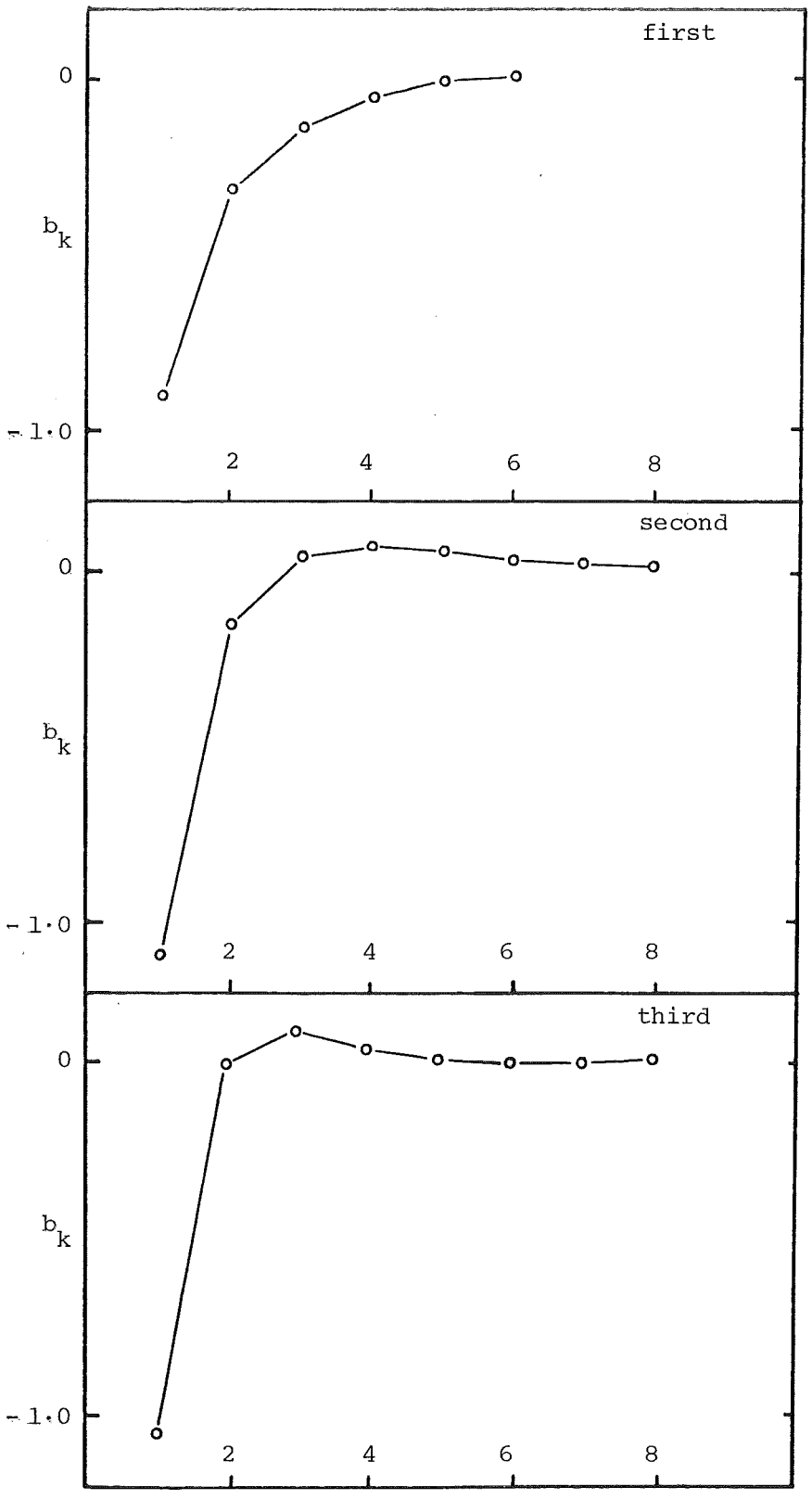

Figure 3.1(f): Interface spectra for the 3 lowest solutions with $\rho = 1{\cdot}05$, $\varepsilon = {\cdot}015$, $\mu = {\cdot}3192$, $S_{max} = {\cdot}06$.

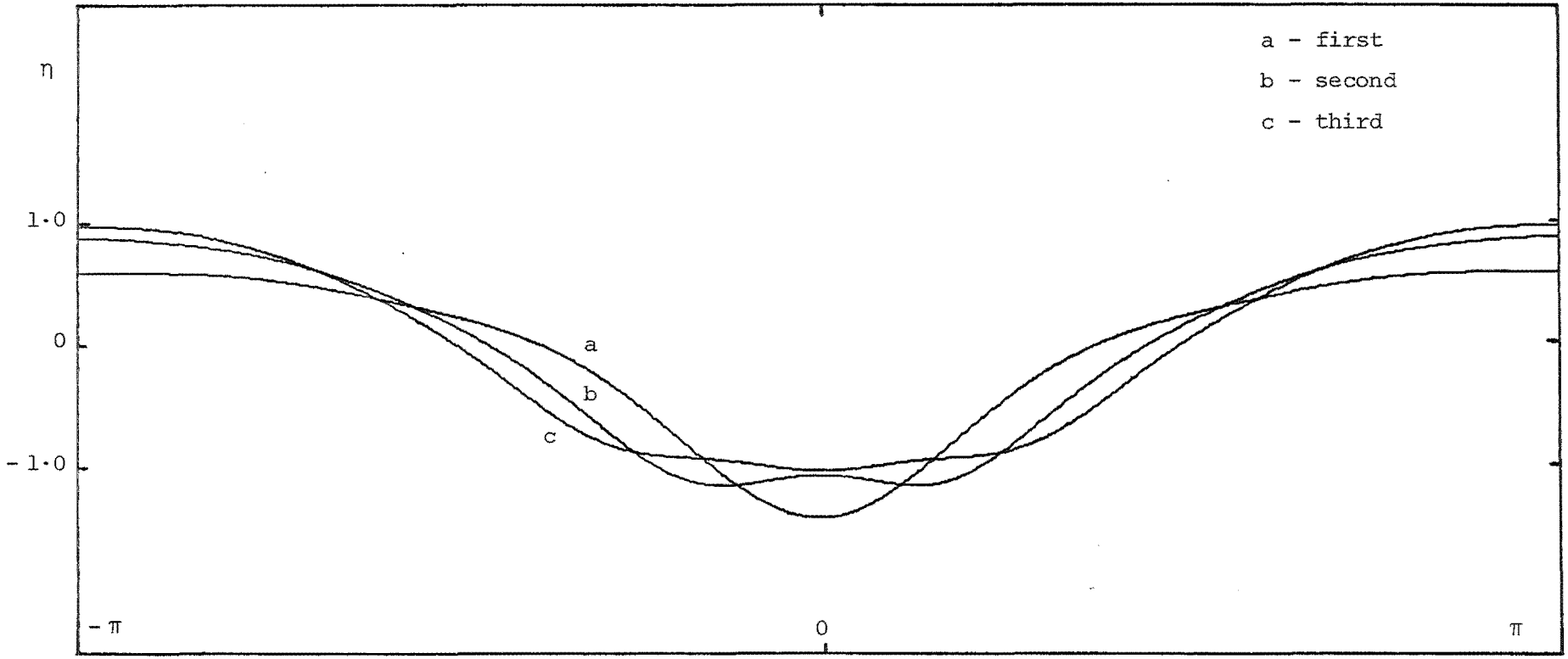

Figure 3.1(g): Interface displacements for the 3 lowest solutions with $\rho = 1{\cdot}05$, $\varepsilon = {\cdot}015$, $\mu = {\cdot}3192$, $S_{max} = {\cdot}06$. The vertical magnification is 75.

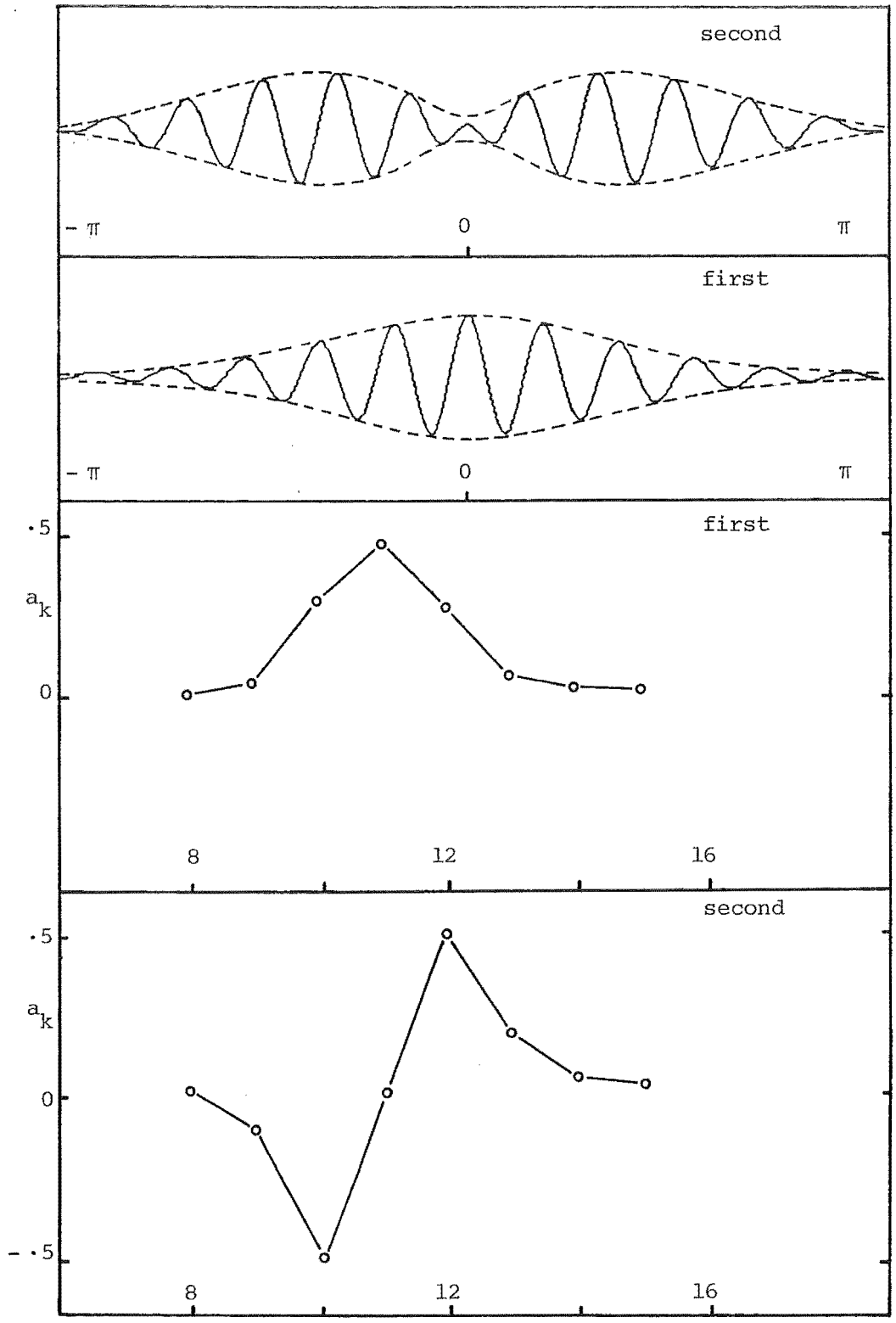

Figure 3.2(a): Free surface wave groups (top) and surface spectra for the 2 lowest solutions with $\rho = 1{\cdot}05$, $\varepsilon = {\cdot}005$, $\mu = 1{\cdot}354$, $S_{max} = {\cdot}04$. The vertical magnification for the wave groups is 30.

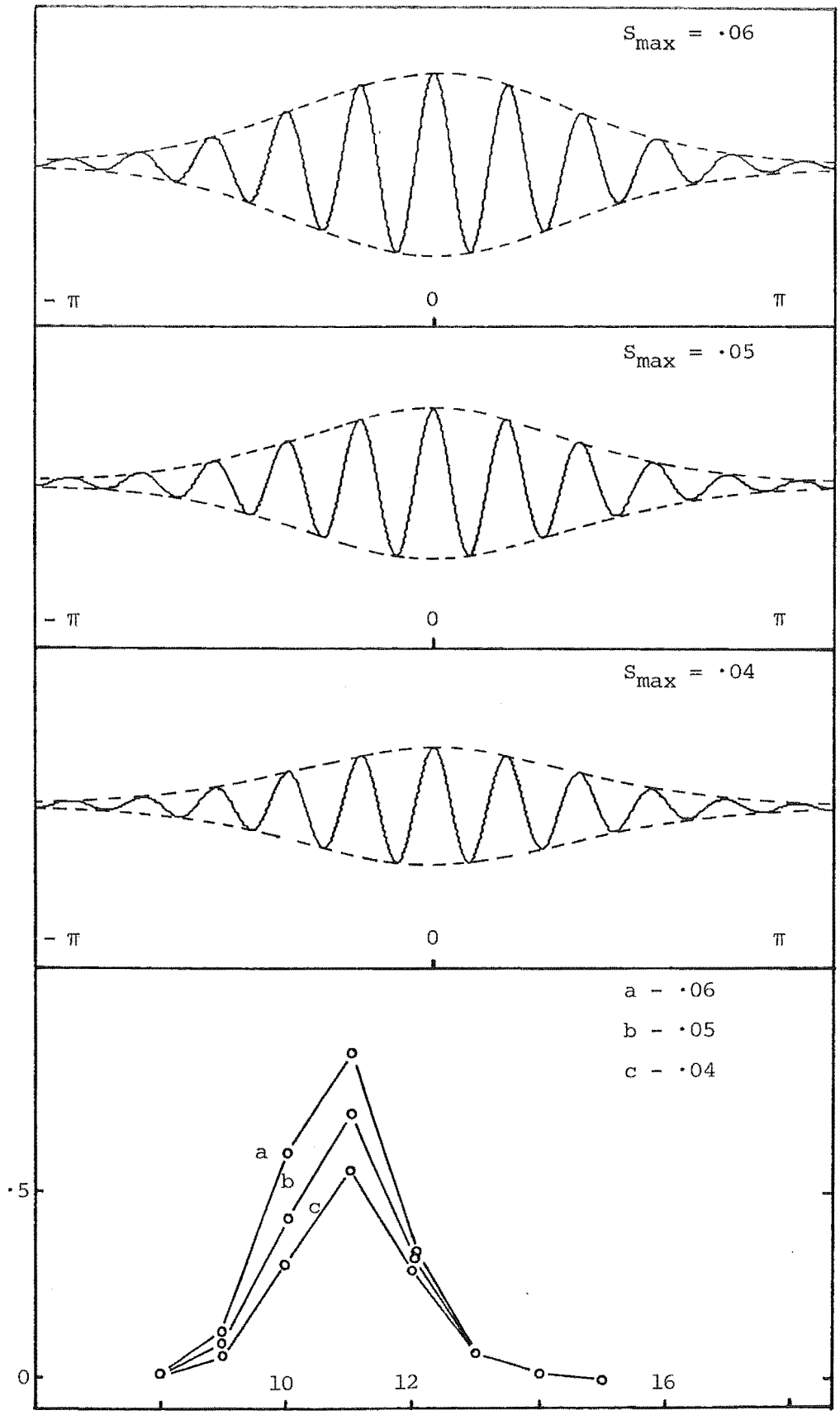

Figure 3.2(b): Free surface wave groups and surface spectra for the lowest solutions with $\rho = 1{\cdot}05$, $\varepsilon = {\cdot}005$, $\mu = 1{\cdot}354$, $S_{max} = {\cdot}04, {\cdot}05, {\cdot}06$. The vertical magnification of the wave groups is 30.

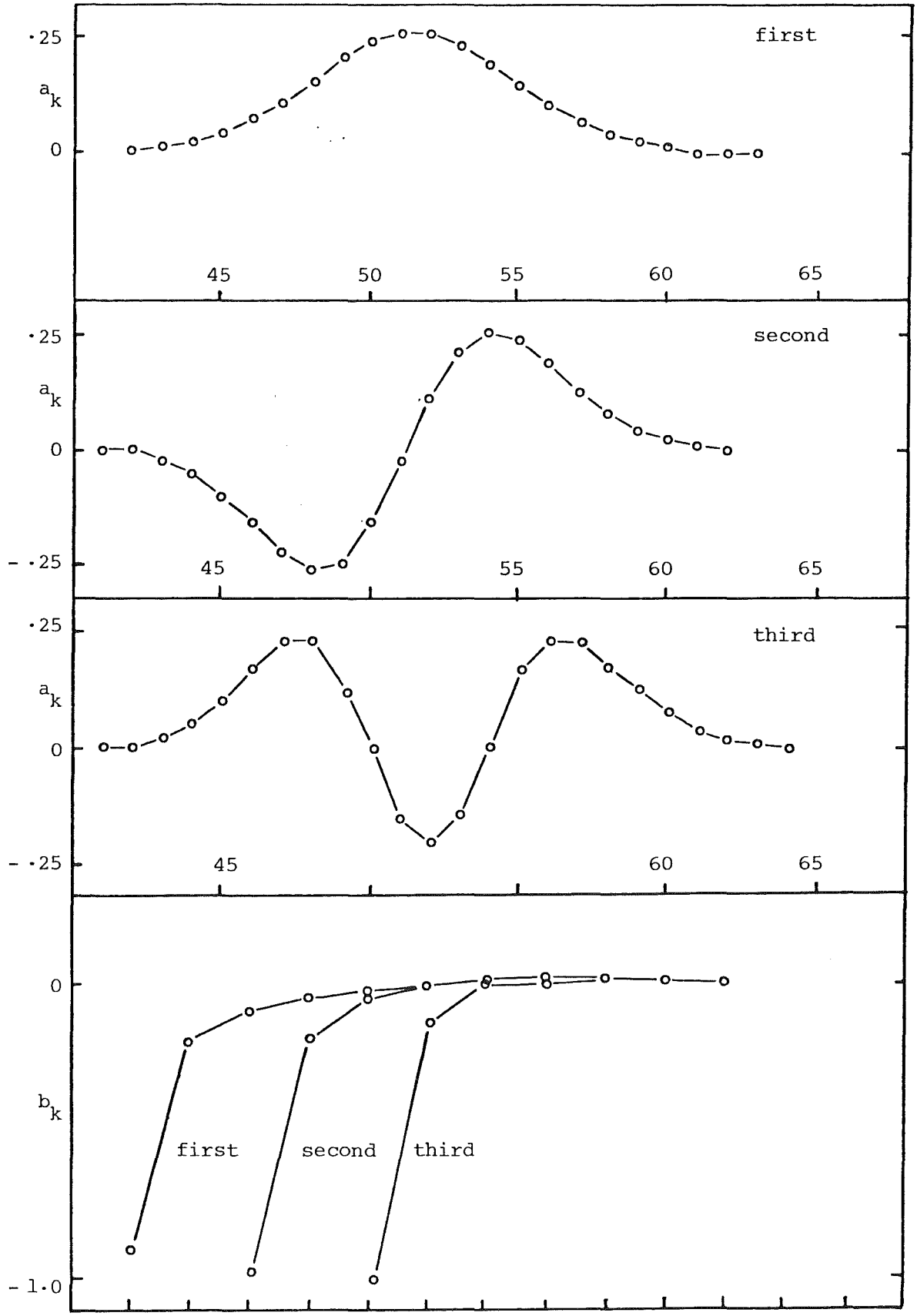

Figure 3.3(a): Surface (top) and interface spectra for the 3 lowest solutions with $\rho = 1{\cdot}02$, $\varepsilon = 0{\cdot}01$, $\mu = {\cdot}3096$, $S_{max} = {\cdot}04$.

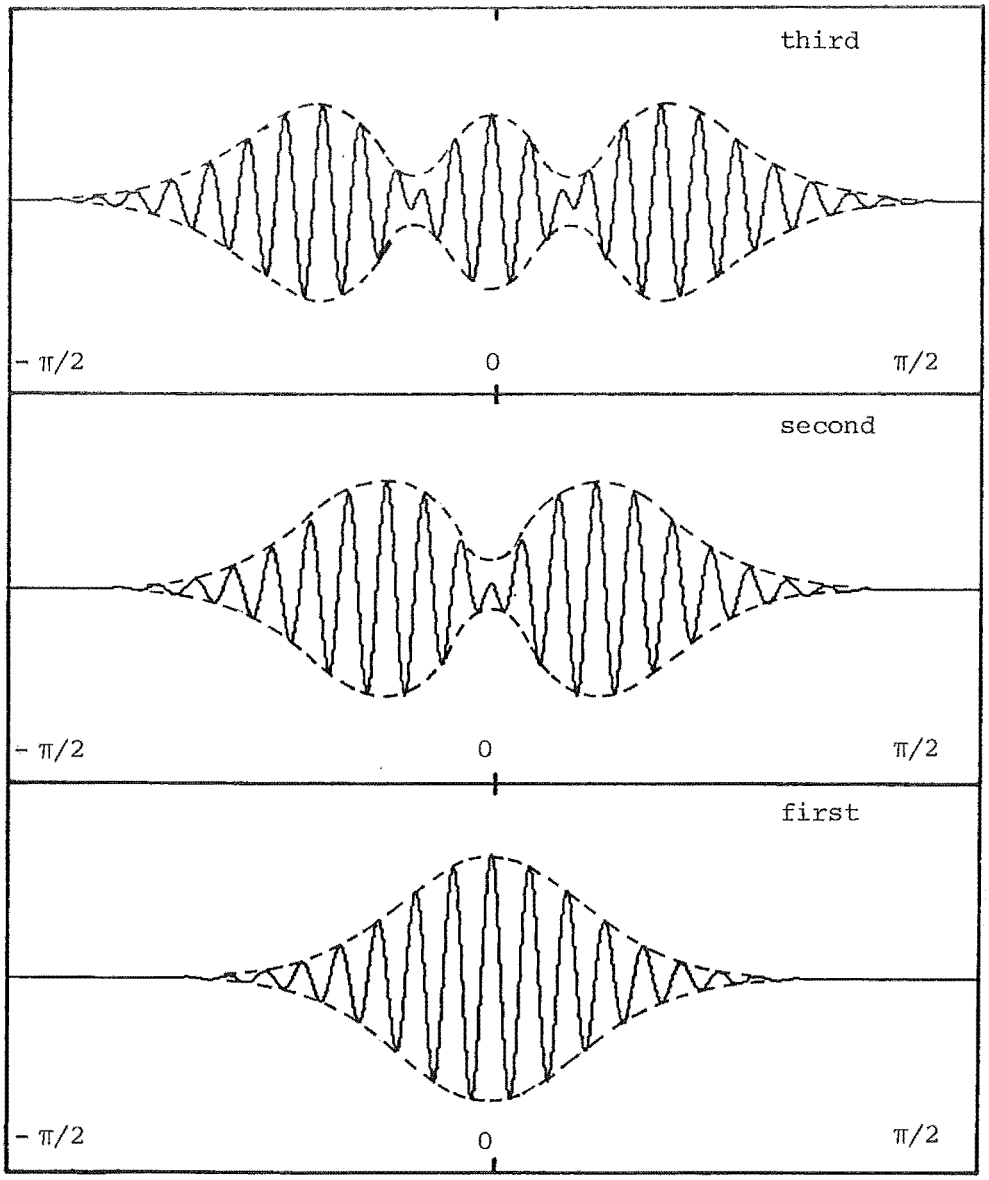

Figure 3.3(b): Free surface wave groups for the 3 lowest solutions with $\rho = 1{\cdot}02$, $\varepsilon = {\cdot}01$, $\mu = {\cdot}3096$, $S_{max} = {\cdot}04$. The vertical magnification is 30.

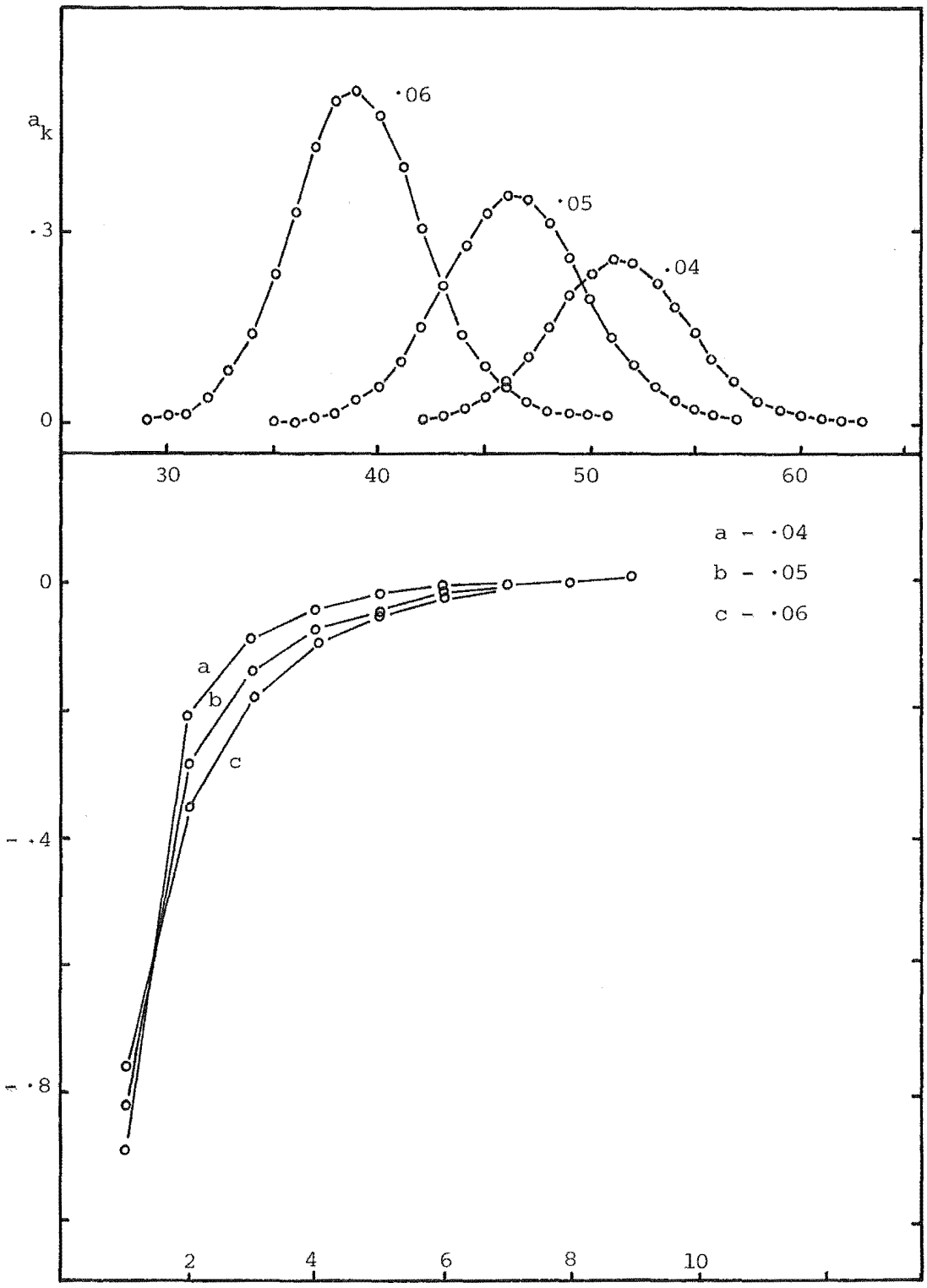

Figure 3.3(c): Surface and interface spectra for the lowest solution with $\rho = 1{\cdot}02$, $\varepsilon = {\cdot}01$, $\mu = {\cdot}3096$, $S_{max} = {\cdot}04, {\cdot}05, {\cdot}06$.

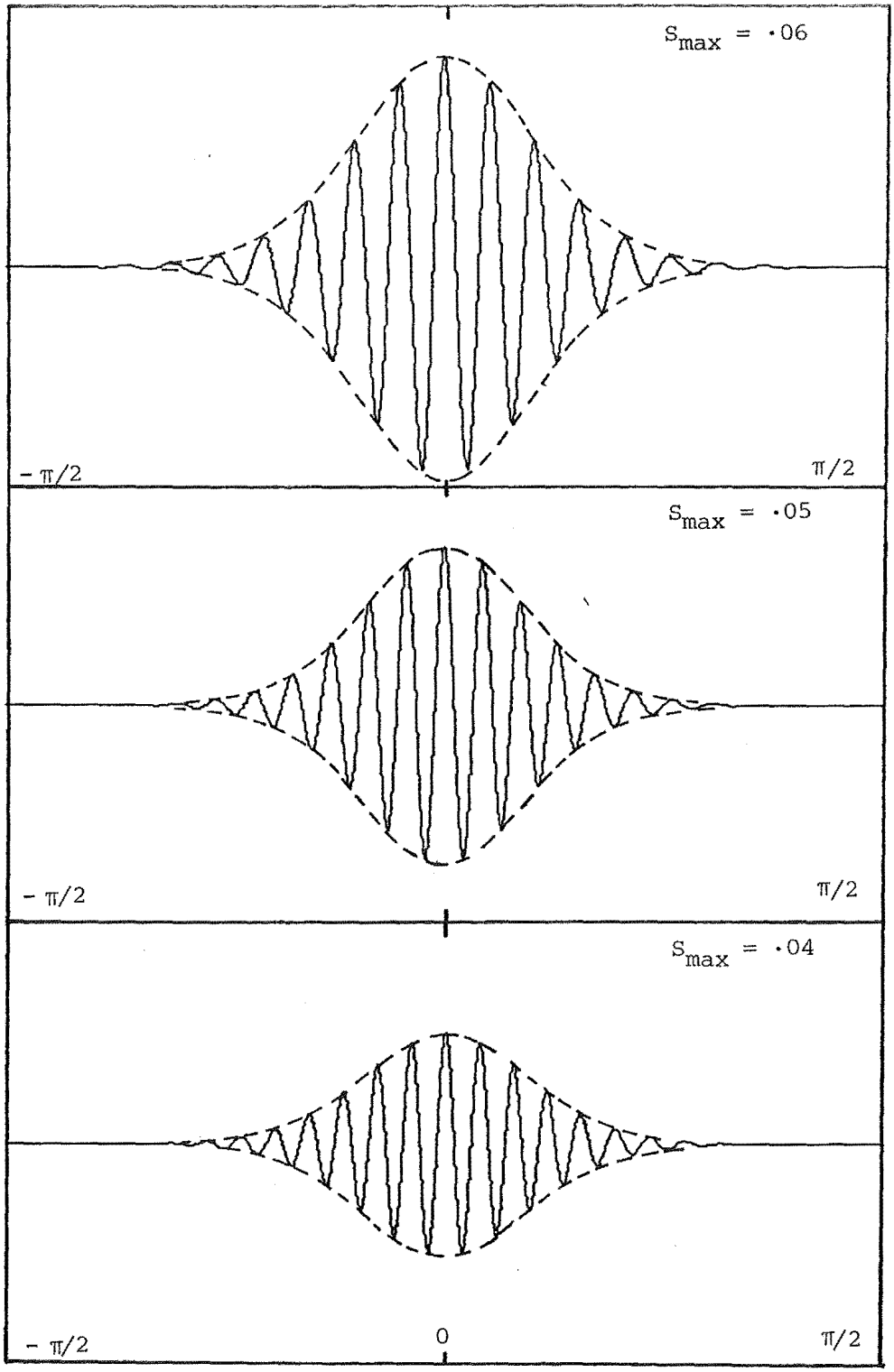

Figure 3.3(d); Free surface wave groups for the lowest solution with ρ = 1·02, ε = ·01, μ = ·3096, S_{max} = ·04, ·05, ·06. The vertical magnification is 30.

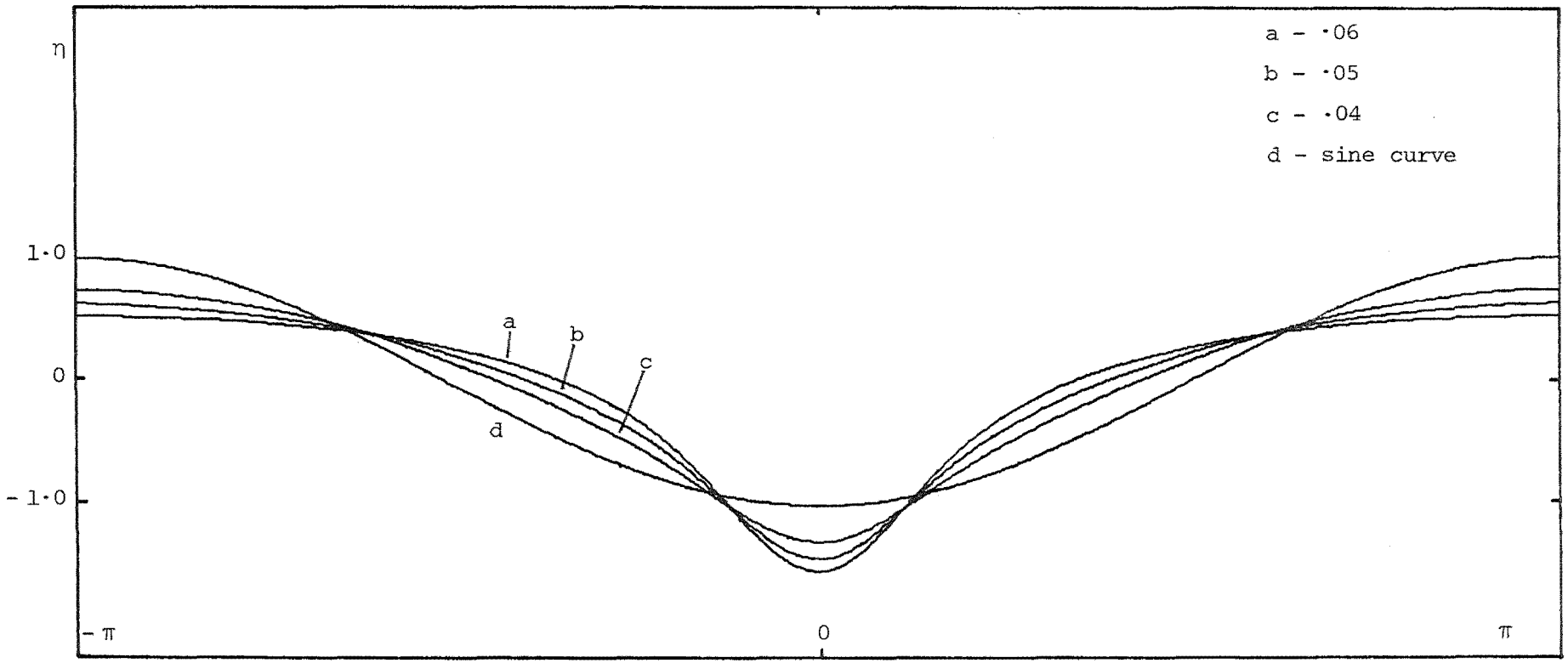

Figure 3.3(e): Interface displacements and sine curve for the lowest solution with $\rho = 1{\cdot}02$, $\varepsilon = {\cdot}01$, $\mu = {\cdot}3096$, $S_{max} = {\cdot}04, {\cdot}05, {\cdot}06$. The vertical magnification is 75.

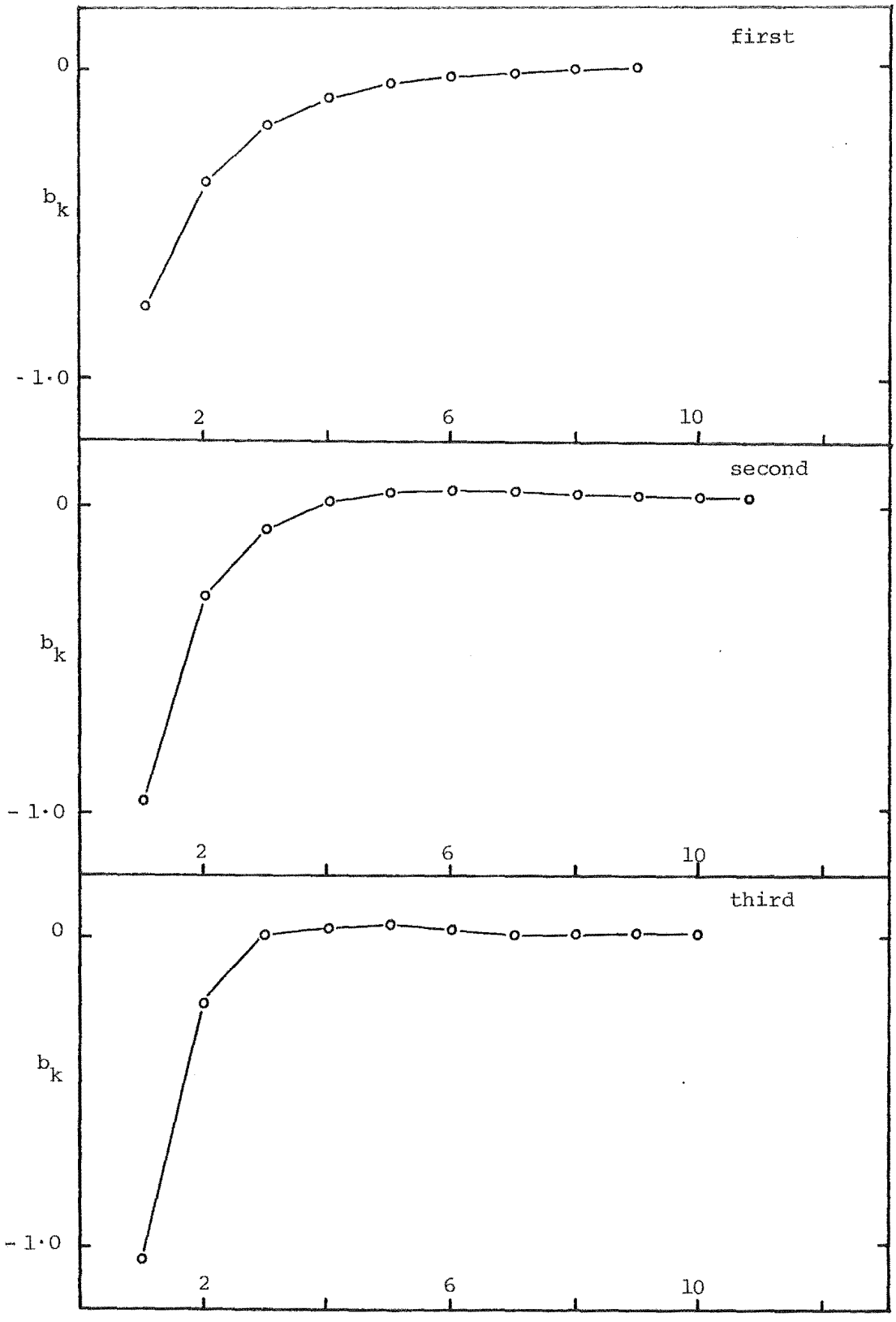

Figure 3.3(f): Interface spectra for the 3 lowest solutions with $\rho = 1{\cdot}02$, $\varepsilon = {\cdot}01$, $\mu = {\cdot}3096$, $S_{max} = {\cdot}06$.

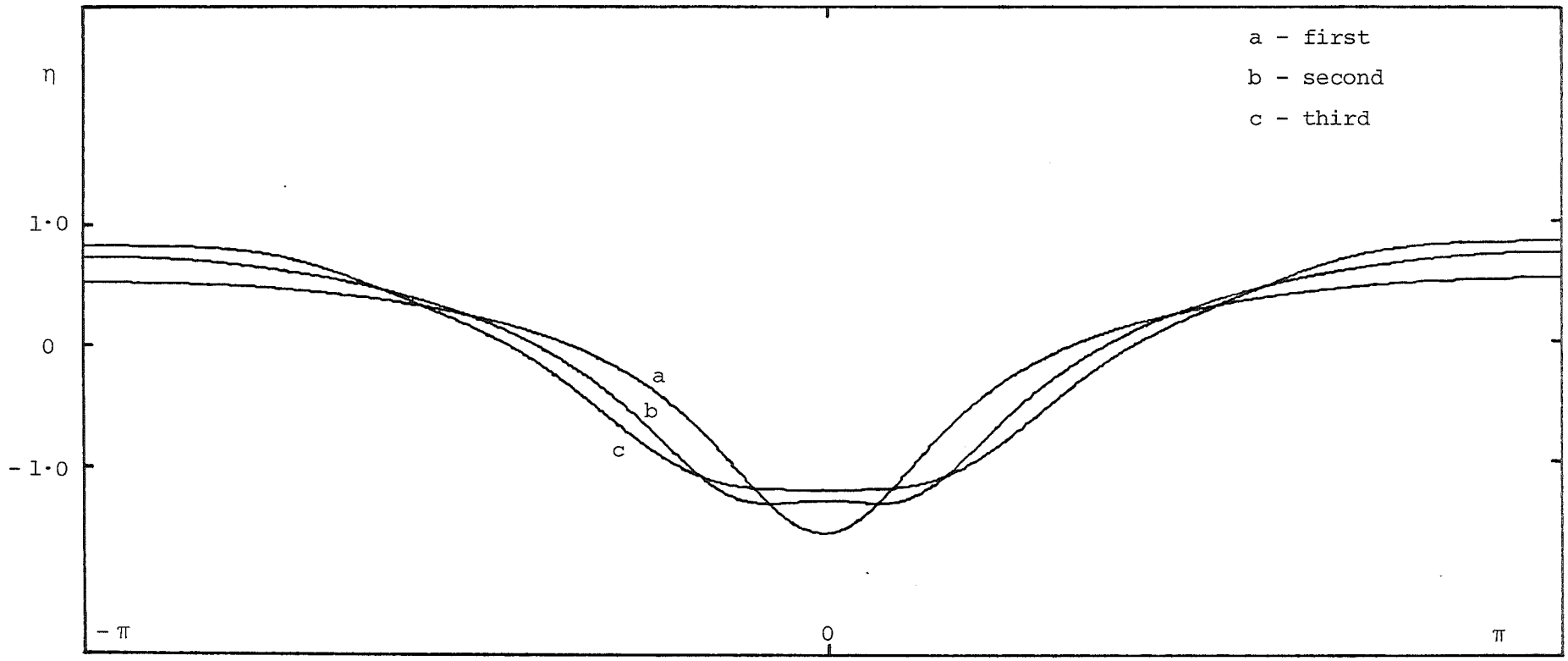

Figure 3.3(g): Interface displacement for the 3 lowest solutions with $\rho = 1{\cdot}02$, $\varepsilon = {\cdot}01$, $\mu = {\cdot}3096$, $S_{max} = {\cdot}06$. The vertical magnification is 75.

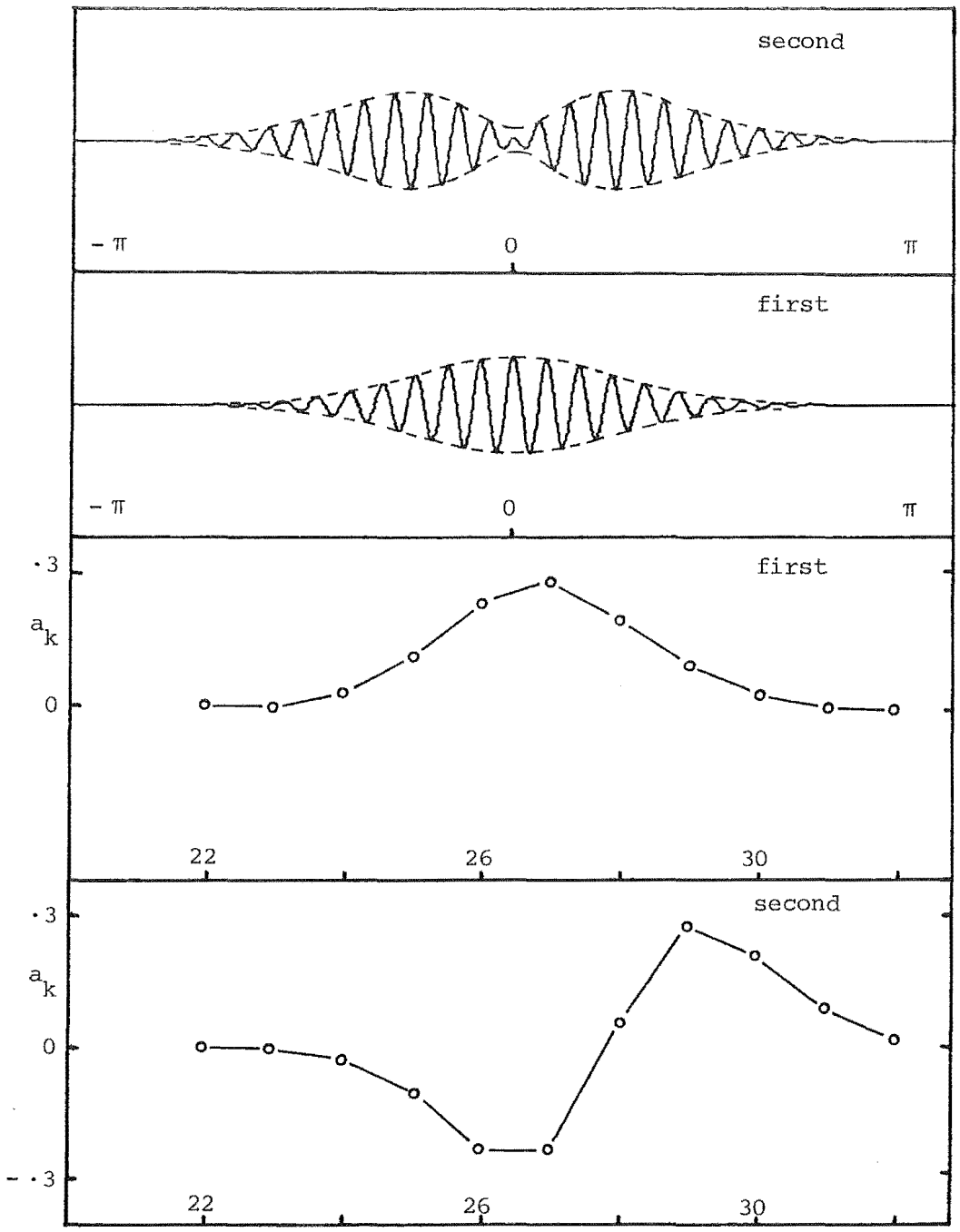

Figure 3.4(a): Free surface wave groups (top) and surface spectra for the 2 lowest solutions with $\rho = 1{\cdot}02$, $\varepsilon = {\cdot}004$, $\mu = 1{\cdot}373$, $S_{max} = {\cdot}04$. The vertical magnification of the wave groups is 30.

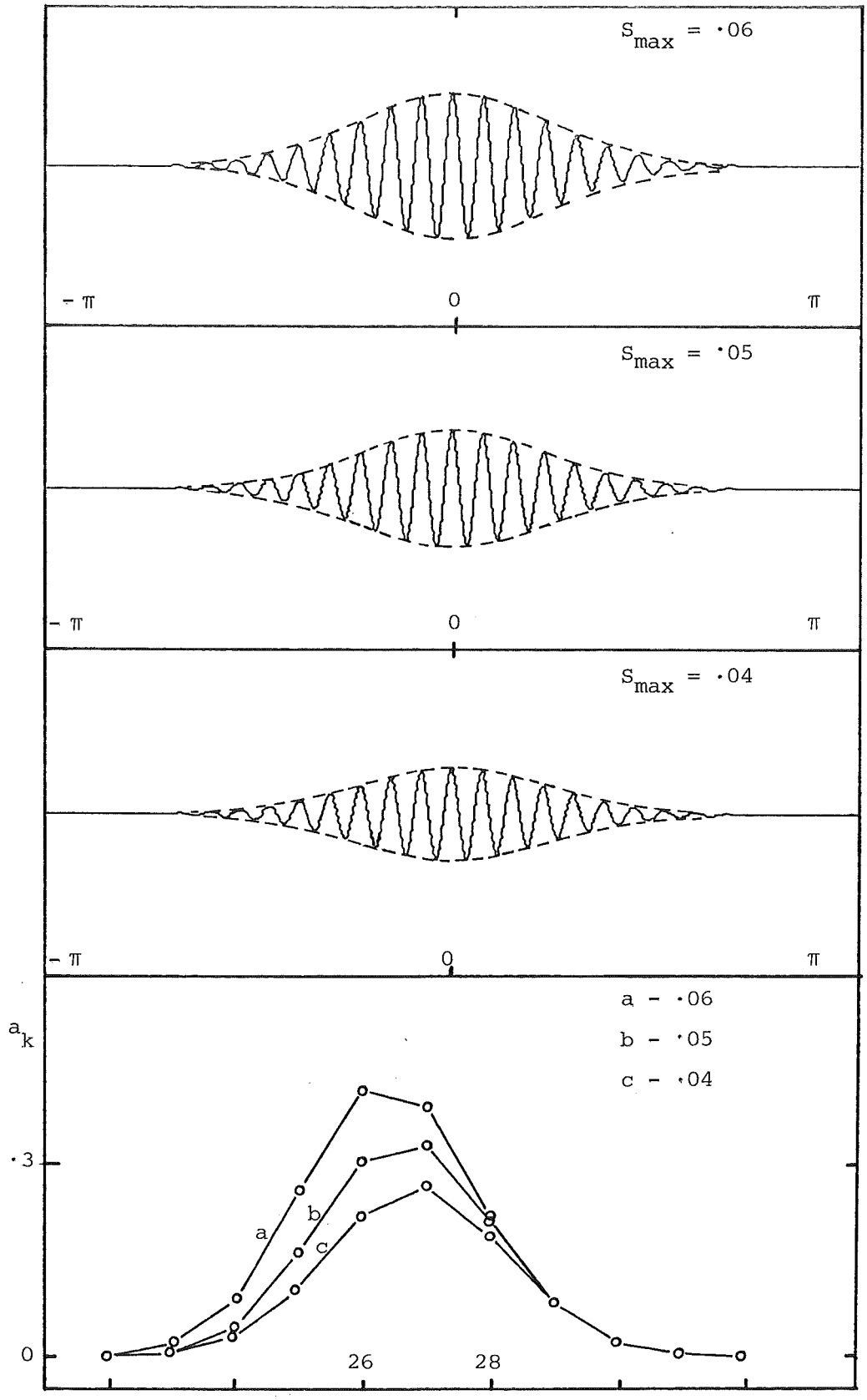

Figure 3.4(b): Free surface wave groups and surface spectra for the lowest solution with $\rho = 1{\cdot}02$, $\varepsilon = {\cdot}004$, $\mu = 1{\cdot}373$, $S_{max} = {\cdot}04, {\cdot}05, {\cdot}06$. The vertical magnification of the wave groups is 30.

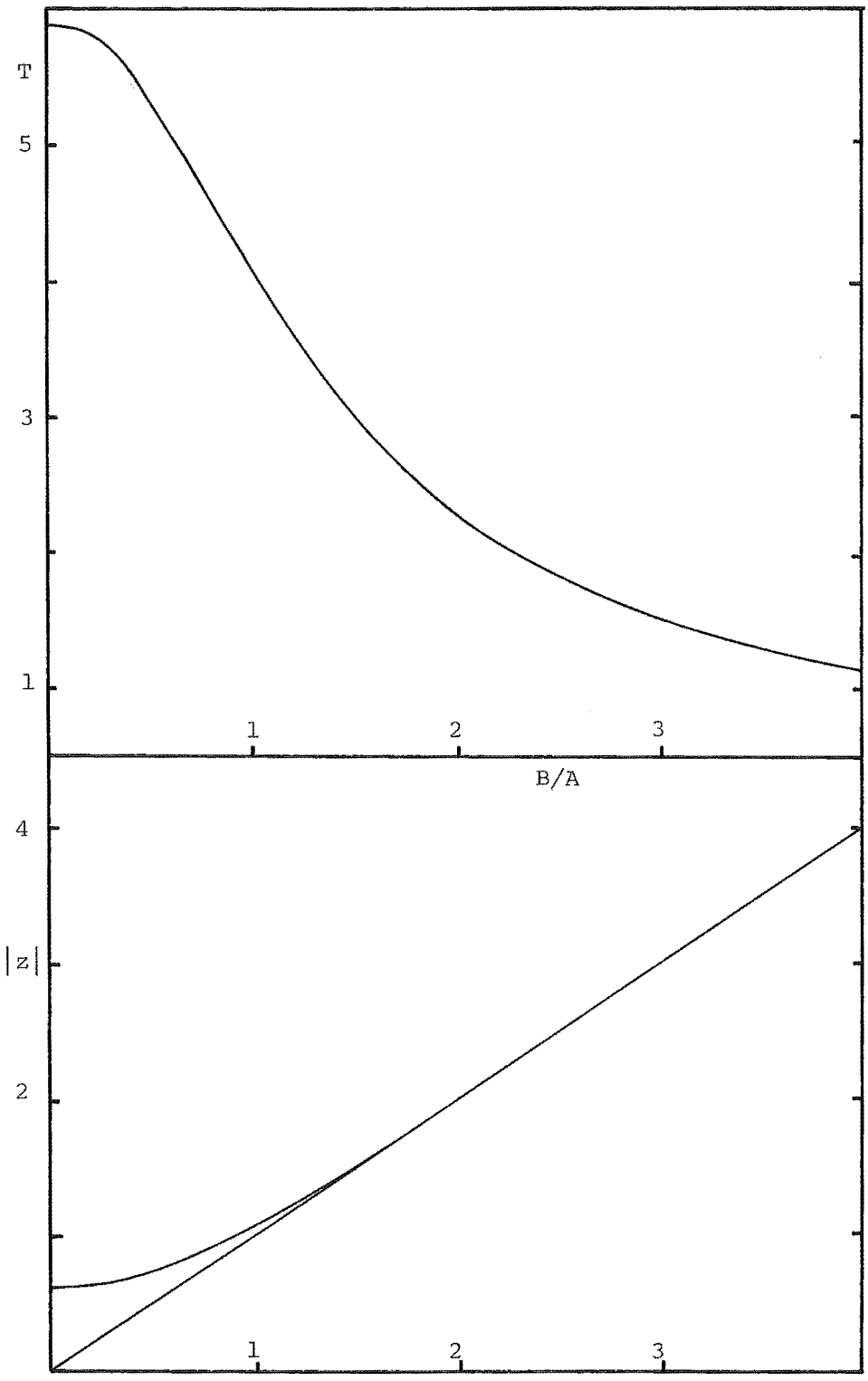

Figures 4.1(a),(b): Period of the energy oscillation (top) and the bounds in $|z|$ for the unsteady three wave solution with $\rho = 1{\cdot}05$, $\varepsilon = {\cdot}015$, $\mu = {\cdot}3096$, $A = 1{\cdot}0$.

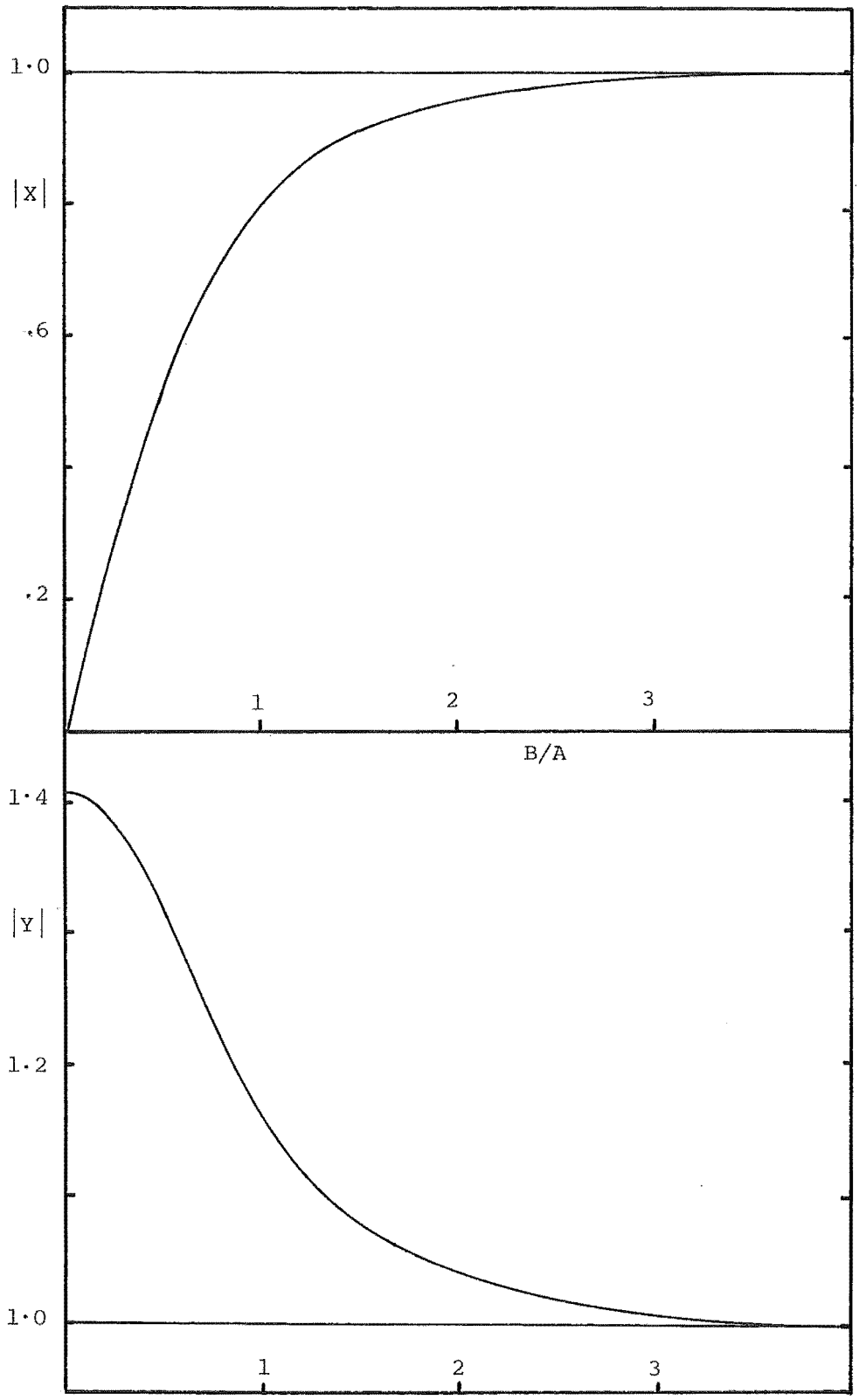

Figure 4.1(c),(d): Bounds on $|X|$ (top) and $|Y|$ for the three wave solution with $\rho = 1{\cdot}05$, $\varepsilon = {\cdot}015$, $\mu = {\cdot}3096$, $A = 1{\cdot}0$.

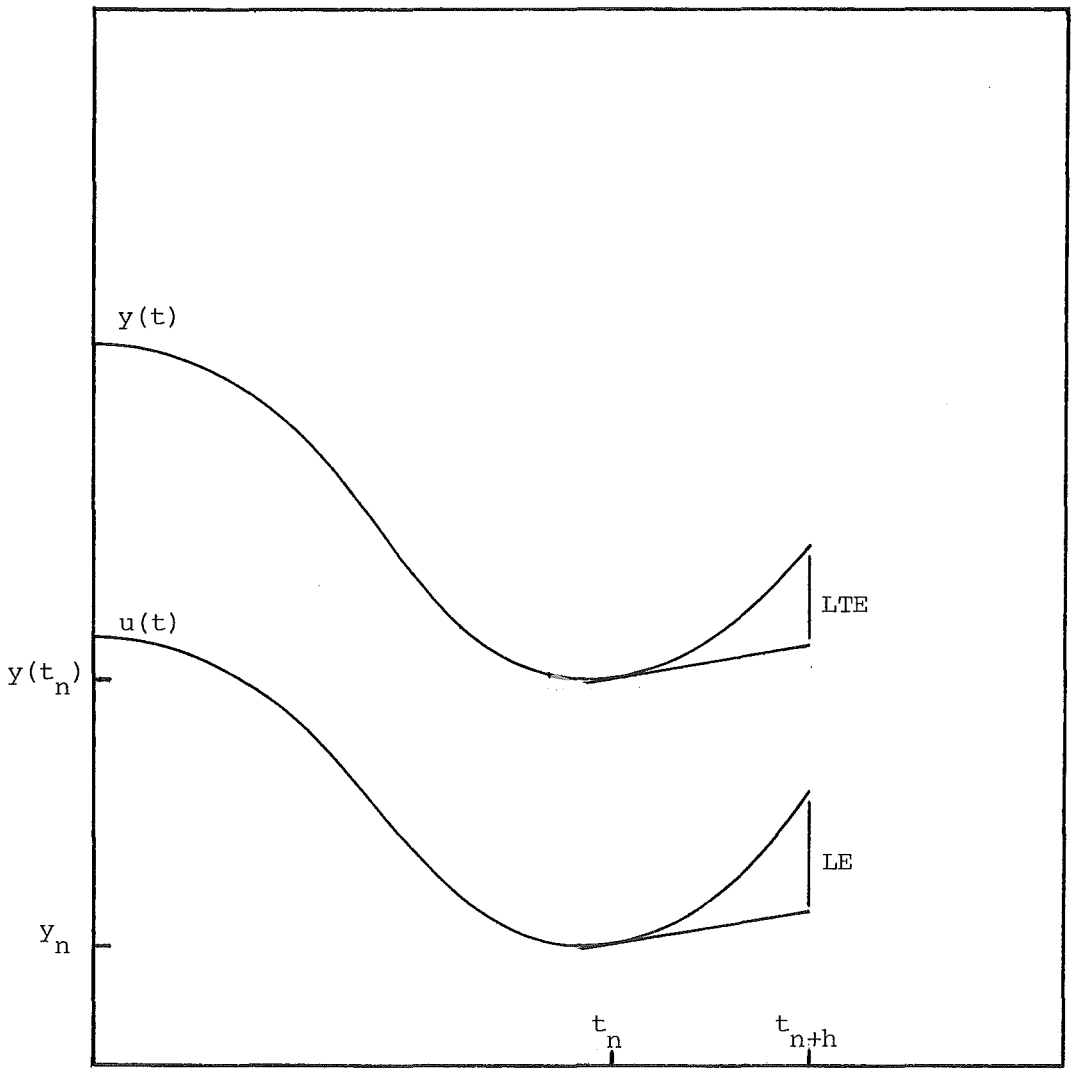

Figure 4.2(a): Relationship between the local truncation error and the local error in the integration of the initial value problem 4.3.2. LTE - local truncation error, LE - local error.

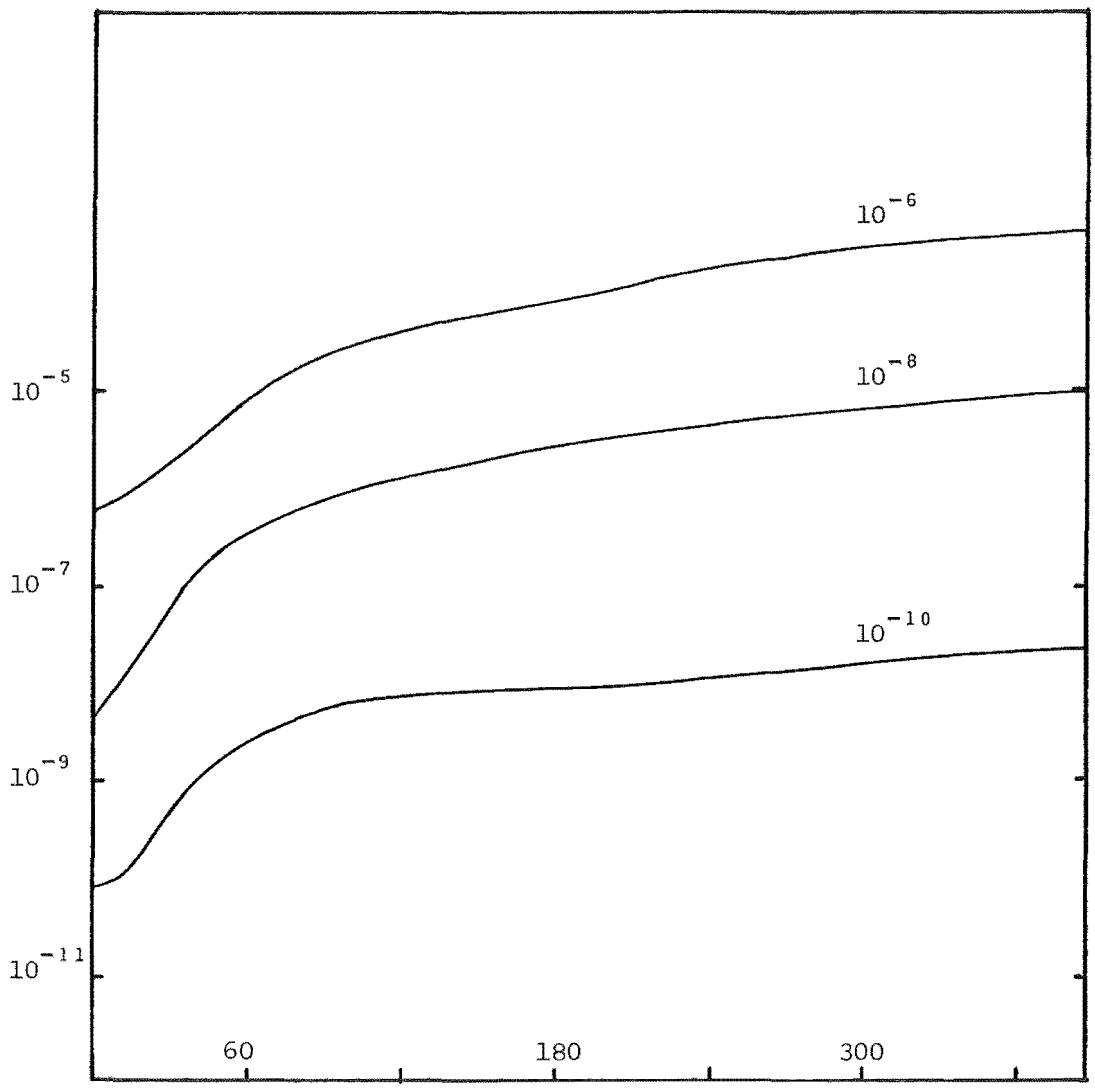

Figure 4.2(b): Global error vs τ for the three wave solution with $\rho = 1{\cdot}05$, $\varepsilon = {\cdot}015$, $\mu = {\cdot}31$, $A = 1$ and local error tolerances 10^{-6}, 10^{-8}, 10^{-10}.

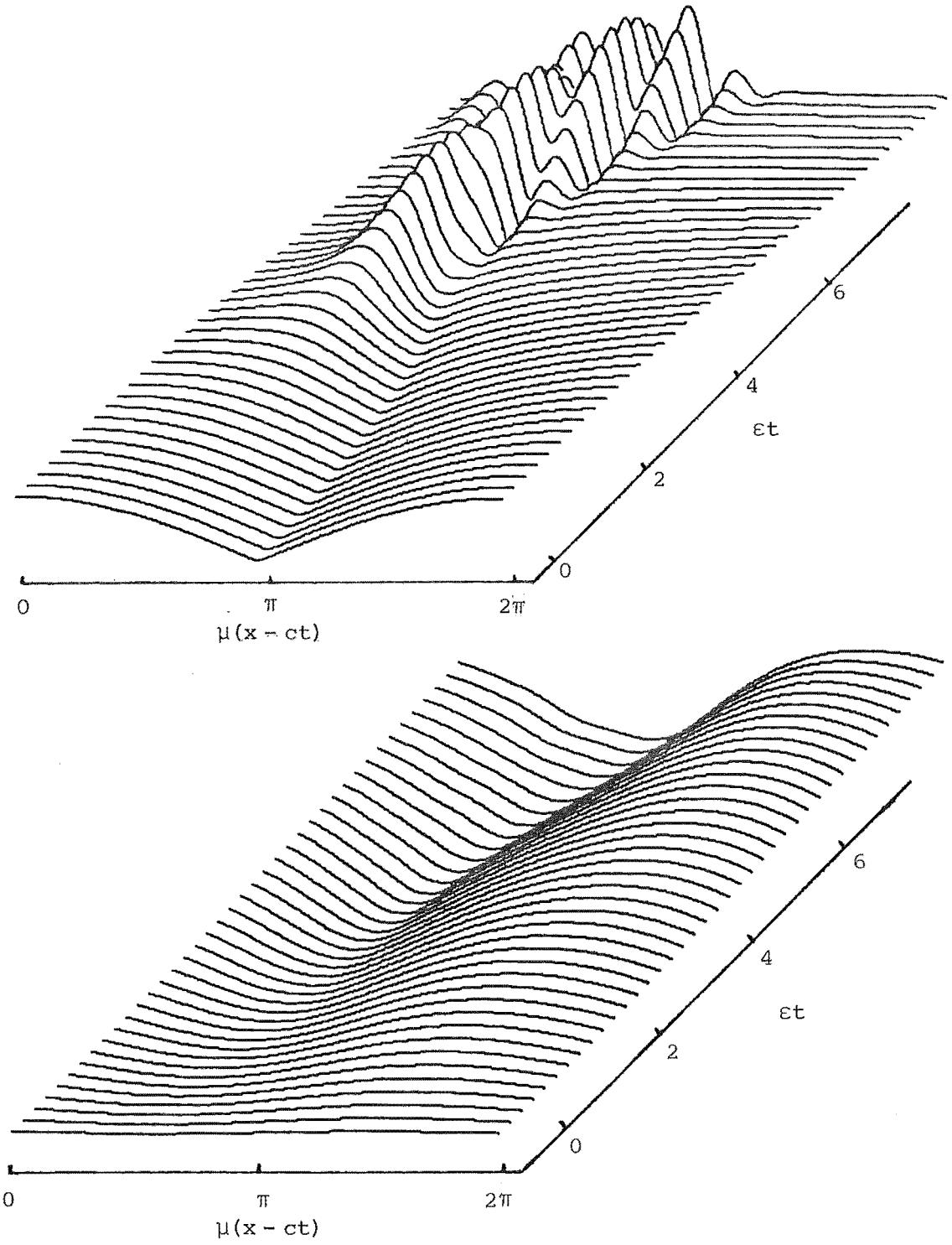

Figure 4.3(a): One wavelength of the surface envelope (top) and interface displacement for $\tau = 0 - 9$ with $\rho = 1{\cdot}05$, $\varepsilon = {\cdot}015$, $\mu = {\cdot}3192$ and the first set of initial conditions.
The vertical magnification is 25.

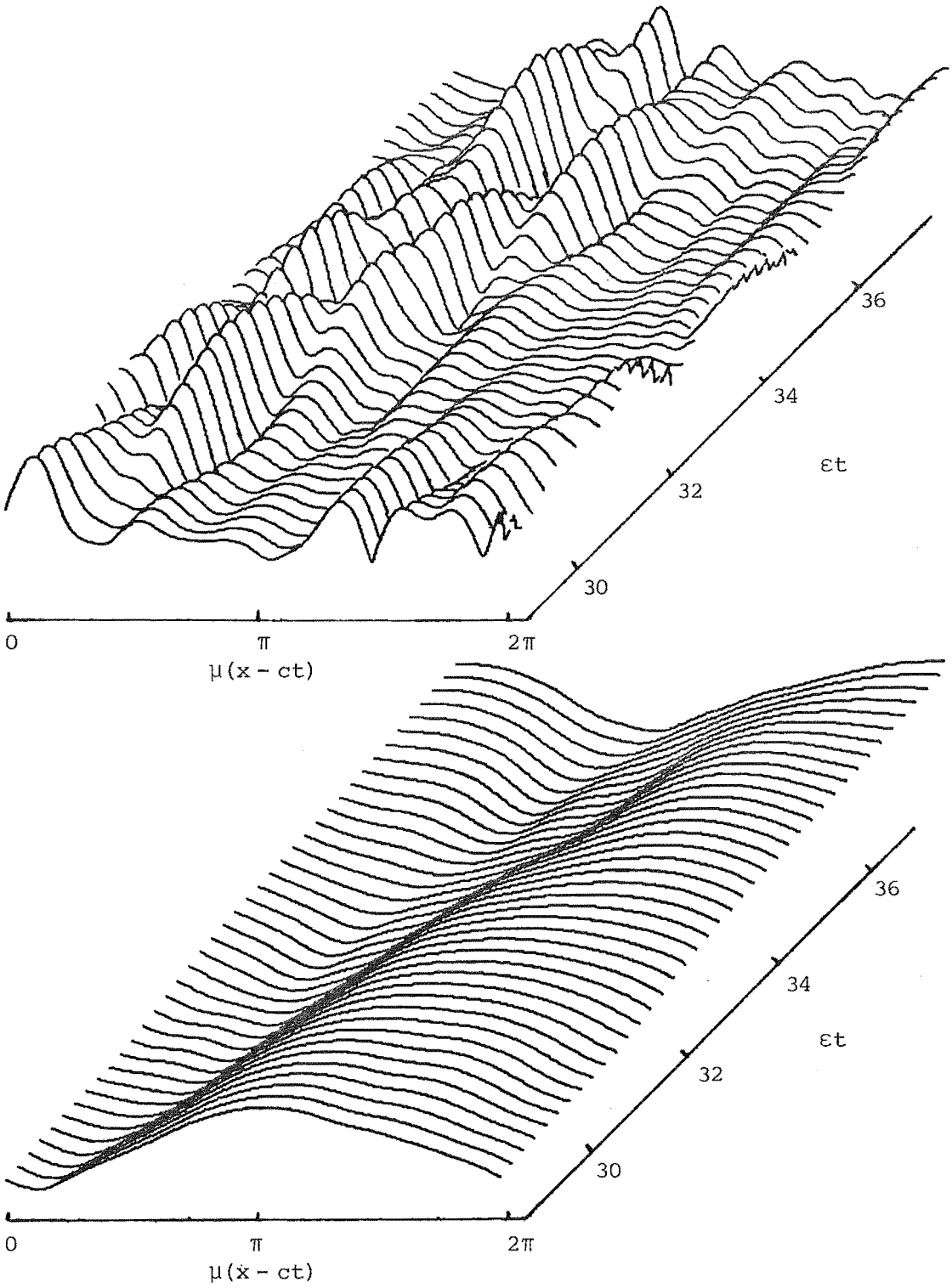

Figure 4.3(b): One wavelength of the surface envelope (top) and interface displacement for $\tau = 30 - 39$ with $\rho = 1{\cdot}05$, $\varepsilon = {\cdot}015$, $\mu = {\cdot}3192$ and the first set of initial conditions.
The vertical magnification is 25.

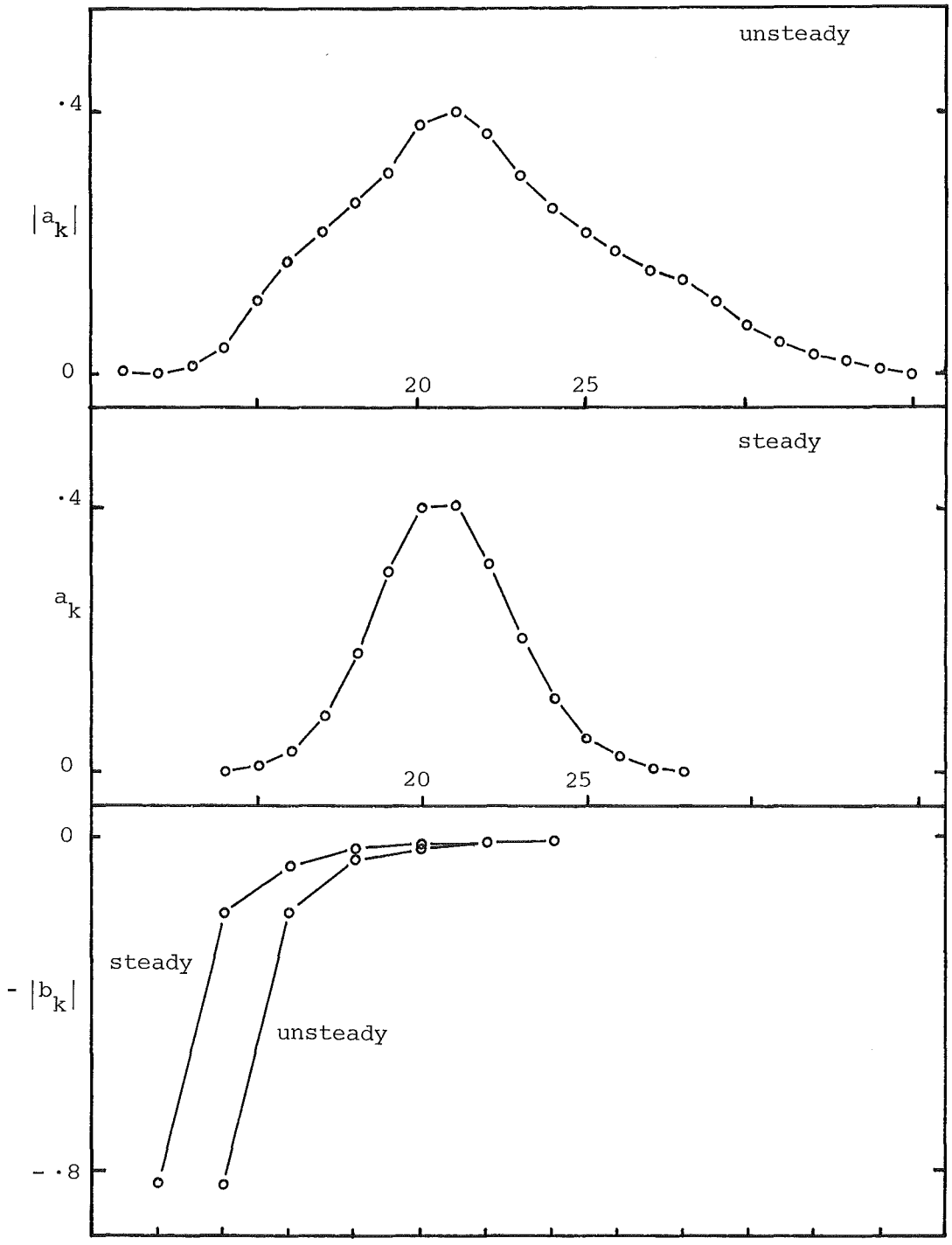

Figure 4.3(c): Averaged unsteady and lowest steady spectra for $\rho = 1{\cdot}05$, $\mu = {\cdot}3192$, $\varepsilon = {\cdot}015$ and the first set of initial conditions.

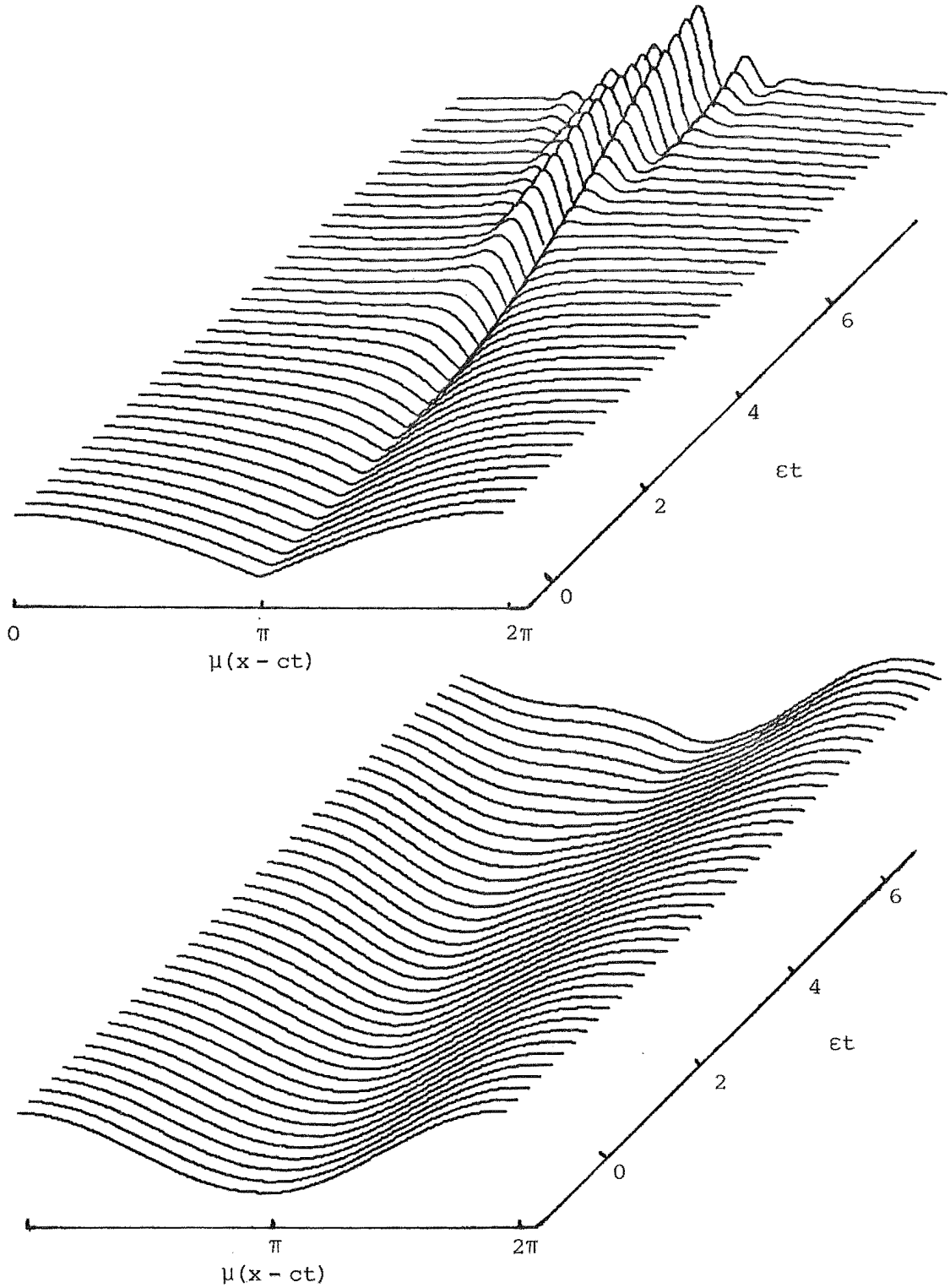

Figure 4.3(d): One wavelength of the surface envelope (top) and interface displacement for $\tau = 0 \cdot 9$ with $\rho = 1 \cdot 05$, $\varepsilon = \cdot 015$, $\mu = \cdot 3192$, and the second set of initial conditions. The vertical magnification is 25.

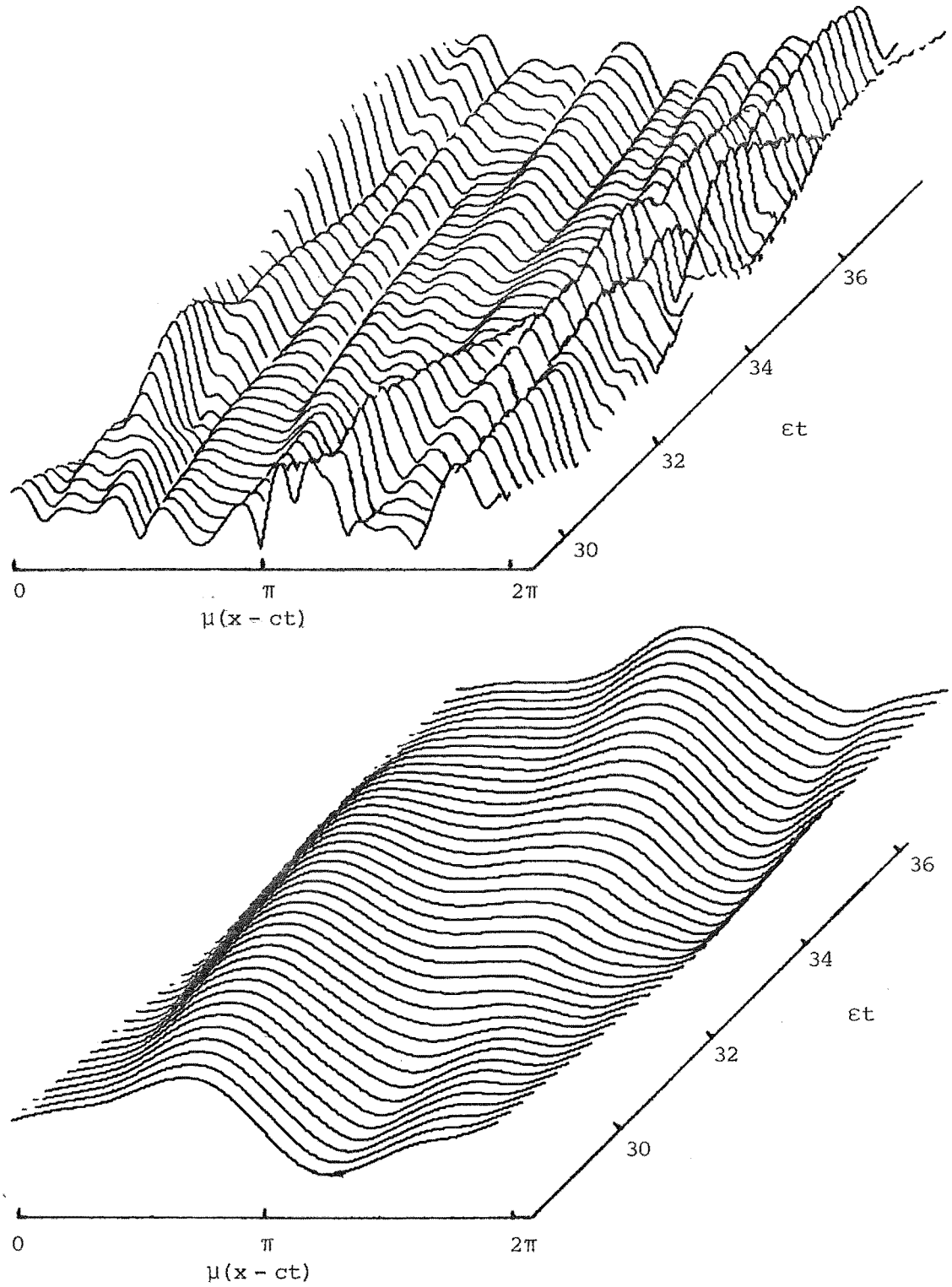

Figure 4.3(e): One wavelength of the surface envelope (top) and interface displacement for $\tau = 30 - 39$ with $\rho = 1{\cdot}05$, $\varepsilon = {\cdot}015$, $\mu = {\cdot}3192$ and the second set of initial conditions.
The vertical magnification is 25.

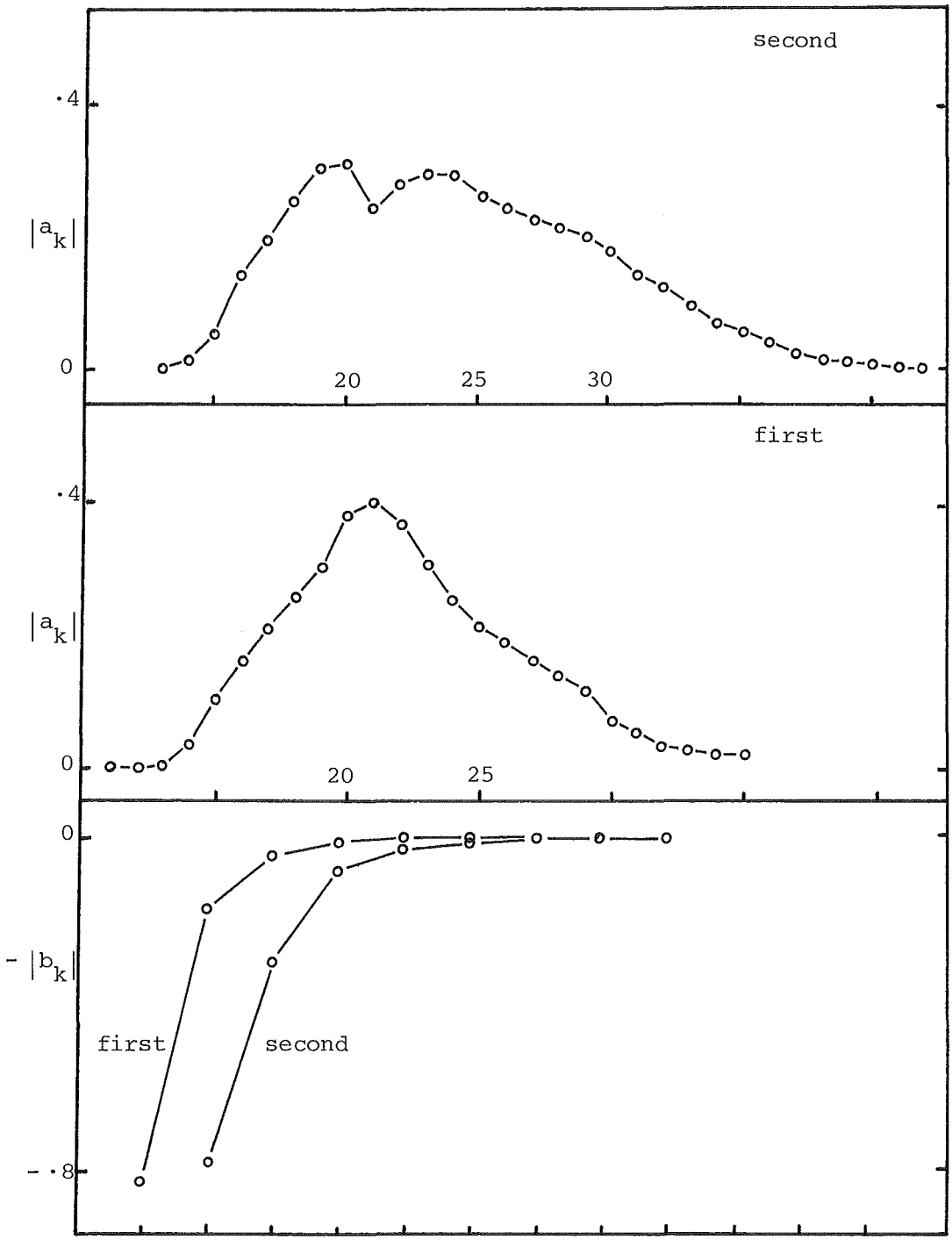

Figure 4.3(f): The averaged unsteady spectra for $\rho = 1{\cdot}05$, $\varepsilon = {\cdot}015$, $\mu = {\cdot}3192$ and the first and second sets of initial conditions.

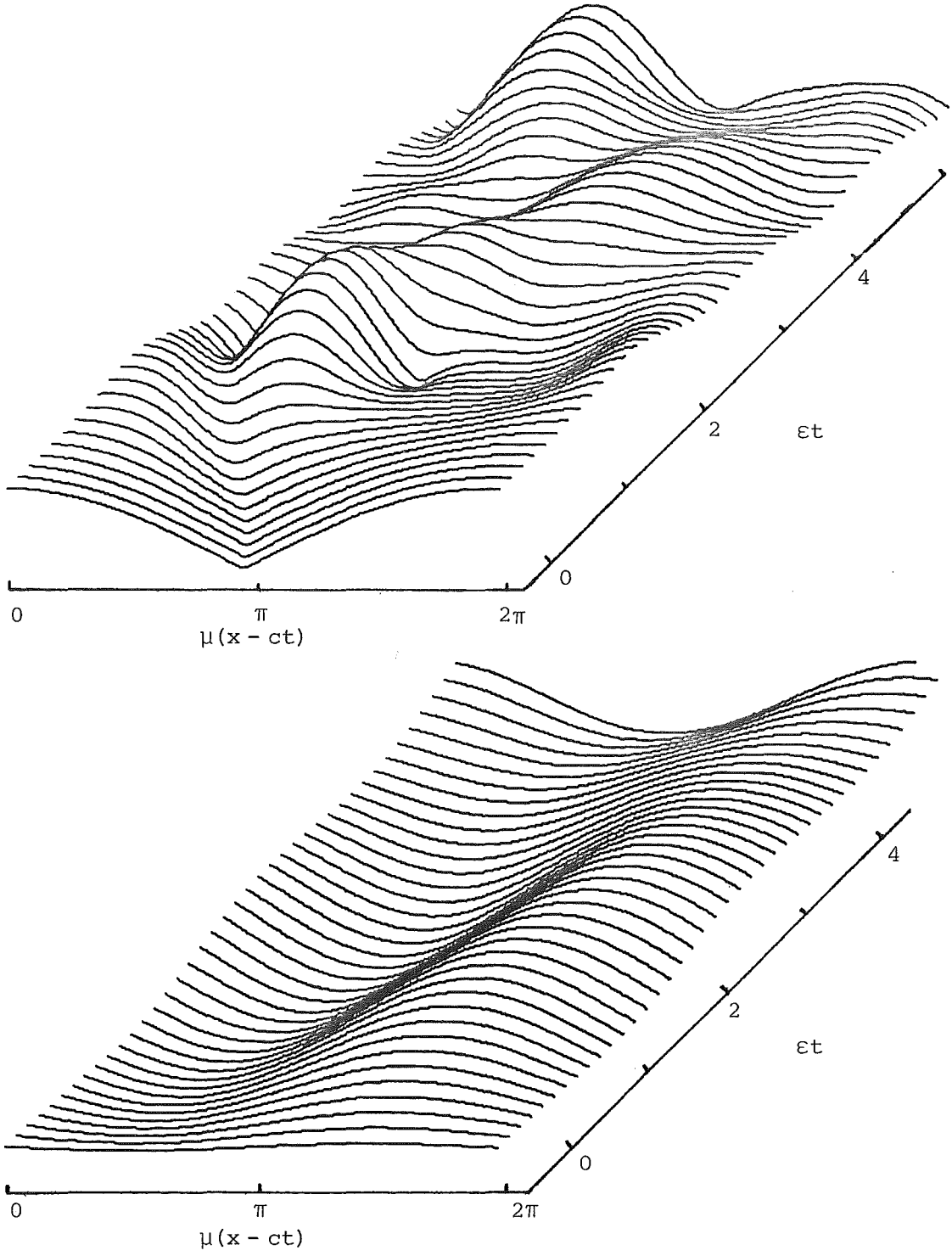

Figure 4.4(a): One wavelength of the surface envelope (top) and the interface displacement for $\tau = 0 - 6$ with $\rho = 1{\cdot}05$, $\varepsilon = {\cdot}005$, $\mu = 1{\cdot}354$ and the first set of initial conditions.
The vertical magnification is 25.

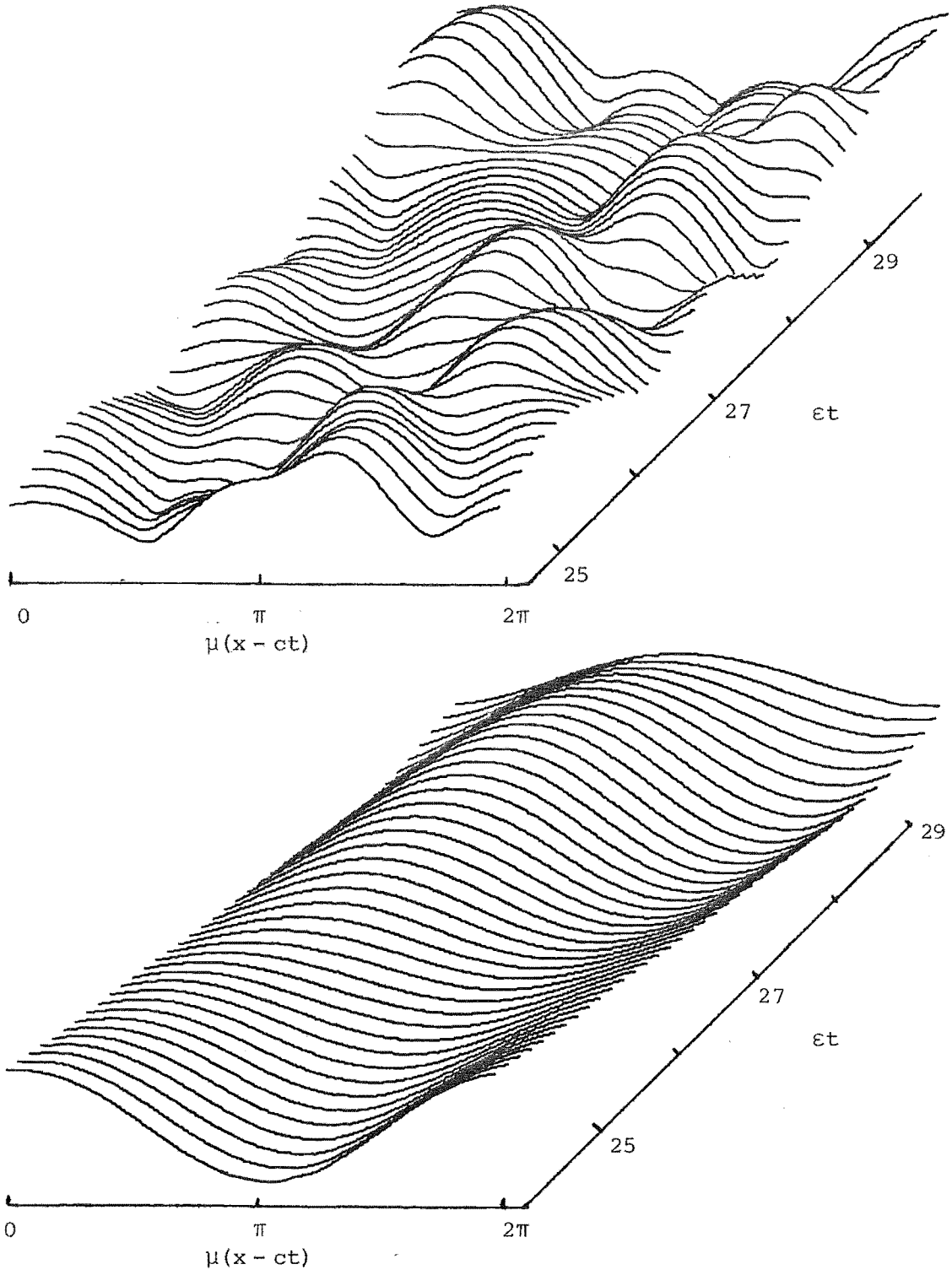

Figure 4.4(b): One wavelength of the surface envelope (top) and the interface displacement for $\tau = 25 - 31$ with $\rho = 1{\cdot}05$, $\varepsilon = {\cdot}005$, $\mu = 1{\cdot}354$ and the first set of initial conditions.
The vertical magnification is 25.

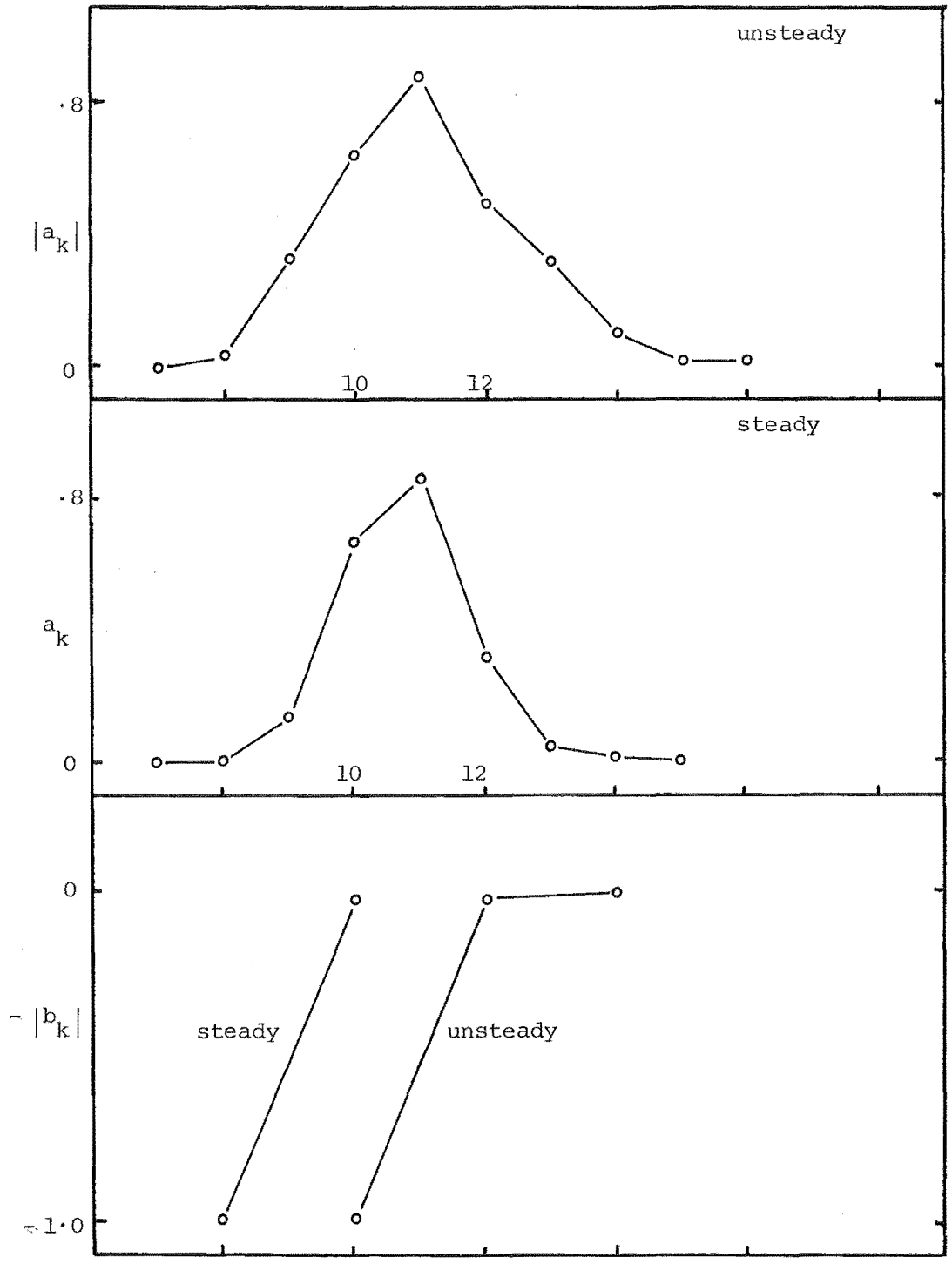

Figure 4.4(c): Averaged unsteady and lowest steady spectra for $\rho = 1{\cdot}05$, $\varepsilon = {\cdot}005$, $\mu = 1{\cdot}354$ and the first set of initial conditions.

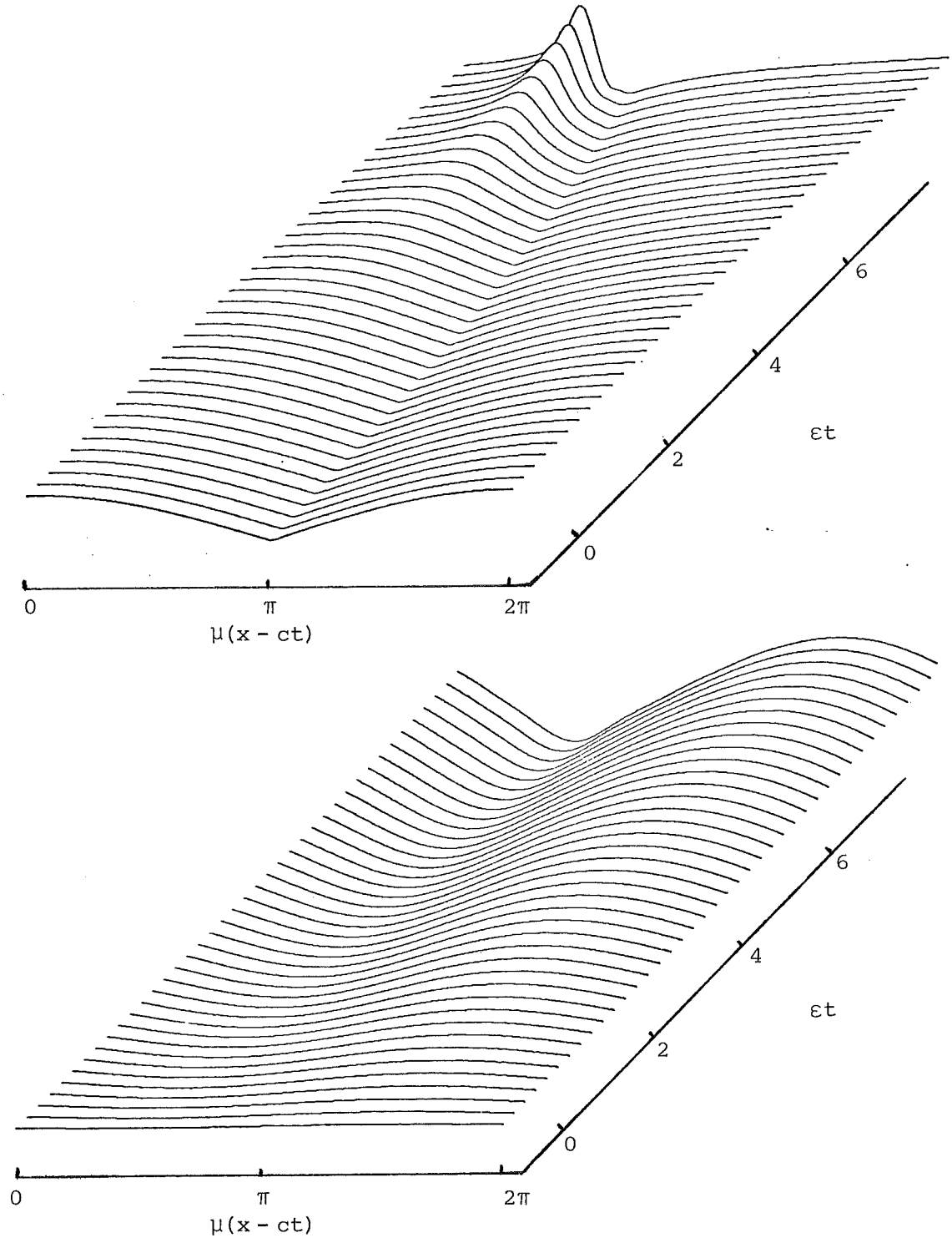

Figure 4.5(a): One wavelength of the surface envelope (top) and interface displacement for $\tau = 0 - 9$ with $\rho = 1{\cdot}02$, $\varepsilon = {\cdot}01$, $\mu = {\cdot}3096$ and the first set of initial conditions. The vertical magnification is 25.

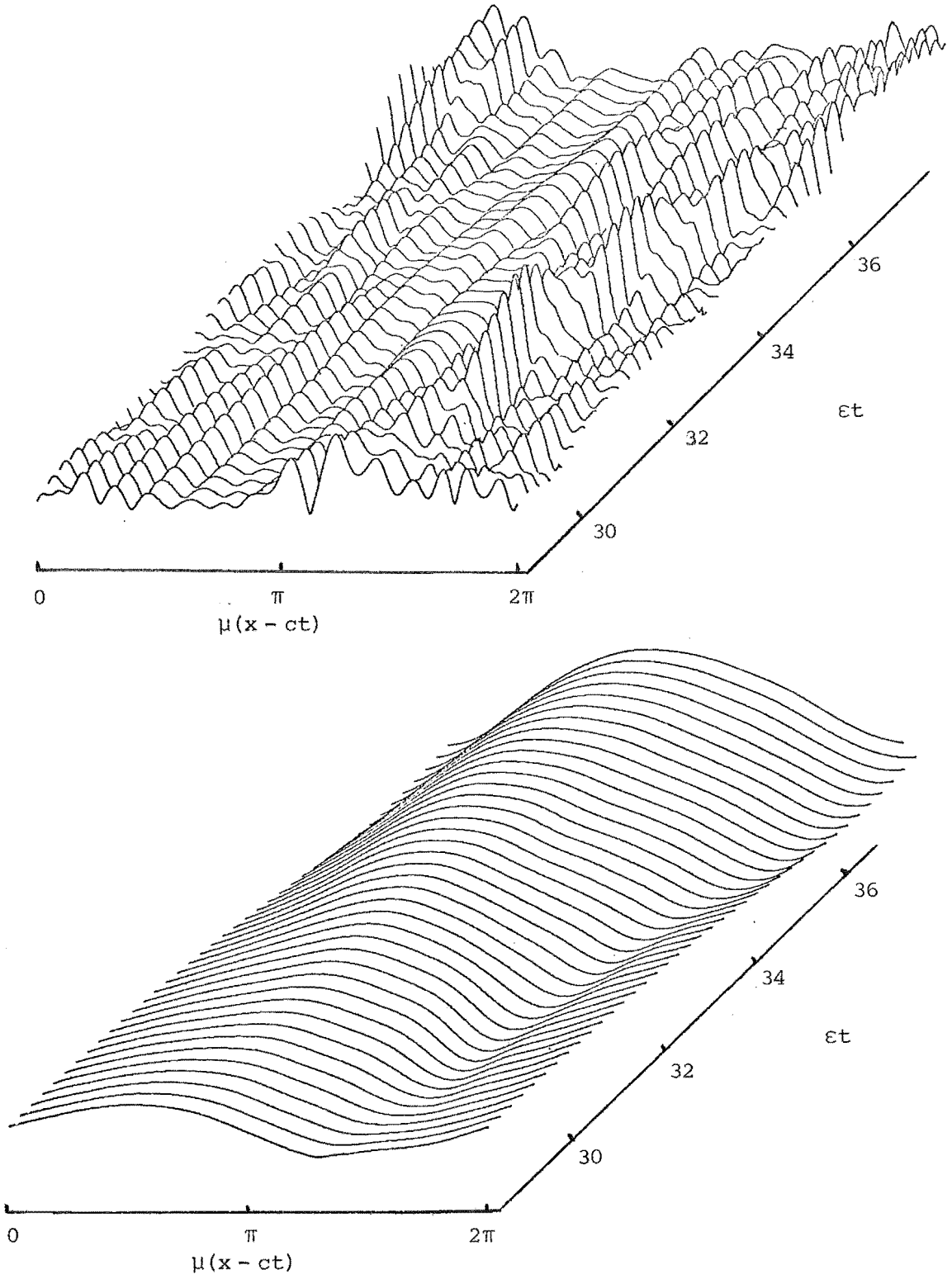

Figure 4.5(b): One wavelength of the surface envelope (top) and interface displacement for $\tau = 30 - 39$ with $\rho = 1{\cdot}02$, $\varepsilon = {\cdot}01$, $\mu = {\cdot}3096$ and the first set of initial conditions.
The vertical magnification is 25.

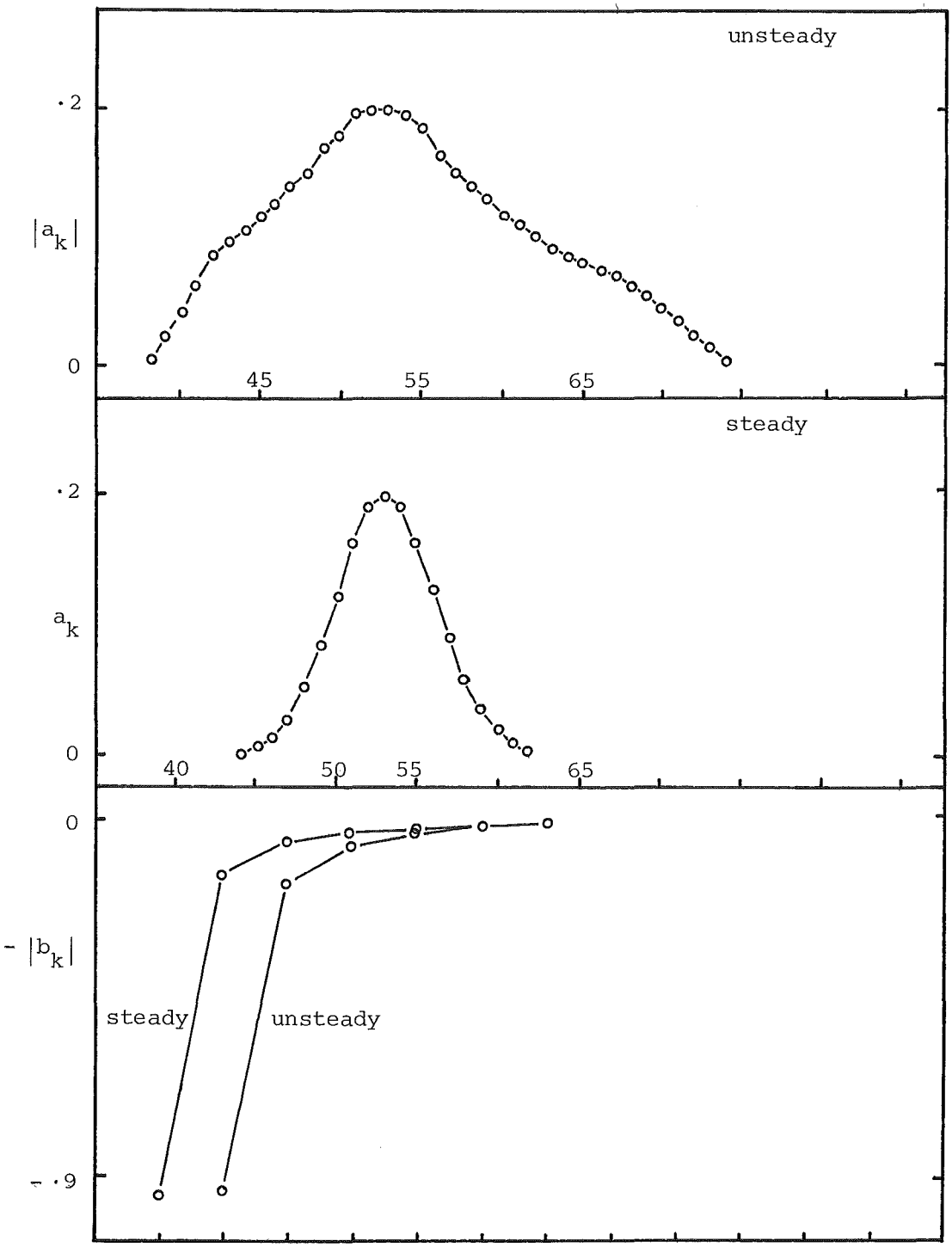

Figure 4.5(c): Averaged unsteady and lowest steady spectra for $\rho = 1{\cdot}02$, $\varepsilon = {\cdot}01$, $\mu = {\cdot}3096$ and the first set of initial conditions.

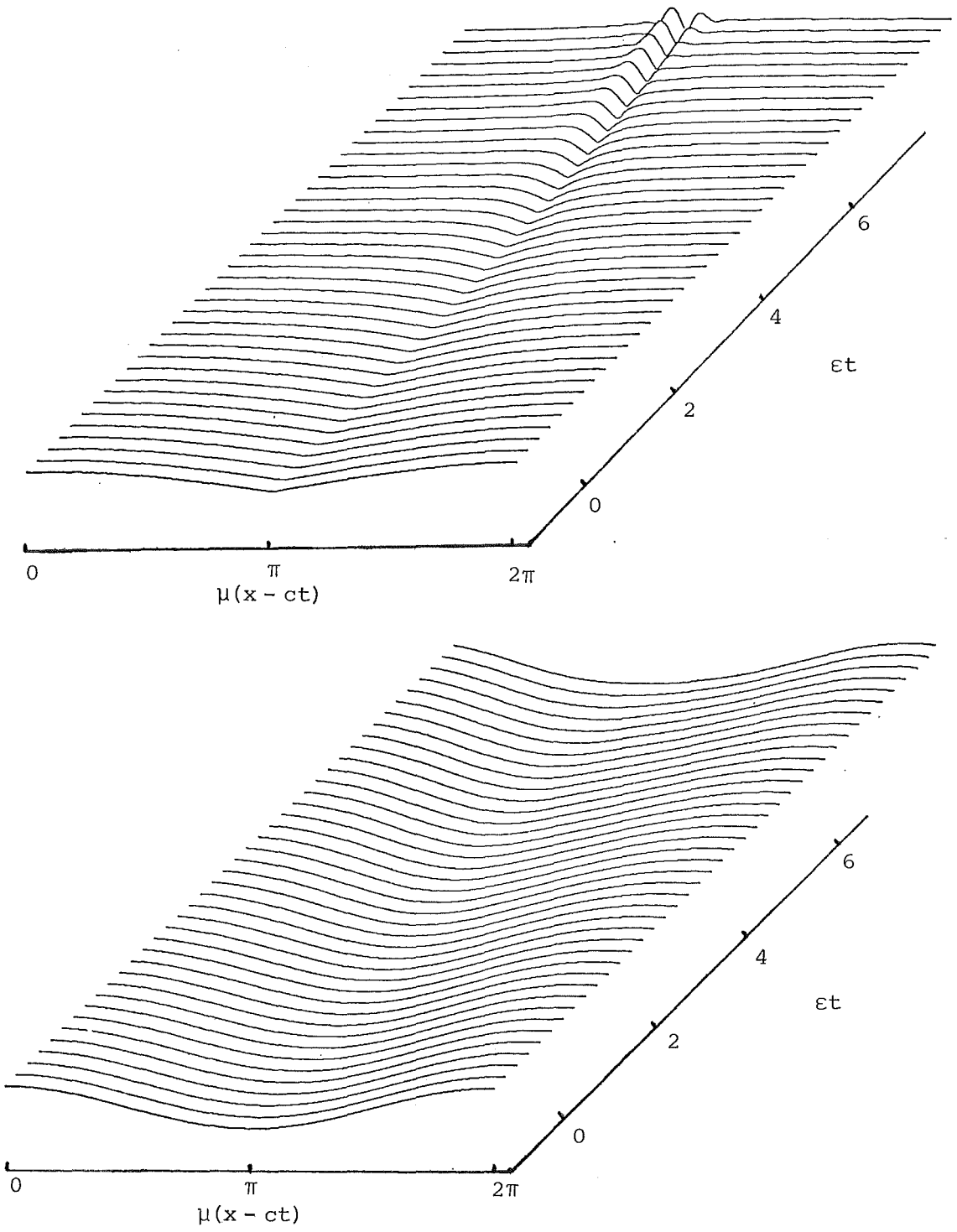

Figure 4.5(d): One wavelength of the surface envelope (top) and interface displacement for $\tau = 0 - 9$ with $\rho = 1{\cdot}02$, $\varepsilon = {\cdot}01$, $\mu = {\cdot}3096$ and the second set of initial conditions. The vertical magnification is 12.

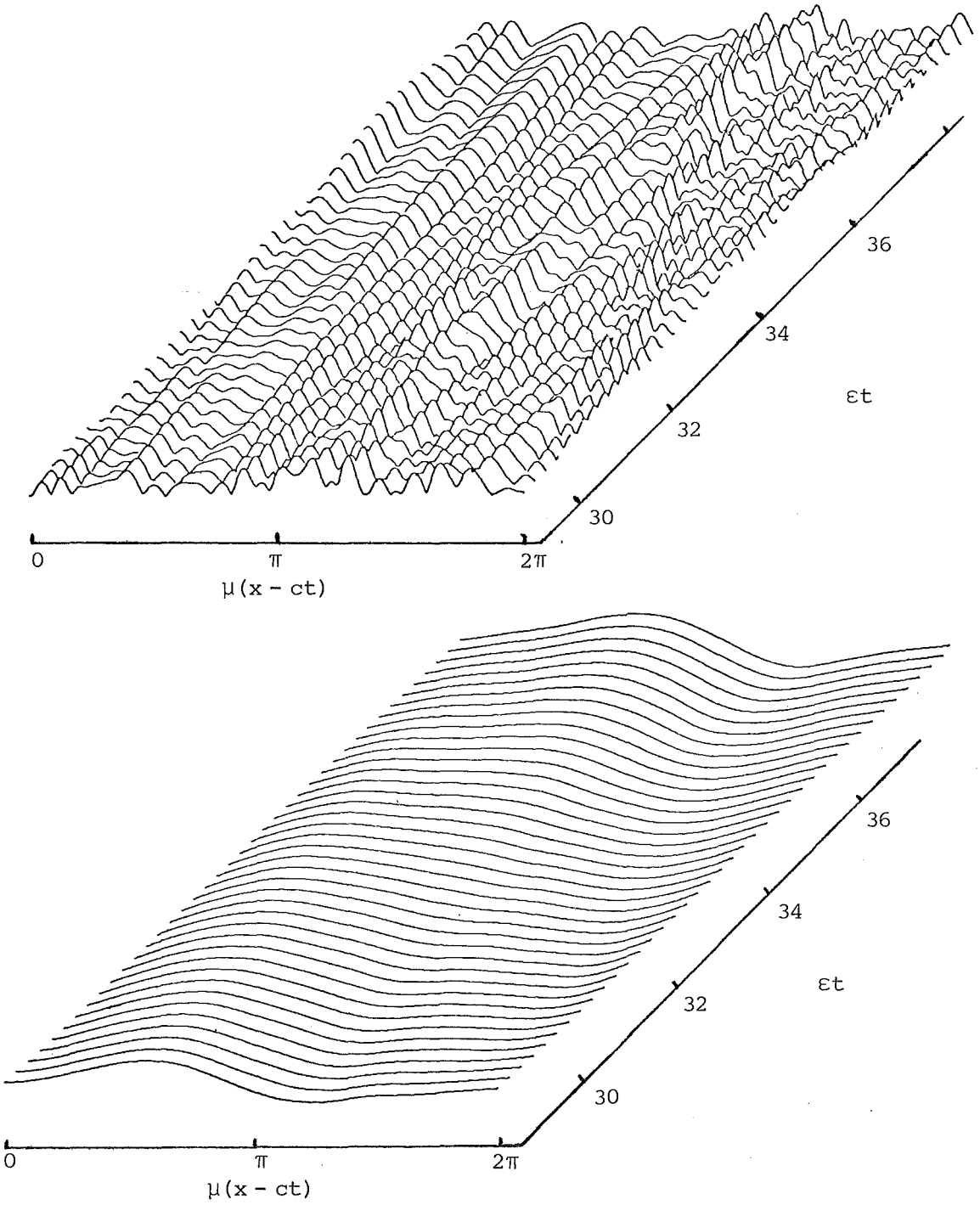

Figure 4.5(e): One wavelength of the surface envelope (top) and interface displacement for $\tau = 30 - 39$ with $\rho = 1{\cdot}02$ $\varepsilon = {\cdot}01$, $\mu = {\cdot}3096$ and the second set of initial conditions. The vertical magnification is 12.

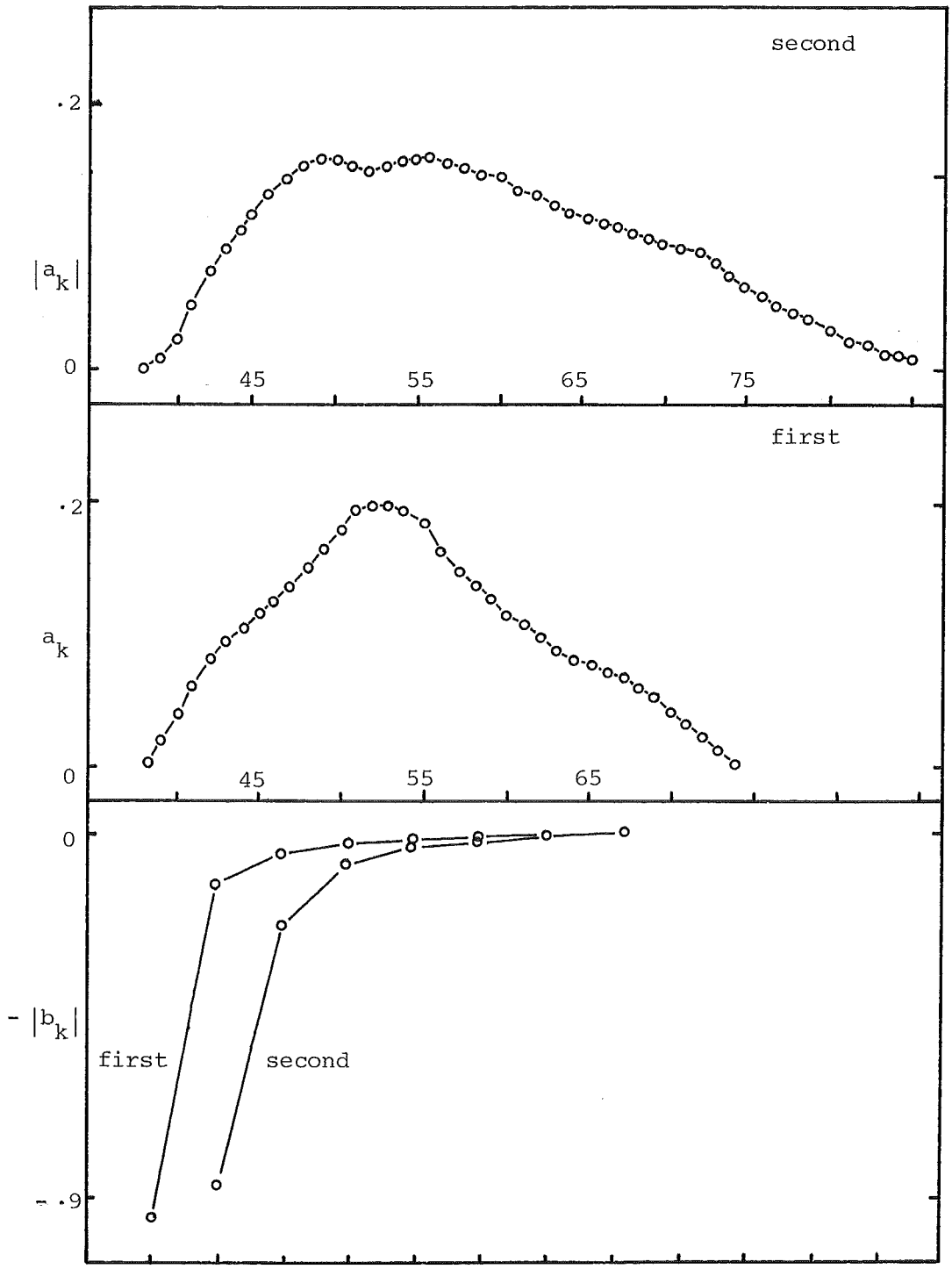

Figure 4.5(f): Averaged unsteady spectra for $\rho = 1{\cdot}02$, $\varepsilon = {\cdot}01$, $\mu = {\cdot}3096$ and the first and second set of initial conditions.

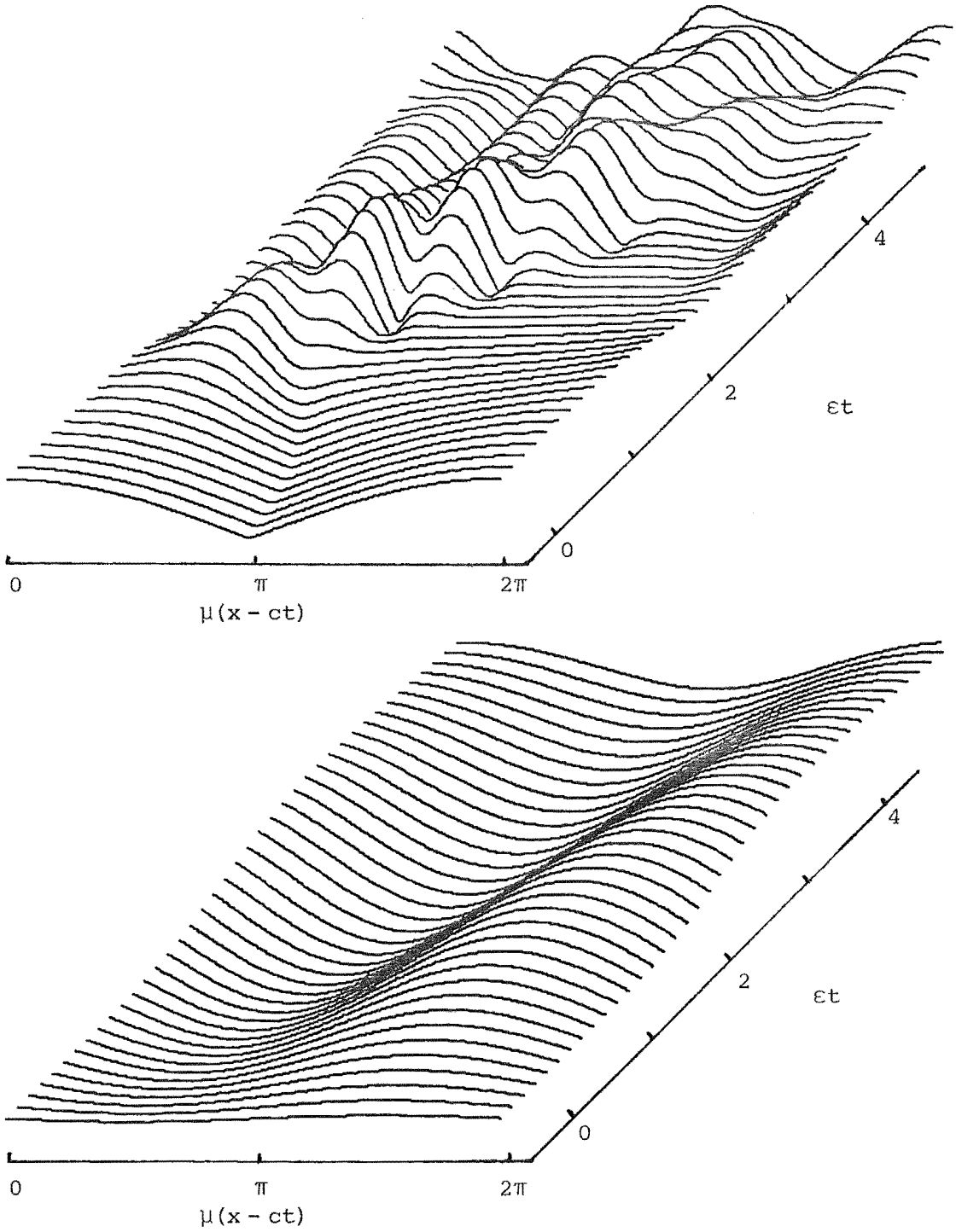

Figure 4.6(a): One wavelength of the surface envelope (top) and interface displacement for $\tau = 0 - 6$ with $\rho = 1{\cdot}02$, $\varepsilon = {\cdot}004$, $\mu = 1{\cdot}373$ and the first set of initial conditions.
The vertical magnification is 25.

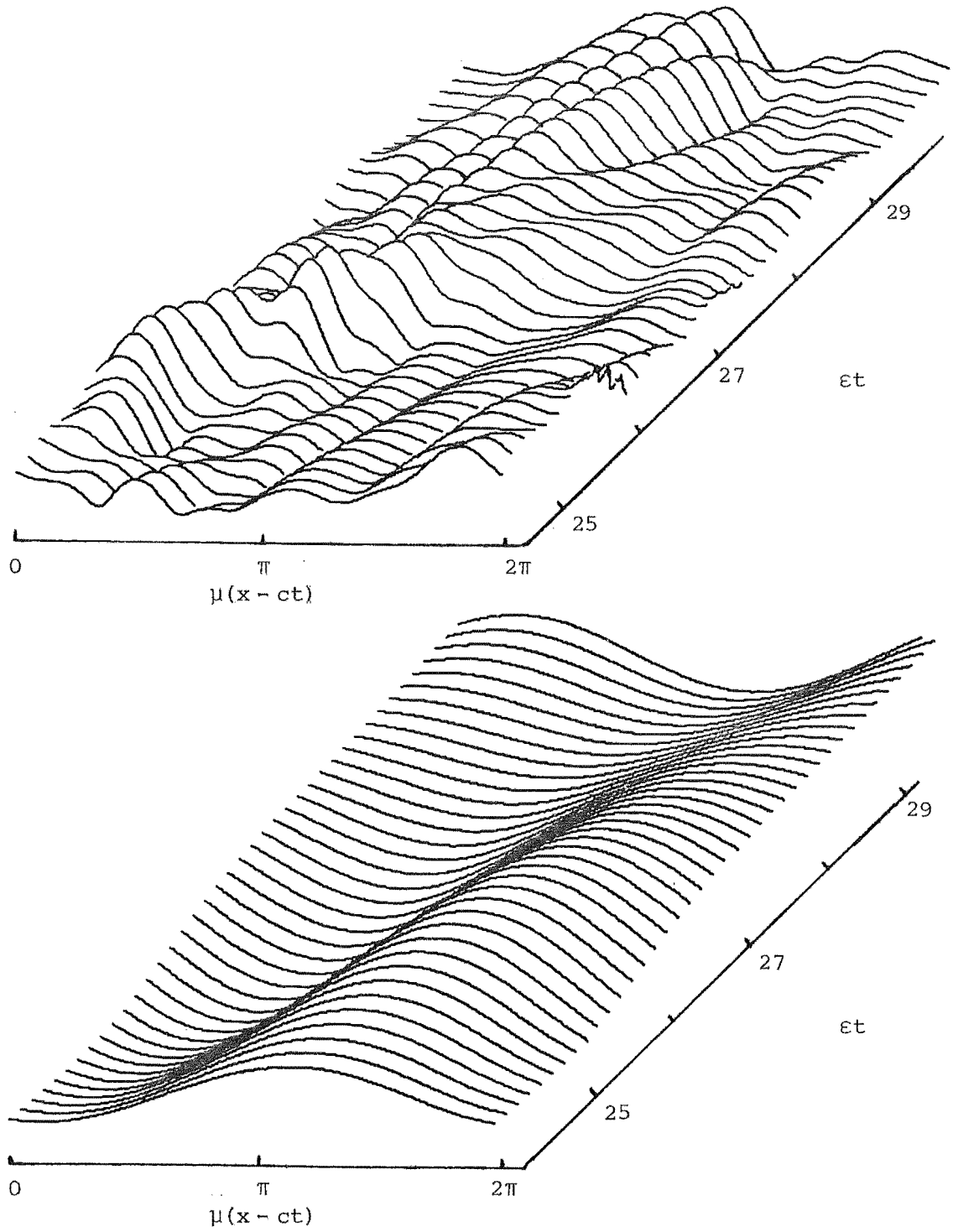

Figure 4.6(b): One wavelength of the surface envelope (top) and interface displacement for $\tau = 25 - 31$ with $\rho = 1{\cdot}02$, $\varepsilon = {\cdot}004$, $\mu = 1{\cdot}373$ and the first set of initial conditions.
The vertical magnification is 25.

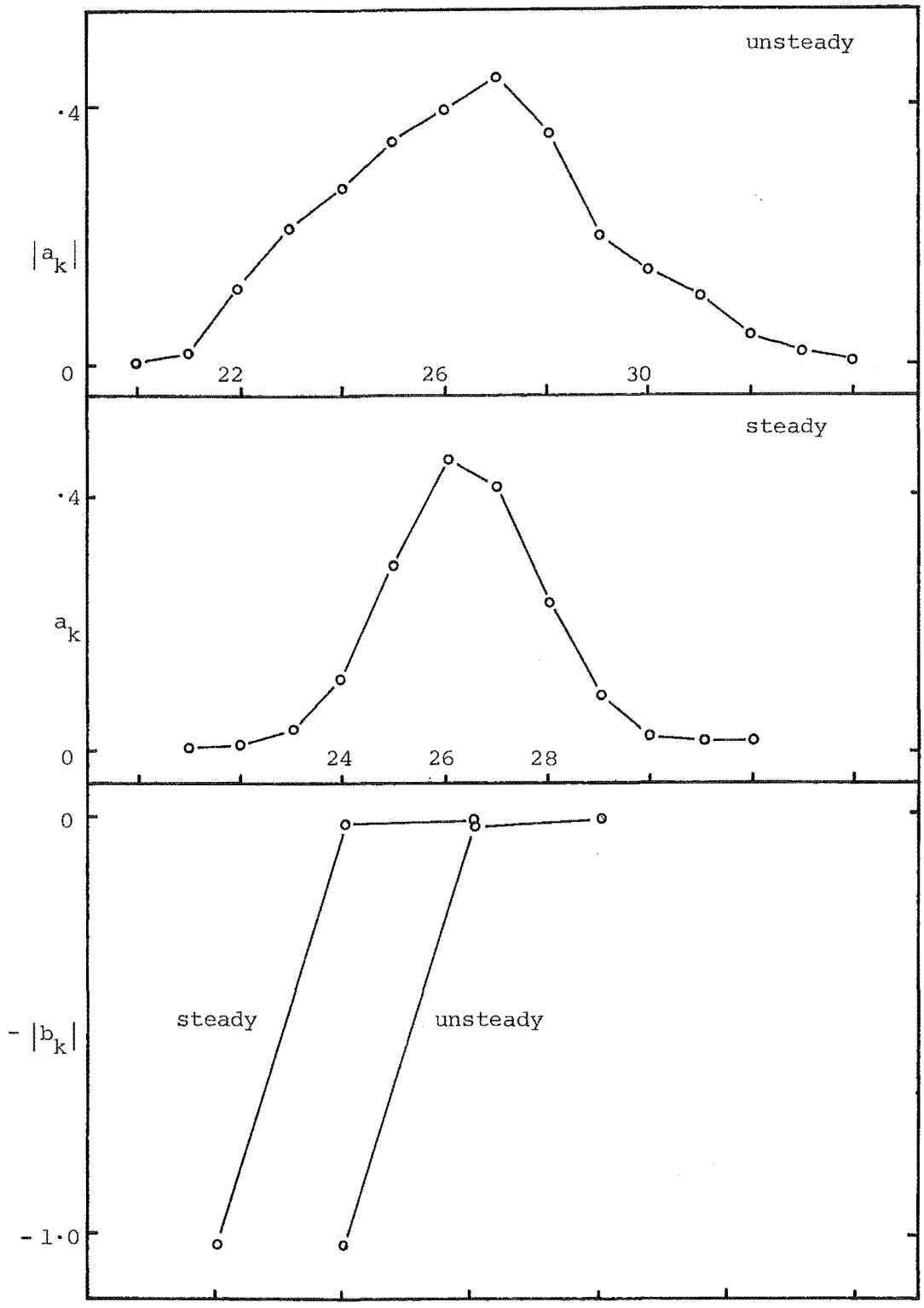

Figure 4.6(c): Averaged unsteady and lowest steady spectra for $\rho = 1{\cdot}02$, $\varepsilon = {\cdot}004$, $\mu = 1{\cdot}373$ and the first set of initial conditions.